Aus dem Institut für Physik der Universität Potsdam

Synchronization in ensembles of nonisochronous oscillators

Dissertation

Zur Erlangung des akademischen Grades
Doktor der Naturwissenschaften
(Dr. rer. nat.)
in der Wissenschaftsdisziplin Theoretische Physik

eingereicht an der
Mathematisch-Naturwissenschaftlichen Fakultät
der Universität Potsdam

von
Ernest Montbrió i Fairen

Potsdam, im April 2004

Contents

Chapter 1

Introduction

This thesis analyses synchronization phenomena occurring in large ensembles of interacting oscillatory units.

The concept of *macroscopic mutual synchronization* (or macroscopic mutual *entrainment*) is essential in order to understand self-organization phenomena arising at many levels in nature. This means that multiple periodic processes with different natural frequencies come to acquire a common frequency (and in some cases also a common phase) as a result of their mutual influence. The importance of the function of synchronization in the self-organization in nature may be realized from the fact that what looks like a single periodic process on a macroscopic level often turns out to be a collective oscillation resulting from the mutual synchronization among an enormous number of the constituent oscillators. This notion was first explored by Norbert Wiener in connection with the human alpha rhythm in the brain: He concluded that some physiological rhythms might reflect mutual synchronization of myriads of individual oscillatory processes (Wiener, 1958).

In general the biological organisms are characterized by complex internal dynamics. In some cases these dynamics are cyclic, so that an organism persistently goes through a closed sequence of states and in this sense, operates as a clock. Thus, these forms of internal dynamics can be viewed as an active motion along a certain cyclic coordinate (Winfree, 1967). The actual processes underlying the cyclic behavior of a biological organism are typically very complex and may differ greatly from one organism to another (Winfree, 1980). Additionally, in biology the oscillators must be self-sustained and nonidentical, in contrast to many-body physics, where the oscillators are usually assumed to be conservative and identical. Here, self-sustained oscillator means that each oscillator is of a dissipative type, or equivalently that it rides a (stable) limit cycle corresponding to the individual's free-running oscillation. This assumption is appropriate, because perturbed biological oscillators generally regulate their amplitude, i.e. they return to their attractor, whereas conservative oscillators would remain in the perturbed state forever.

Very often enormous communities of biological oscillators are found. In such cases, the interaction between individual oscillators may lead to mutual entrainment of their cycles and thus to the emergence of coherent internal dynamics. There are many examples of collective synchronization in nature. For instance, an impressive example is that performed by the fireflies in the jungles of Southeast Asia. Male fireflies emit light at regular intervals, typically twice per second. Large communities of such insects may cover the trees and when the cycles of the individual insects are synchronized these trees are seen rapidly flashing (Buck and Buck, 1968). In addition, visual and acoustic interactions also make crickets and frogs chorus (Walker, 1969; Winfree, 1980) and an audience clap in synchrony (Néda et al., 2000). Synchronization is therefore a phenomenon of *self-organization in time*.

Similar phenomena are known at a cellular level. For instance, oscillations of the glycolysis in suspensions of yeast cells (Richard et al., 1996; Dano et al., 2001), or in the cells forming pacemaker nodes, may become synchronous so that a large amplitude periodic signal is generated (Winfree, 1980; Glass and Mackey, 1988). Moreover, synchronization is related with several central issues in neuroscience (Singer, 1999; Varela et al., 2001): the simultaneous spiking in a neuronal population is a typical response to visual (Eckhorn et al., 1988; Gray et al., 1989), odorous (Stopfer et al., 1997) or tactile (Steinmetz et al., 2000) stimuli and it is the mechanism that maintains vital rhythms as respiration (Koshiya and Smith, 1999). In contrast, synchronization is sometimes regarded as dangerous as in the case of several neurological diseases, e.g. epilepsy (Engel and Pedley, 1975).

Another important example in nature is the synchronization of population cycles in ecology that takes place in very broad geographic regions (Blasius et al., 1999). In this context it is known that synchronization of fluctuating population numbers is strongly connected to the risk of global species extinction (Heino et al., 1997; Earn et al., 2000). On the other hand applications of synchronization of many systems in physics and engineering may be found in chemical reactions (Ertl, 1991; Mikhailov and Loskutov, 1996), lasers (Garcia-Ojalvo et al., 1999; Garcia-Ojalvo and Roy, 2001), digital-logic circuitry (Wiesenfeld et al., 1996, 1998) and in neural networks (Hoppensteadt and Izhikevich, 1998, 1999, 2000). Moreover, the emergence and breakdown of coherent collective motion are not a unique property of the internal dynamics of the oscillators. Similar effects are possible when cyclic collective motions of swarms in physical coordinate space are considered (Gray, 1928; Taylor, 1951).

The problem of synchronization can be formulated mathematically in terms of coupled nonlinear differential equations and hence, in the case of weak interactions, it becomes a problem of perturbations. In this context the concept '*isochron*' was developed by Winfree (1967) in order to treat with oscillators perturbed off their limit cycles. This is important because biological oscillators are almost never

on their attracting cycles. In the present thesis these ideas are incorporated into the *Kuramoto model*, which is a paradigmatic model to investigate mathematically macroscopic mutual synchronization (Kuramoto, 1974; Pikovsky et al., 2001).

This work is organized as follows: Chapters 2 and 3 intend to give the necessary background information. Chapter 2 briefly describes the two canonical models that will be used to study synchronization. First the *Landau-Stuart model*, that describes a general dissipative system close to the onset of oscillations (Hopf bifurcation). This model contains two independent parameters: the natural frequency and the nonisochronicity, that is a parameter related with the isochrons, and describes the amplitude dependence of the frequency. The second model describes the oscillators dynamics in terms of a single phase variable: Taking the effect of the perturbations on the evolution of the oscillators into account allows to reduce a *weakly* perturbed oscillatory system to a single equation which describes the evolution of the phase. Therefore, the so called *phase equations* permit to write a generic system of N weakly coupled, nearly identical, limit cycle oscillators as a system consisting of N coupled differential equations of N phase variables. Finally, the synchronization of two phase oscillators is studied and compared with that of two diffusively coupled Landau-Stuart oscillators. This helps to determine the restrictions imposed by the phase approximation and, particularly, to introduce the concept of *nonisochronicity*.

Chapter 3 presents the most remarkable results concerning mutual synchronization in large populations of oscillators. The Kuramoto model (Kuramoto, 1974), that is the simplest possible phase model, is introduced and analyzed. Despite its simplicity it still retains very fundamental information about the synchronization process [1]. In particular, if an order parameter (measuring the degree of phase coherence in the model) is defined, the sudden transition from incoherent to synchronized motion at a critical value of the coupling strength, is strikingly similar to a thermodynamic second-order phase transition. Using the language of bifurcations theory, the transition occurs through a Hopf bifurcation. In the course of Chapter 3 several analytical techniques that will be used later are developed and finally the phase reduction of the Landau-Stuart model is presented.

In Chapter 4 the phenomenon called 'anomalous synchronization' is described. Generally, it is assumed that diffusive interaction between nonlinear oscillators in one dynamical variable will eventually lead to synchronization of the phases of such oscillators. However, it has been shown that weak diffusive interaction can also lead to dephasing of the oscillators, which then entails a variety of new dynam-

[1] In fact, ensembles of superconducting Josephson junctions (Wiesenfeld et al., 1996; Kiss et al., 2002), lasers (Oliva and Strogatz, 2001) and electrochemical oscillators (Kiss et al., 2002) show a transition to synchronization exactly as the Kuramoto model predicts.

ical phenomena such as chemical turbulence (Kuramoto, 1974; Kurrer, 1997) and intermittency (Han et al., 1995). Here, a novel mechanism is presented where the coupling can enlarge the natural disorder of frequencies, desynchronizing the ensemble of oscillators (in the regime of weak coupling) (Blasius et al., 2003; Montbrió and Blasius, 2003; Montbrió et al., 2004a). This effect arises due to the presence of nonisochronicity of the oscillators in the ensemble. In particular, the nonisochronicity must be correlated with the natural frequency of oscillation. This premise is pertinent because the inhomogeneities in the ensemble may, firstly, affect all the parameters in the system and, secondly, maintain certain correlations.

On the other hand, when nonisochronicity and natural frequency have negative covariance synchronization can be enhanced. This allows for synchronization control: With a careful choice of oscillator parameters the effect of anomalous synchronization can be used to either enhance or inhibit the synchronization in the ensemble. Similar strategies can be used in biological systems and thus anomalous synchronization might play an important role in living systems.

Chapter 5 is devoted to a different problem where, again the effects of the nonisochronicity are remarkable (Montbrió et al., 2004b). In particular, in this chapter it is argued that nonisochronicity may have a fundamental influence in the synchronization process taking place between two interacting populations of oscillators, as it happens in the case of two coupled nonisochronous oscillators (Aronson et al., 1990).

The problem of coupling two different macroscopic populations has been mostly unexplored, so far. The paradigmatic examples of synchronization in populations of many interacting oscillators are typically modelized as a single population of oscillators coupled via an equally weighted mean field coupling - all oscillators interact identically with the mean field. This problem has been extensively studied considering the distribution of natural frequencies to be unimodal (Kuramoto, 1974), symmetric (Kuramoto, 1974; Bonilla et al., 1992; Crawford, 1994) and asymmetric bimodal (Acebrón et al., 1998), or multimodal (Acebrón et al., 2001). However, all these studies do not account for the fact that many of such biological populations may, in fact, be composed of sub-populations, that could be of different type and that may interact in a different fashion internally and externally. For example, synchronization seems to be a central mechanism for neuronal information processing within a brain area as well as for communication between different brain areas (Singer and Gray, 1995; Singer, 1999). Moreover, Eckhorn et al. (1988) and Gray et al. (1989) have shown experimentally that synchronization arises between different neighboring visual cortex columns, and also between different cortical areas. It is believed that such mechanisms play a crucial role in the pattern recognition tasks. The last experiments motivated the first study about synchronization of two different populations composed of identical phase oscillators under the influence of white noises (Okuda and Kuramoto, 1991).

Here, in Chapter 5, the results of Okuda and Kuramoto (1991) are generalized for the case of nonidentical oscillators. Moreover, in our study the coupling function is of a more general form: The oscillators are considered to be phase oscillators of a Landau-Stuart type, i.e. the coupling possesses a parameter (a phase shift in the Kuramoto's coupling function), that accounts for the nonisochronicity effects (Sakaguchi and Kuramoto, 1986). Such a coupling function has also been proved to be useful in modeling information concerning the synaptic connections in a neural network (Hoppensteadt and Izhikevich, 1998) and time delays (Izhikevich, 1998). On the other hand it also appears naturally in the phase reduction of an array of superconducting Josephson junctions (Wiensenfeld and Swift, 1995; Wiesenfeld et al., 1996).

In contrast to Chapter 4, the inhomogeneity in the ensemble is now introduced simply through the natural frequencies, and not through the parameters related with nonisochronicity. Additionally, the synchronization transition in the regime of stronger interactions is considered. Here strong coupling means that the systems are in regions of the parameter space close to criticality, i.e. close to the transition between the incoherent and the synchronized motion.

The case of two coupled populations is especially interesting also from a theoretical perspective, because is combines the concept of macroscopic synchronization (Chapter 3) with that of mutual synchronization of two oscillators (Chapter 2). In this respect the presence of nonisochronicity plays a prominent role.

Finally, in Chapter 6, the results of this work are summarized, discussed and some directions for future work are proposed.

Chapter 2

Dynamics of perturbed oscillatory systems

In this Chapter two fundamental models for oscillatory systems are presented which will be mainly used for analyzing synchronization phenomena.

The first model is the Landau-Stuart equation (Landau, 1944; Stuart, 1960) which describes a general dissipative system near a Hopf bifurcation point.

The second model are the so called *phase equations* (Kuramoto, 1974). They are based on a fundamental approximation applicable in general to *weakly* perturbed limit cycle oscillators, and therefore to *weakly coupled* oscillators in general. Here the simplification of the dynamics comes essentially from the fact that the amplitude disturbances decay much faster than the phase disturbances and thus the original dynamics is contracted to a much simpler one, which still retains a sufficiently large number of degrees of freedom to admit a variety of self-organization phenomena.

Finally the synchronization of two coupled Landau-Stuart systems is studied and compared with the synchronization process taking place between the corresponding phase oscillators for the Landau-Stuart system. This permits to check the validity of the phase approximation as well as to study the influence of the nonisochronicity of the original limit cycle system, into the corresponding phase equations.

2.1 Fundamental models for synchronization studies

2.1.1 The Landau-Stuart model

Many theories on the nonlinear dynamics of dissipative systems are based on the first order ordinary differential equations

$$\frac{d\mathbf{x}}{dt} = \mathbf{F}(\mathbf{x}; \chi) \tag{2.1}$$

where $\mathbf{x} \in \mathbb{R}^n$ and χ represents some parameters of the system. Assume that for some range of the parameters χ the system has a stable steady state which loses stability at some critical value of χ_c, giving rise to a periodic motion. This phenomenon is generally called Hopf bifurcation. As the parameter χ is increased further, the system may show more complex behavior through a number of bifurcations, that may lead to quasi-periodic, chaotic or a variety of non-periodic behaviors. However, all the systems come to behave in a similar manner sufficiently close to the Hopf bifurcation. This important fact permits to reduce the system (2.1) to a very simple universal equation sometimes called the Landau-Stuart (or $\lambda - \omega$) equation.

The Landau-Stuart model in complex variables writes

$$\dot{z} = z[1 + i(\omega + q) - (1 + iq)z\bar{z}], \tag{2.2}$$

or in polar coordinates, $z = re^{i\theta}$,

$$\begin{aligned} \dot{r} &= r(1 - r^2) && (2.3)\\ \dot{\theta} &= \omega + q(1 - r^2). && (2.4) \end{aligned}$$

The parameter ω is the *natural frequency* of the oscillator and q is the *non-isochronicity*, or shear term. It reflects that the oscillation frequency is a function of the amplitude of the oscillations [1]. From Eq.(2.3 in follows that the origin ($r = 0$) is always an unstable fixed point, and that there are stable oscillations of radius $r = 1$.

The solution of Eq.(2.2) with initial conditions $r_0 = r(0)$ and $\theta_0 = \theta(0)$ is

$$\begin{aligned} r(t) &= \left(1 + \frac{1 - r_0^2}{r_0^2} e^{-2t}\right)^{-1/2}, \\ \theta(t) &= \theta_0 + \omega t - \frac{q}{2} \ln(r_0^2 + (1 - r_0^2)e^{-2t}). \end{aligned} \tag{2.5}$$

For the case of zero nonisochronicity, $q = 0$, the Landau-Stuart system rotates with constant velocity ω for all initial conditions (r_0, θ_0). However, if the nonisochronicity deviates from zero, the system still rotates with the natural frequency ω on the limit cycle C, but it can have different frequencies in the other regions of the phase space (r, θ).

2.1.2 Isochrons

In such a situation, when the rotation frequency depends on the location in the phase space, it is not clear a priori how to define the phase outside the limit cycle C. In order to deal with oscillatory systems perturbed off their limit cycles, Winfree

[1] The Landau-Stuart equations are not derived here. Some derivations can be found for instance in (Kuramoto, 1974; Aronson et al., 1990; Hoppensteadt and Izhikevich, 1998)).

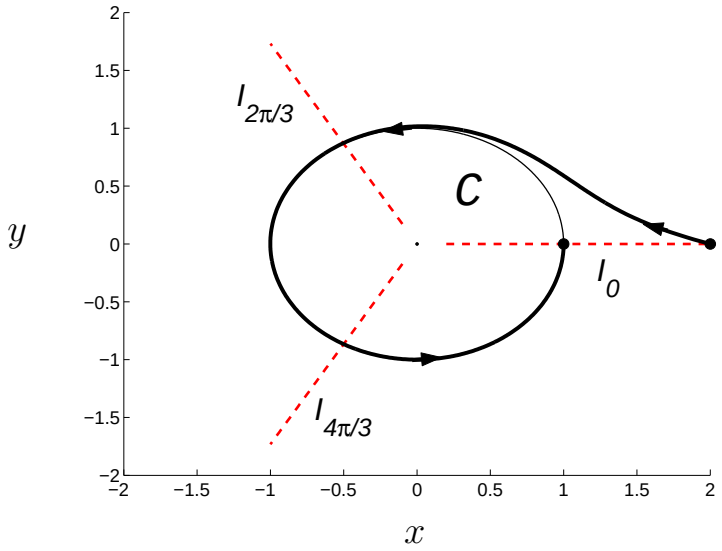

Figure 2.1: *Isochronous ($q = 0$)* Landau-Stuart system (2.2). The isochrons (dashed lines) are orthogonal to the limit cycle C. A trajectory starting at time t with initial position $\phi_0 = \theta_0$ at the isochron I_0, crosses the isochron I_0 at times $t + n(2\pi/\omega)$, where $n = 1, 2, \ldots$. The depicted trajectory (bold face line) is obtained through the solution (2.5) taking $(r_0 = 2, \theta_0 = 0)$.

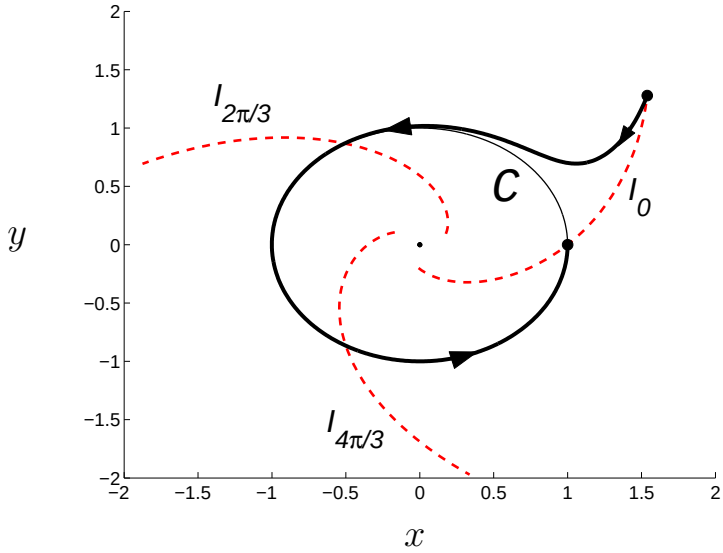

Figure 2.2: *Nonisochronous ($q = 0.66$)* Landau-Stuart system (2.2). The isochrons (dashed lines) are given by (2.6). A trajectory starting at time t with initial position ϕ_0 at the isochron I_0, crosses the isochron I_0 at times $t + n(2\pi/\omega)$, where $n = 1, 2, \ldots$. The depicted trajectory (bold face line) is obtained through the solution (2.5) taking $(r_0 = 2, \theta_0 = 0)$.

(1967) developed the concept '*isochron*'. According to Winfree the phase variable ϕ is defined by the condition that all the points are rotating uniformly with the same frequency ω in the neighborhood of C. Thus, the phase in not necessarily a simple angle in the phase space. Instead points of constant phase define curves in phase space which are called the isochrons. This concept is very useful for studying systems consisting of many interacting oscillators, because they will almost never be on their attractors.

In the case of the Landau-Stuart oscillator, from Eq. (2.5) we see that the new phase ϕ can be defined in a small region around cycle C as

$$\phi(r, \theta) = \theta - q \ln r,$$

since the additional phase shift of a trajectory starting at (r_0, θ_0) is $-q \ln r_0$. Therefore the isochrone I_{ϕ_0} is the curve of constant phase ϕ_0 defined, for the Landau-Stuart system, as

$$I_{\phi_0}: \quad \phi_0 = \theta - q \ln r. \tag{2.6}$$

- The isochrons for the case $q = 0$ are just lines perpendicular to the cycle C (see Fig. 2.1). In this case the definition of the new phase ϕ coincides with the angle variable θ of the Landau-Stuart system (2.2). In general, we refer to the systems with amplitude-independent frequency (defined as the time derivative of the angle variable of the original system) as *isochronous oscillators*.

- The isochrons of the Landau-Stuart system (and thus of any oscillatory system close to the onset of oscillations) for $q \neq 0$ are logarithmic spirals (see Fig. 2.2). We refer to such systems with an amplitude-dependent frequency (defined as the time derivative of the angle variable of the original system) as *nonisochronous oscillators*.

Similarly the isochrons can be defined for any system (2.1) as $n-1$ dimensional surfaces of constant phase.

2.1.3 Phase dynamics

In this section we describe a fundamental approximation which will be very much used in this work. In the previous Section the individual system was supposed to be in the neighborhood of the Hopf bifurcation point. The description here is related with *perturbations* acting on the system: when the perturbations are *weak*, there exists another asymptotic regime where the description of the dynamics is greatly simplified. In this context the concept of isochrons becomes very useful.

Later such perturbations will play the role of the coupling strength, i.e. the interaction among the oscillators that will lead to collective behavior.

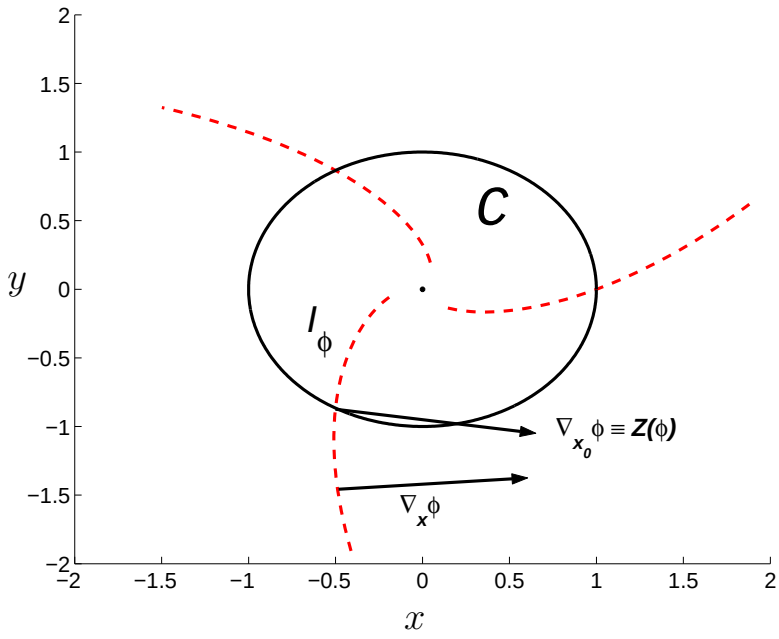

Figure 2.3: The geometrical meaning of the vector $\nabla_{\mathbf{x_0}}\phi$. When the state point $\mathbf{x}$ is in the vicinity of the limit cycle, the gradient can be evaluated approximately by assuming that $\mathbf{x}$ is on the limit cycle trajectory C (The limit cycle system is the nonisochronous Landau-Stuart (2.2) with three isochrons I_ϕ corresponding to Eq.(2.6) with $q = 0.47$ and for the angles $\phi = 0, 2\pi/3, 4\pi/3$ rad.).

We first consider a single limit cycle oscillator, with natural frequency ω, represented by a n-dynamical system (2.1). We then can define the phase ϕ corresponding to an arbitrary $\mathbf{x}$ in the space state representing the system. The most natural treatment is to define a phase variable ϕ in such a way that, with the time development of $\mathbf{x}$ given by Eq.(2.1) the phase evolves uniformly. Therefore ϕ satisfies

$$\dot{\phi} = \omega, \tag{2.7}$$

and using the original system (2.1), the new definition (2.7) implies

$$\nabla_{\mathbf{x}}\phi \cdot \mathbf{F}(\mathbf{x}) = \omega.$$

The phase dynamics method is extremely effective in describing systems of weakly coupled oscillators. In this case, we can treat the interactions effect on a single oscillator as being generated by a weak external force $\mathbf{p}(t)$. Let us proceed in this manner, writing the forced system

$$\frac{d\mathbf{x}}{dt} = \mathbf{F}(\mathbf{x}) + \mathbf{p}(t).$$

Then, we consider the correspondingly perturbed motion of ϕ. Formally, we have

$$\dot{\phi} = \nabla_{\mathbf{x}}\phi \cdot (\mathbf{F}(\mathbf{x}) + \mathbf{p}(t)).$$

The vector $\nabla_{\mathbf{x}}$ is perpendicular to the isochron (surface of constant phase) I_ϕ (see Fig.2.3). If the perturbation in question is sufficiently weak, we expect that the point $\mathbf{x}$ representing the system's state will be close to the limit cycle orbit C of the unperturbed system. Thus, we can replace $\nabla_{\mathbf{x}}$ by its realization at the intersection of I_ϕ and C, so that $\nabla_{\mathbf{x}_0}\phi \equiv \mathbf{Z}(\phi)$, as it is shown in Fig. 2.3. In other words, we write

$$\dot{\phi} = \omega + \mathbf{Z}(\phi) \cdot \mathbf{p}.$$

Clearly, we have that $\mathbf{Z}(\phi + 2\pi) = \mathbf{Z}(\phi)$.

2.1.4 Two coupled phase oscillators

Let us now consider the situation in which the system consists in two coupled identical oscillators in which the interaction between oscillators can be represented by a perturbation of the form $\mathbf{p} = \mathbf{V}(\mathbf{x_1}, \mathbf{x_2})$, where $\mathbf{x_1}$ is the state of the first oscillator and $\mathbf{x_2}$ the state of the second one. Now, with $\mathbf{x_1}$ and $\mathbf{x_2}$ having the isochrons I_{ϕ_1} and I_{ϕ_2}, with the same reasoning used above. We can replace $\mathbf{x_1}$ and $\mathbf{x_2}$ in $\mathbf{V}$ by their values at the intersections of C with I_{ϕ_1} and C with I_{ϕ_2} by $\mathbf{x_{1}}_0$ and $\mathbf{x_{2}}_0$. We thus obtain for the first oscillator the following evolution equation involving only the phases

$$\dot{\phi}_1 = \omega + G(\phi_1, \phi_2), \tag{2.8}$$

where

$$G(\phi_1, \phi_2) \equiv \mathbf{Z}(\phi_1) \cdot \mathbf{V}(\mathbf{x}_0(\phi_1), \mathbf{x}_0(\phi_2)),$$

is a 2π-periodic function in both ϕ_1 and ϕ_2. We further simplify this equation as follows. First, introducing the *phase disturbances* ψ_1 and ψ_2 as $\phi_1 = \omega t + \psi_1$, and $\phi_2 = \omega t + \psi_2$. Replacing ϕ_1 and ϕ_2 in Eq.(2.8) with these expressions, we have

$$\dot{\psi}_1 = G(\omega t + \psi_1, \omega t + \psi_2). \tag{2.9}$$

Since the coupling between the oscillators is weak, G is small and ψ_1 and ψ_2 change slowly in time. Thus, in one period $2\pi/\omega$, ψ_1 and ψ_2 change only very slightly, and we can approximate them as constants. We thus average the right hand side of Eq.(2.9) over one period and obtain, (in terms of ϕ_1 and ϕ_2)

$$\dot{\phi}_1 = \omega + \Gamma(\phi_1 - \phi_2),$$

with

$$\Gamma(\phi_1 - \phi_2) = \frac{1}{2\pi}\int_0^{2\pi} G(\phi_1, \phi_2) d(\omega t).$$

The function Γ is called the *interaction function*, and it is a 2π periodic function of the phase difference $\phi_1 - \phi_2$.

Next we generalize the previous discussion to two *nonidentical* (but nearly identical) oscillators. Considering the vector fields to be slightly different

$$\mathbf{F}(\mathbf{x_1}) = \mathbf{F}_0(\mathbf{x_1}) + \delta\mathbf{F}(\mathbf{x_1}), \quad \mathbf{F}(\mathbf{x_2}) = \mathbf{F}_0(\mathbf{x_2}) + \delta\mathbf{F}(\mathbf{x_2}) \tag{2.10}$$

the full equation of motion for each oscillator can be written in the form $d\mathbf{x}/dt = \mathbf{F}(\mathbf{x})$, the vector field $\mathbf{p}$ can be included in the deviations $\delta\mathbf{F}(\mathbf{x})$, and under the approximation made above, in which $\mathbf{x}$ is replaced by $\mathbf{x}_0(\phi)$, G comes to possess the additional term $\mathbf{Z}(\phi)\delta\mathbf{F}(\mathbf{x}_0(\phi))$. Again, taking the average over one period, this additional term yields the constant value $\delta\omega$. This represents a constant shift from the characteristic frequency. With this, if the interaction is symmetric Eqs.(2.10) come to assume the form

$$\begin{aligned} \dot{\phi}_1 &= \omega_1 + \delta\omega_1 + \Gamma(\phi_1 - \phi_2), \\ \dot{\phi}_2 &= \omega_2 + \delta\omega_2 + \Gamma(\phi_2 - \phi_1). \end{aligned} \tag{2.11}$$

2.2 Synchronization of two oscillators

In the two oscillator model described in the previous section, if the phase difference remains finite, i.e.

$$|\phi_1(t) - \phi_2(t)| < \text{ct.} \quad \text{for } t \to \infty \tag{2.12}$$

then the average frequencies (or observed frequencies)

$$\Omega = \lim_{t\to\infty} \frac{\phi(t)}{t}. \tag{2.13}$$

for the two oscillators are identical. If this case we say that the oscillators are mutually *phase-synchronized* (Pikovsky et al., 2001). When the phase difference diverges as $t \to \infty$, the synchronization is said to be broken, and the oscillators *drift*.

2.2.1 Synchronization of two phase oscillators

If we write Eqs. (2.11) in terms of the phase differences $\phi = \phi_1 - \phi_2$, the time evolution of ϕ can be expressed in a closed form

$$\dot{\phi} = \Delta\omega + 2\Gamma_{\text{odd}}(\phi), \tag{2.14}$$

where $\Delta\omega \equiv \omega_1 - \omega_2$, and $\Gamma_{\text{odd}}(\phi)$ is the anti-symmetric part of the interaction function $\Gamma(\phi)$. Since $\Gamma_{\text{odd}}(\phi)$ is both anti-symmetric and 2π periodic, it satisfies

$$\Gamma_{\text{odd}}(0) = \Gamma_{\text{odd}}(\pi) = 0.$$

For simplicity let us first assume that the oscillators are identical, i.e. $\Delta\omega = 0$. Then there exist at least two synchronized solutions, one with $\phi = 0$ and one with $\phi = \pi$. In order for these solutions to be stable, their corresponding differential coefficients $\Gamma'(0)$ and $\Gamma'(\pi)$ must be negative. For example, let us take

$$\Gamma(\phi) = -\frac{K}{2}\sin(\phi + \alpha), \tag{2.15}$$

with the coupling constant defined as $K > 0$. When synchronization has occurred then ϕ has to remain constant and therefore if $\alpha < \pi/2$ the motion of the oscillators becomes synchronized (with frequency Ω_-) *in-phase*, i.e. $\phi = 0$. However, if $\alpha > \pi/2$ the oscillators synchronize (with frequency Ω_+) *in anti-phase*, that is $\phi = \pi$. For more complicated coupling functions Γ, states in which the pase difference is neither 0 nor π can result. On the other hand, it is interesting to note that the oscillators synchronize to the frequencies

$$\Omega_\mp = \phi_\mp = \omega \mp \frac{K}{2}\sin\alpha, \tag{2.16}$$

that deviate from the individual frequencies of the oscillators if α is nonzero. Thus, although the oscillators are identical the oscillators modify their frequencies due to the coupling.

When the oscillators are considered to be nonidentical, it is also clear that the solutions exist over some finite range of $\Delta\omega$ around 0. If we write the Eqs. (2.11) using the same coupling function (2.15) we have

$$\begin{aligned} \dot{\phi}_1 &= \omega_1 - \frac{K}{2}\sin(\phi_1 - \phi_2 + \alpha), \\ \dot{\phi}_2 &= \omega_2 - \frac{K}{2}\sin(\phi_2 - \phi_1 + \alpha). \end{aligned} \tag{2.17}$$

and the corresponding closed differential equation for the evolution of the phase difference is given by

$$\dot{\phi} = \Delta\omega - K\cos\alpha\sin\phi. \tag{2.18}$$

This equation it is known as the Adler equation. There are two cases in the dynamics of ϕ, as depicted in Fig.2.4. If the frequency detuning lies in the interval

$$-K\cos\alpha < \Delta\omega < K\cos\alpha \tag{2.19}$$

then there is one pair of fixed points, i.e. a pair of stationary solutions for ϕ. It is easy to see that one of this fixed points is (asymptotically) stable and the other one unstable. Therefore, if (2.19) is fulfilled, the system evolves to one of

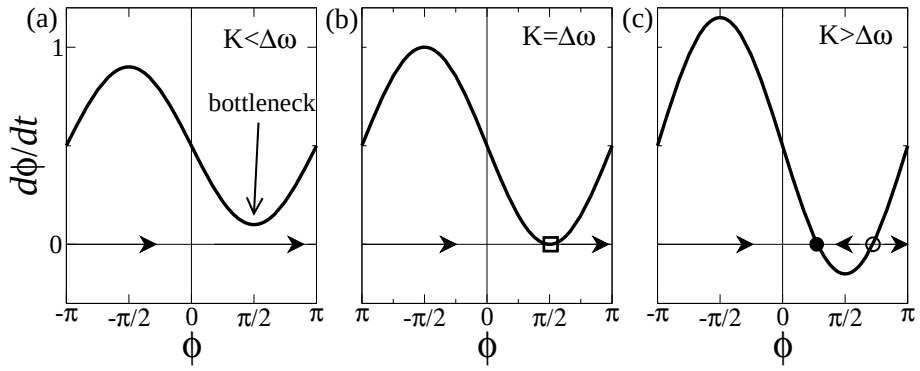

Figure 2.4: The right hand side of Eq.(2.18) with $\alpha = 0$ outside (a), at the border (b), and inside the synchronization region (c). The stable and the unstable fixed points are shown with the filled and open circles. In panel (b) the synchronization transition is shown. Here the stable and the unstable fixed points collide and form a half-stable fixed point which has been born in a saddle-node bifurcation.

the stable fixed points and stays there, so that the oscillators maintain a constant phase difference given by

$$\phi^* = \arcsin\left(\frac{\Delta\omega}{K\cos\alpha}\right). \tag{2.20}$$

This regime determines when the oscillators are synchronized, i.e. they posses a common frequency Ω that in general ($\alpha \neq 0$) deviates from the mean $\bar{\omega} = (\omega_1 + \omega_2)/2$ (see Fig.2.5). This regime exists inside the domain (2.19) on the parameter plane $(\Delta\omega, K)$, called the *synchronization region*, or range of entrainment.

Another situation is observed if the frequency detuning lies outside the synchronization region (2.19). Then the time derivative of ϕ is permanently positive (or negative) and thus increases indefinitely, corresponding to *phase drift* (Fig. 2.4(a)). Notice that the phases do not separate at a uniform rate: ϕ increases most slowly when it passes under the minimum of the sine function (bottleneck), in Fig. 2.4(a) at $\phi = \pi/2$, and most rapidly when it passes under the maximum at $\phi = -\pi/2$. Moreover, the period of phase drift may be calculated as

$$T = \int_0^{2\pi} \frac{d\phi}{\dot{\phi}} \tag{2.21}$$

which yields

$$T = \frac{2\pi}{\sqrt{\Delta\omega^2 - (K\cos\alpha)^2}}. \tag{2.22}$$

The state of the system in the phase drift regime is quasiperiodic with two fundamental frequencies: the *beat frequency*

$$\Delta\Omega = 2\pi/T, \tag{2.23}$$

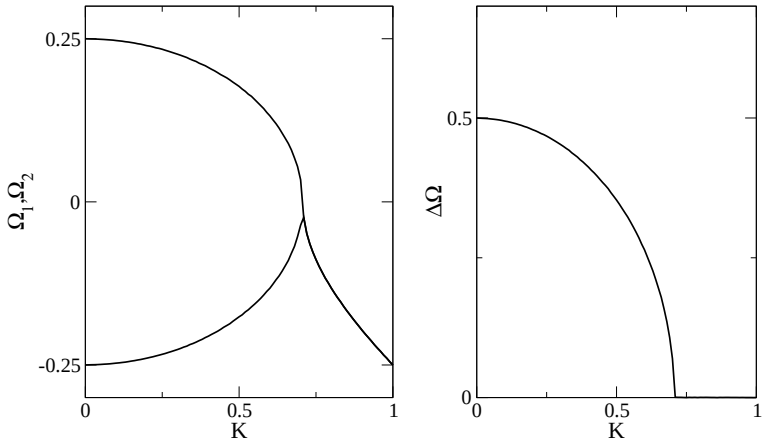

Figure 2.5: Synchronization of two phase oscillators (2.17). Plotted is the averaged frequencies (2.13) of each oscillator (left) and the beat frequency (2.23) $\Delta\Omega(K)$ (right) as a function of the coupling strength, K.

and the observed frequency $\langle\dot{\phi}\rangle = \Omega$, (Eq. (2.13)).

The transition between phase drift and synchronization occurs in a saddle-node bifurcation at

$$(\Delta\omega)_c = \frac{K}{\cos\alpha}, \quad \text{or} \quad K_c = \frac{\Delta\omega}{\cos\alpha}. \tag{2.24}$$

Close to the synchronization region (2.19) it it possible to estimate the behavior beat frequency $\Delta\Omega$, that gives

$$\Delta\Omega \sim \sqrt{\Delta\omega - K\cos\alpha}.$$

This shows that $\Delta\Omega$ obeys the characteristic square root scaling law of a system close to a saddle-node bifurcation (see Fig. (2.4(b)). Therefore the oscillators spend a long time with some constant phase difference that it is interrupted by short intervals where the phase difference ϕ increases (or decreases) by 2π: these events are called *phase slips*.

2.2.2 Synchronization of two Landau-Stuart oscillators

In the following section we obtain the phase equations of a system consisting in two diffusively coupled Landau-Stuart oscillators,

$$\dot{z}_{1,2} = z_{1,2}[1 + i(\omega_{1,2} + q_{1,2}) - (1 + iq_{1,2})z_{1,2}\bar{z}_{1,2}] + \frac{K}{2}(z_{2,1} - z_{1,2}), \tag{2.25}$$

where the subscripts refer to the oscillator 1 or 2. Aronson et al. (1990) showed that the dynamics of (2.25) close to the transition to synchronization are greatly

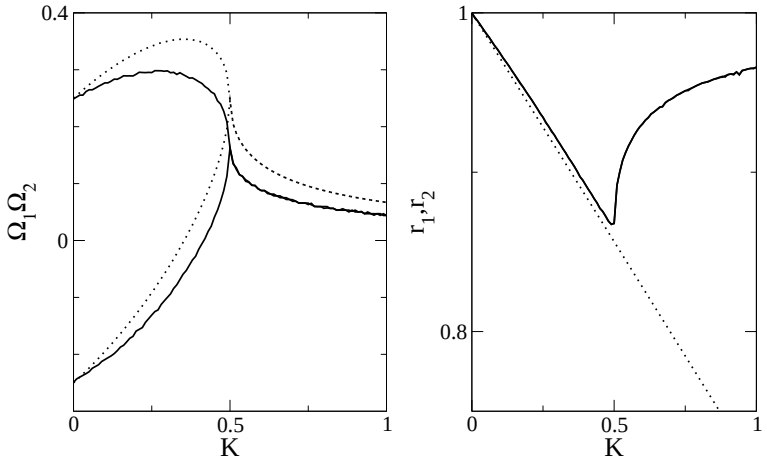

Figure 2.6: Frequencies (left) and averaged radius (right) of two coupled Landau-Stuart oscillators (2.25) (solid lines) versus coupling strength K. The dotted lines in the left panel correspond to the phase approximation (2.30) and the dotted lines in the right one correspond to Eq. (2.28) ($q_1 = q_2 = 0.666$, $\omega_1 = 0.25$, $\omega_2 = -0.25$).

complicated due to the presence of the nonisochronicity. However, the weakly coupled system presents an interesting property that was investigated and that will be the the subject of Chapter 4. However, we first discuss briefly an important phenomenon called *oscillation death* arising in the presence of both large parameter mismatch and strong coupling strength. In such circumstances the diffusive coupling acting in limit cycle systems can lead to the suppression of the oscillations (Bar-Eli, 1985; Aronson et al., 1990). The system (2.25) in polar coordinates writes

$$\dot{r}_{1,2} = r_{1,2}(1 - \frac{K}{2} - r_{1,2}^2) + \frac{K}{2} r_{2,1}\cos(\theta_{2,1} - \theta_{1,2}), \tag{2.26}$$

$$\dot{\theta}_{1,2} = \omega_{1,2} + q_{1,2}(1 - r_{1,2}^2) + \frac{K}{2}\frac{r_{2,1}}{r_{1,2}}\sin(\theta_{2,1} - \theta_{1,2}). \tag{2.27}$$

In order to understand how oscillation death arises in the Landau-Stuart oscillators (2.25) let us assume that the oscillators are not synchronized. In this case, Eqs.(2.26) can be time-averaged over one period T of the phase difference $\phi(t) = \theta_2 - \theta_1$ in order to estimate the mean radius of the oscillators. Since the oscillators are unlocked, the phases perform a quasiperiodic motion on a torus with coordinates θ_1 and θ_2, and therefore the integration of the trigonometric terms in the right-hand side of Eqs. (2.26) and (2.27) vanish. In particular, the equation for the radius has a stable fixed point located at

$$r_{1,2} = \sqrt{1 - \frac{K}{2}}, \tag{2.28}$$

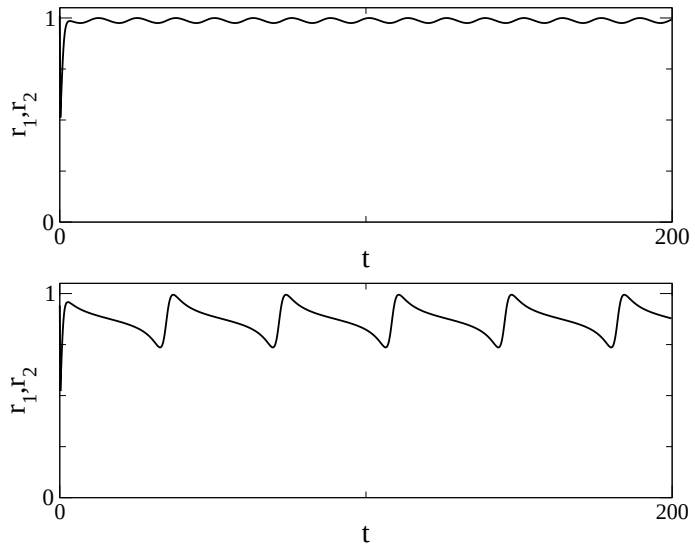

Figure 2.7: Time evolution of the radius of two coupled Landau-Stuart oscillators (2.25) for $K = 0.05$ (up) and for $K = 0.47$ (down). ($q_1 = q_2 = 0.666$, $\omega_1 = 0.25$, $\omega_2 = -0.25$).

and an unstable one at $r_{1,2} = 0$. Eq.(2.28) describes the effect of oscillation death: At $K = 2$ the unstable and the stable solutions meet and thus the origin $r_{1,2} = 0$ becomes stable.

In Fig. (2.6) the transition to synchronization for two Landau-Stuart oscillators is shown numerically integrating Eqs.(2.25) and computing the frequencies Ω_1, Ω_2, as the coupling strength K is continuously increased from zero. The right panel shows, in solid lines, the time-average of the radius r_1 and r_2. The approximation (2.28) is plotted with dotted lines and presents good agreement with the numerics as far as the oscillators are not synchronized. As soon as the oscillators become locked, their radius increases reflecting the lower degree of interaction between the oscillators.

In the left panel of Fig. (2.6) the frequencies of the oscillators are depicted (as solid lines) as the coupling strength K is continuously increased from zero. Note that there exists an important difference between Figs. (2.6)(left) and (2.5)(left). In the present case the oscillators increase their frequencies despite the fact that they are not synchronized: This reflects the presence of nonisochronicity in the Landau-Stuart systems. In addition, note that as soon as the synchronization is achieved the frequencies begin to decrease and tend to the mean $\bar{\omega} = (\omega_1 + \omega 2)/2$ as $K \to \infty$. This can be better understood by writing the corresponding phase equations for the Landau-Stuart oscillators.

Next, we derive the phase equations corresponding to the Landau-Stuart system (2.25). If we assume that for weak coupling the time evolution of the radial part is approximately constant (see Fig. 2.7), $\dot{\rho} \approx \dot{r}_1 \approx \dot{r}_2 \approx 0$, then the Eqs.(2.26) for

the radius become

$$r_{1,2}^2 = 1 - \frac{K}{2} + \frac{K}{2}\frac{r_{2,1}}{r_{1,2}}\cos(\theta_{2,1} - \theta_{1,2}), \tag{2.29}$$

and substituting this into Eqs. (2.27) we obtain

$$\dot{\theta}_{1,2} = \omega_{1,2} + \frac{K}{2}q_{1,2} + \frac{K}{2}\frac{r_{2,1}}{r_{1,2}}\left[2\sin(\theta_{2,1} - \theta_{1,2}) - q_{1,2}\cos(\theta_{2,1} - \theta_{1,2})\right], \tag{2.30}$$

In Fig (2.6) a comparison of the phase Eqs.(2.30) with the original system (2.25) is shown. Clearly, the phase approximation is valid as far as the systems interact weakly and the amplitude of the oscillators remains constant in time. The validity of the phase approximation can be better understood comparing the left panel of Fig (2.6) with Figs. (2.7), where the time evolution of the oscillators amplitudes for weak and for large (close to synchronization) coupling are shown.

Chapter 3

Synchronization in an ensemble of nonidentical oscillators

"Below a threshold, anarchy prevails; above it, there is a collective rhythm (...)"

A. Winfree (2002)

This Chapter gives an overview on some of the main results that are known about macroscopic synchronization, especially for the case of global coupling. The material here can be mostly found in the book of Kuramoto (1974), the book of Pikovsky et al. (2001) and in the papers Strogatz and Mirollo (1991) and Strogatz (2000). On one side, our aim is to put the results of this thesis in a general context. On the other, to present mathematical techniques that will be very much used in the following chapters.

A starting date for the study of synchronization of many oscillators with different natural frequencies can be probably set in the context of cybernetics, when Wiener (1958) suggested to approach the alpha rhythm in the brain as the entrainment of a large number of neurons with different period. About ten years later the problem of synchronization was reconsidered by Winfree (1967) as an ubiquitous and central issue of biological systems.

Instead of the Fourier formalism used by Wiener, Winfree investigated the problem looking at synchronization as a phase transition. As a simplified case, he studied the behavior of a population of limit cycle oscillators with different natural frequencies and all-to-all coupling. He numerically found that for low values of the coupling strength, the system was *incoherent*: On average no collective oscillations appear in the ensemble. Increasing the coupling term, a critical value is reached, at which a small cluster of oscillators, rotating at the same frequency, emerges. With further increase of coupling the cluster increases in size and the system enters

a region of partial locking. Using the centroid of the population of oscillators as an *order parameter* and the the coupling strength, or alternatively the width of the distribution of natural frequencies, as a control parameter, a phenomenon analogous to a second order phase transition appears.

Later this phenomenon was studied in more detail by Kuramoto (1974), who introduced the model that now is the standard framework for studying synchronization phenomena, and is usually referred to as the *Kuramoto model*.

3.1 The Kuramoto model

We start analyzing the synchronization process in a macroscopic ensemble of N oscillators using the simplest possible model. In the Chapter 2 the phase equations corresponding to two coupled oscillators were derived, under the assumption of weak coupling and nearly identical natural frequencies (see Eq.(2.11)). Using the same arguments, the phase equations for an ensemble of nearly identical, weakly coupled oscillators can be obtained. Thus we have

$$\dot{\theta}_i = \omega_i - \frac{K}{N}\sum_{j=1}^{N}\Gamma(\theta_i - \theta_j), \quad i = 1, \dots N \tag{3.1}$$

where θ_i denotes the phase of the oscillator i in the ensemble and the frequencies ω_i are distributed according to some probability density $g(\omega)$. The simplest possible form of the coupling function corresponds to the Kuramoto model

$$\dot{\theta}_i = \omega_i - \frac{K}{N}\sum_{j=1}^{N}\sin(\theta_i - \theta_j) \tag{3.2}$$

where the frequency distribution $g(\omega)$ is assumed to be unimodal of width γ and symmetric about its mean frequency $\bar{\omega}$, i.e. $g(\bar{\omega}+\omega) = g(\bar{\omega}-\omega)$, for all ω. Moreover, we set $\bar{\omega} = 0$. This last assumption can be made without loss of generality (unlike the hypothesis of symmetry) because the frequency distribution can be arbitrarily shifted by choosing a frame of reference rotating with frequency $-\bar{\omega}$. In that case, the phase variables are tranformed according to $\theta_i \to \theta_i + \bar{\omega}t$, and using this change of variables, Eq. (3.2) goes over to

$$\dot{\theta}_i = \omega_i - \bar{\omega} - \frac{K}{N}\sum_{j=1}^{N}\sin(\theta_i - \theta_j). \tag{3.3}$$

In order to study phase transitions, it is important to introduce an appropriate order parameter, that is a macroscopic quantity defined between 0 and 1 whose value (first order phase transitions) or the value of whose derivative (second order

phase transitions) is discontinuous at a critical point. A natural choice is the centroid of the oscillator positions on the circle, defined as (Kuramoto, 1974)

$$Z = Re^{i\psi} = \frac{1}{N}\sum_{j=1}^{N} e^{i\theta_j}, \tag{3.4}$$

where j is an index that characterizes each oscillator in the ensemble. Clearly the quantity Z is an important measure for characterizing the amount of phase clustering in large populations of oscillators. The order parameter R measures the phase coherence of the oscillators whereas ψ measures the average phase. When the phases of the oscillators get closer to each other R tends to one whereas its value fluctuates around zero when the oscillator phases are uncorrelated (with standard deviation scaling as $1/\sqrt{N}$ with the population size) and vanishes in the thermodynamic limit. Intermediate values of R correspond to configurations where the oscillator density is neither localized nor uniform on the unit circle, like in the case of clustering. Thus, R quantifies the degree of synchronization of the population and a phase transition can be detected looking at discontinuities in its value when one of the control parameters is changed. On the other hand, note that in contrast to the frequency disorder σ (see Chapter 4), the order parameter R does not provide direct information about the oscillator frequencies.

The order parameter as it has been defined in Eq.(3.4) has another important advantage beyond those discussed previously: thanks to the trigonometrical identity obtained multiplying both sides of the order parameter equation (3.4) by $e^{i\theta_i}$, the Eqs.(3.2) can be written in terms of the centroid as

$$\dot{\theta}_i = \omega_i - RK\sin(\theta_i - \psi). \tag{3.5}$$

In this form the mean-field character of the Kuramoto model becomes very clear: The dynamical equation for each oscillator appears to be uncoupled from all the others. In fact, each of them interacts only with the population as a whole, or equivalently with the mean field quantities R and ψ. The phase θ_i of each oscillator is pulled toward the mean phase ψ, rather than toward the phase of each individual oscillator. Moreover, the effective strength of the coupling is proportional to the coherence of the mean field R and therefore, in the incoherent state $R = 0$, all the oscillators are uncoupled and the distribution of natural frequencies remains unperturbed [1]. This proportionality sets up a positive feedback loop between coupling and coherence: as the population becomes more coherent, R grows and so the effective coupling increases, which tends to recruit even more oscillators into the synchronized cluster. If the coherence is further increased by new recruits, the process will continue. Otherwise, it becomes self-limiting.

[1] We will see in the next section that this is a specific property of the system Eq. (3.2). Therefore this is not always true, for instance for the case of globally coupled *nonisochronous* oscillators.

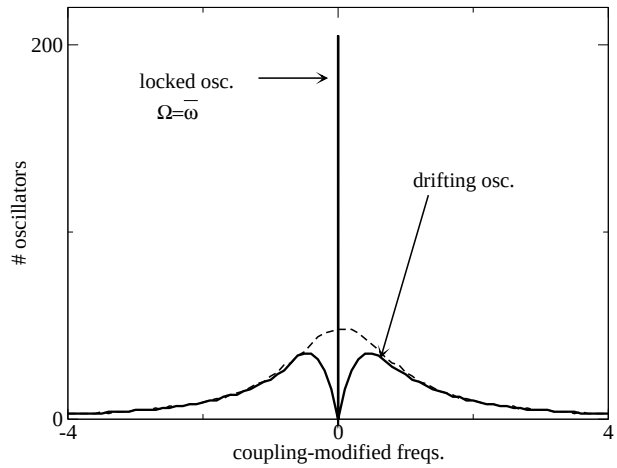

Figure 3.1: Histogram of the coupling-modified frequencies $\tilde{\omega}_i$ of an ensemble of 400 oscillators with a Lorentzian frequency distribution $g(\omega)$. The dotted line represents the distribution of frequencies in the incoherent state (which coincides with $g(\omega)$) whereas the solid line represents the synchronized state. The synchronized cluster appears at a frequency value $\Omega = 0$ ($\gamma = 0.985$, $K = 2$ for a Lorentzian frequency distribution).

From what we have seen until now, it is important to stress that we expect the process of synchronization in a large population of oscillators to occur in a very different fashion as it happens between two oscillators. As we have discussed in the previous Chapter (2), the synchronization of two non-identical oscillators is through a saddle-node bifurcation and thus the difference of the observed frequencies $\Delta\Omega$ goes to zero continuously as one control parameter is varied (see Figs.2.4, 2.5, 4.1 where the control parameter is the coupling strength K). In contrast to this, Eq.(3.5) shows that in a large ensemble of oscillators the individual frequencies do not vary when the parameter K is increased, or equivalently when the dispersal of the frequency distribution is decreased.

Let us now look for the steady solutions of Eq.(3.5). First we choose a reference frame rotating with the frequency of the order parameter Ω -that it is assumed to be constant. Changing variables, $\theta_i \rightarrow, \theta_i - \Omega t$ the model (3.5) becomes

$$\dot{\theta}_i = \omega_i - \Omega - RK \sin\theta_i. \tag{3.6}$$

Since R is assumed to be also constant, Eq.(3.6) implies that the solution shows distinct features depending on the parameter values. Specifically, the population splits into two clusters (see Fig. (3.1)):

- $|\omega_i - \Omega| \leq KR$: The oscillators having frequencies close to Ω approach a fixed point defined by

$$\omega_i - \Omega = RK \sin\theta_i, \quad |\theta_i| \leq \pi/2. \tag{3.7}$$

The oscillators of this group are locked to the frequency Ω of the mean field. From Eq.(3.7) one can understand the basic mechanism of synchronization: In order to compensate the difference between the natural frequency ω_i and the frequency of the mean field Ω, the oscillators phases are shifted (with respect to the centroid) by $\Omega - \omega_i$, so that the frequency mismatch can be exactly balanced according to Eq.(3.7). Hence, in a typical locked state, the oscillators describe an arch of circumference around the centroid. The arch is symmetric because of the symmetry of the sinusoidal coupling function and because of the distribution of natural frequencies. The oscillators are located along the arch in order of natural frequency, the one with $\omega_i = \Omega$ being in the middle and thus having the same phase as the centroid. From the symmetry properties of the frequency distribution it also follows that the locking frequency Ω coincides with the average natural frequency $\bar{\omega}$. Thus, from Eq.(3.7) the locked oscillators have phases distributed according to

$$\theta_i^* = \arcsin\left(\frac{\omega_i}{RK}\right). \tag{3.8}$$

Fig. 3.2(d) presents a snapshot of the phases at a certain time t beyond the transient period. The synchronized oscillators correspond to the central cluster described by Eq.(3.8). Observe that the oscillators with natural frequency $\omega_i = \bar{\omega}$ do not modify their frequencies whereas the rest of oscillators belonging to the synchronized cluster form a frequency plateau depicted in Fig. 3.2(c).

- $|\omega_i - \Omega| > KR$: The oscillators of this group are called *drifting oscillators* and consists in those which fail to be entrained to the macroscopic field. Note that Eq.(3.8) states that any finite population admits a fully locked solution for sufficiently large coupling strength, which increases with the width γ of the parameter distribution. Since the sine function is bounded, though, the oscillators with natural frequency very different from $\bar{\omega}$, i.e. those belonging to the tails of the frequency distribution $g(\omega)$, in practice can never be locked and even large values of the coupling constant will lead at most to a partially synchronized solution. This is always the case for an infinite population size when the distribution of natural frequencies is unbounded.

  The Eq.(3.6) for the drifting oscillators can be integrated and gives

$$\theta_i = \tilde{\omega}_i t + f((\tilde{\omega}_i - \Omega)t), \tag{3.9}$$

  where the coupling-modified frequencies $\tilde{\omega}$ are given by

$$\tilde{\omega}_i = \Omega + (\omega_i - \Omega)\sqrt{1 - \left(\frac{KR}{\omega_i - \Omega}\right)^2}, \tag{3.10}$$

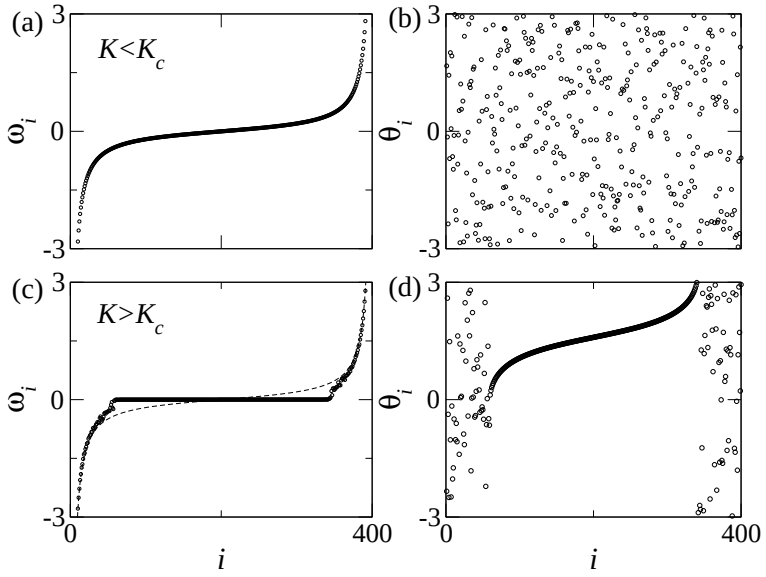

Figure 3.2: Ensemble of 400 phase oscillators governed by Eqs.(3.5). Plotted are the oscillator index i versus coupling-modified frequencies $\tilde{\omega}_i$ ((a) and (c)) and the instantaneous phase θ_i ((b) and (d)), below ($K < K_c$) (top) and above ($K > K_c$) (bottom) the synchronization threshold. In figure (c) the frequency distribution below criticality (dotted line, same as (a)) is also shown. The natural frequencies were distributed according to a Lorentzian distribution, with $\bar{\omega} = 0$.

and f is a certain 2π-periodic function that modulates the time evolution of the phase. From Eq.(3.10), an oscillator having natural frequency far away from the centroid's frequency Ω finds its natural frequency almost unperturbed, in contrast with those oscillators with frequencies close to that of the mean field Ω. This is shown in Fig. 3.2(c), where the coupling-modified frequencies $\tilde{\omega}_i$ for each oscillator i have been computed as in Eq.(2.13). Without considering the central plateau corresponding to the oscillators locked to the mean field, note that only the drifting oscillators close to such plateau have a frequency that differs substantially from their original natural frequencies.

Moreover, the drifting oscillators behave as if they were uncoupled but externally forced via the mean field, with strength KR. Note that Eq.(3.10) reflects the generic square root scaling law close to a saddle node bifurcation (see for instance Strogatz (1994); Guckenheimer and Holmes (1996)).

The next step is to find the contributions of the clusters of locked and drifting oscillators to the mean field. Indicating with $\langle\ \rangle_l$ the average over the locked oscillators and with $\langle\ \rangle_d$ the average over the drifting ones, we have

$$R = \langle e^{i\theta} \rangle_l + \langle e^{i\theta} \rangle_d, \tag{3.11}$$

where the index corresponding to the oscillator number has been dropped, since in the thermodynamic limit $N \to \infty$.

The contribution of the locked oscillators is simplified due to the symmetry of the distribution of the locked phases (3.8): Since the distribution of frequencies is symmetric, an oscillator with frequency ω gives exactly the opposite contribution as the corresponding oscillator with natural frequency $-\omega$. Thanks to this fact, the imaginary part of $\langle e^{i\theta} \rangle_l$ averages out and hence in the thermodynamic limit

$$\langle e^{i\theta} \rangle_l = \langle \cos\theta \rangle_l = KR \int_{|\omega - \Omega| \leq KR} \cos\theta \; g(\omega) \; d\theta.$$

From Eq.(3.7) it is possible to express the natural frequencies as a function of the angular position, and the contribution of the synchronized oscillators to the centroid is

$$\langle e^{i\theta} \rangle_l = KR \int_0^{2\pi} \cos^2\theta \; g(KR\sin\theta + \Omega) \; d\theta. \tag{3.12}$$

Now let us consider the drifting oscillators. In order to proceed Kuramoto made the following additional hypothesis that he did not prove: the oscillators move on a unit circle with a speed that may change in time, but their distribution is stationary. If we define a density function so that $\rho(\theta, \omega)d\theta$ describes the number of oscillators with natural frequency ω that lie between θ and $\theta + d\theta$, Kuramoto's hypothesis implies that ρ must be stationary. The expression for $\rho(\theta, \omega)$ is straightforwardly obtained thinking that the oscillators will spend more time in a given small interval when they have lower speed, and less where their velocity is higher. In other words, the function $\rho(\theta, \omega)$ must be inversely proportional to the velocity (3.5), which again is a function of θ

$$\rho(\theta, \omega) = \frac{C}{|\omega - RK\sin\theta|}. \tag{3.13}$$

The normalization constant C is determined through the normalization condition for the density ρ

$$1 = \int_0^{2\pi} \rho(\theta, \omega) d\theta = \int_0^{2\pi} \frac{C}{|\omega - RK\sin\theta|} d\theta$$

which yields

$$C = \frac{1}{2\pi} \sqrt{\omega^2 - (KR)^2}.$$

The contribution of the drifting oscillators can now be written as follows

$$\langle e^{i\theta} \rangle_d = \int_0^{2\pi} \int_{|\omega - \Omega| > KR} e^{i\theta} \rho(\theta, \omega) g(\omega) d\omega d\theta. \tag{3.14}$$

Again we can use symmetry arguments to see that this integral vanishes, since $g(\omega)$ is an even function and, from Eq.(3.13), $\rho(\theta + \pi, \omega) = \rho(\theta, -\omega)$.

The sums (3.12) and (3.14) yield the exact self-consistent equation

$$R = KR \int_0^{2\pi} \cos^2\theta \; g(KR\sin\theta + \Omega) \; d\theta,$$

that is always satisfied if $R = 0$, i.e., in the incoherent case. However, a nontrivial solution, corresponding to the locked regime, can be found by eliminating R

$$1 = K \int_0^{2\pi} \cos^2\theta \; g(KR\sin\theta + \Omega) \; d\theta. \tag{3.15}$$

Now the condition for the onset of synchronization can be obtained by solving the integral for $R \to 0^+$. This leads to the critical value of K

$$K_c = \frac{2}{\pi g(\bar{\omega})}, \tag{3.16}$$

which is the Kuramoto's critical coupling for the onset of collective synchronization.

The behavior of the order parameter in the vicinity of the onset of synchronization can be studied performing an expansion of Eq.(3.15) for K close to the critical value

$$1 - \frac{\pi}{2} K g(\bar{\omega}) - \frac{\pi}{16} K^3 g''(\bar{\omega}) R^2 + O(R^3) = 0. \tag{3.17}$$

It turns out that the character of the bifurcation, that is whether the centroid's oscillations amplitude increases for coupling larger (supercritical) or smaller (subcritical) than K_c, is determined by the value of $g''(\bar{\omega})$. In particular, we will consider the supercritical case $g''(\bar{\omega}) < 0$, when R can be estimated as

$$R \approx \sqrt{\frac{16}{-\pi K_c^3 g''(\bar{\omega})}} \sqrt{\frac{K - K_c}{K_c}}. \tag{3.18}$$

This relation also tells us that the order parameter scales as the square root of the distance from the critical point, which is a generic feature of infinite dimensional systems and corresponds, from a dynamics systems perspective, to the order parameter undergoing a supercritical Hopf bifurcation.

We want to stress that this self-consistent method has two important limitations:

- The analysis is concerned only with steady-state behavior and it therefore provides no information about stability. This important question will be discussed in the Section 3.2.
- It depends crucially on the sinusoidal form of the coupling in the model (3.2). Because of a convenient trigonometric identity, the order parameter (3.4) appears in the governing equation (3.5). This is the coincidence which allows the order parameter to be determined self-consistently.

3.1.1 Asymmetric coupling function

This section is devoted to compare the results obtained for the Kuramoto model with the results obtained by Sakaguchi and Kuramoto (1986) using a more general coupling function Γ in Eq.(3.1)

$$\dot{\theta}_i = \omega_i - \frac{K}{N}\sum_{i=1}^{N}\sin(\theta_i - \theta_j + \alpha), \tag{3.19}$$

where $|\alpha| < \pi/2$. Using the order parameter (3.4), the model (3.19) becomes

$$\dot{\theta}_i = \omega_i - KR\sin(\theta_i - \theta_j + \alpha). \tag{3.20}$$

The model (3.20) is essentially the Kuramoto model with a phase shift α in the coupling function. This term in especially important when nonisochronicity is considered, as it will be shown in Section 3.3. On the other hand Eqs. (3.20) have also been proved to be useful in modeling information concerning the synaptic connections in a neural network (Hoppensteadt and Izhikevich, 1998) and time delays (Izhikevich, 1998) and they also appear naturally in the phase reduction of an array of superconducting Josephson junctions (Wiensenfeld and Swift, 1995; Wiesenfeld et al., 1996).

The fundamental difference between Eq.(3.19) and the Kuramoto model (3.2) is that the in the present case the cluster of synchronized oscillators (i.e. the velocity of the order parameter Ω) is not determined trivially as in the previous case as the mean bare frequency $\bar{\omega}$, and therefore Ω must be determined self-consistently as well as the order parameter R. Sakaguchi and Kuramoto (1986) showed that the quantities R and Ω can be determined from the following self-consistency relation

$$Re^{i\alpha} = KR\left(iJ + \int_{\pi/2}^{\pi/2} g(\Omega + KR\sin\xi)e^{i\xi}\cos\xi\ d\xi\right), \tag{3.21}$$

where

$$J = \int_0^{\pi/2} \frac{\cos\xi(1-\cos\xi)}{\sin^3\xi}[g(\Omega+\mu) - g(\Omega-\mu)]\ d\xi \tag{3.22}$$

with $\mu = KR/\sin\xi$. Specifically, the critical point $K = K_c$ is located at the point where the $R > 0$ solution branches off the $R = 0$ solution.

Thus the synchronized cluster is Ω-shifted with respect the mean frequency. This fact in general is able to break the symmetry imposed through the choice of a reflection-symmetric frequency distribution. In other words, the locked oscillators are in general not equally distributed around $(\bar{\omega} - \Omega)$, as it is shown in Fig 3.3.

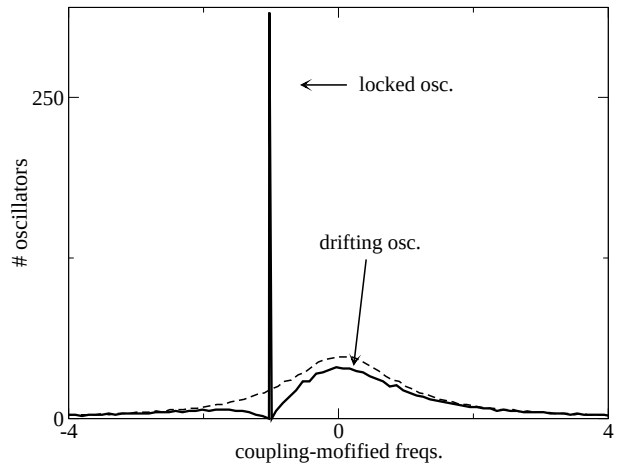

Figure 3.3: Histogram of the coupling-modified frequencies $\tilde{\omega}_i$ of the model (3.19) (compare with Fig.3.1). The synchronized cluster appears at a frequency value Ω that differs from the mean of $g(\omega)$ (compare with Fig.3.1). ($\gamma = 0.985$, $K = 2.8$, $\alpha = \pi/4 rad.$ for a Lorentzian frequency distribution.)

3.2 Stability of incoherence in the Kuramoto model

As we have seen in the previous section, the stability properties of the steady solutions of the Kuramoto model can not be understood from the classical Kuramoto's analysis. Since the incoherent state and the partially synchronized state emerge when the initial value problem is solved numerically, each must be stable in the appropriate range of K at least in an operational sense. However, the theoretical explanation of this stability has proved to be rather subtle even for the incoherent state (Strogatz and Mirollo, 1991; Strogatz et al., 1992; Strogatz, 2000). This section is devoted to explain the appropriate theoretical tools for the study of the stability of the possible dynamical states of the Kuramoto model. The theoretical treatment will be very much used in the rest of this PhD thesis.

3.2.1 Continuum limit of the Kuramoto model

The infinite system should be visualized as follows: for each frequency ω, there is a continuum of oscillators distributed along the circle. Suppose then that this distribution is characterized by a density function ρ defined so that $Ng(\omega)\rho(\theta, \omega, t)d\theta d\omega$ describes the number of oscillators with natural frequencies in $[\omega, \omega + d\omega]$ and phases in $[\theta, \theta + d\theta]$. Thus $\rho(\theta, \omega, t)d\theta$ denotes the fraction of oscillators with natural frequency ω and phase in $[\theta, \theta + d\theta]$ and satisfies the normalization

$$\int_{-\pi}^{\pi} \rho(\theta, \omega, t)d\theta = 1,$$

for all ω and t. Furthermore, the density ρ is required to be 2π-periodic in θ and nonnegative. The evolution of ρ is governed by the continuity equation

$$\frac{\partial \rho}{\partial t} = -\frac{\partial(\rho v)}{\partial \theta}, \tag{3.23}$$

which expresses conservation of oscillators of frequency ω. Here the velocity $v(\theta, t, \omega)$ is interpreted in an Eulerian sense as the instantaneous velocity of an oscillator at position θ, given that it has natural frequency ω. From (3.5) that velocity is

$$v_i(\theta, t, \omega) = \omega_i - RK\sin(\theta_i - \psi). \tag{3.24}$$

The *incoherent state* is described by the uniform distribution

$$\rho_0 = \frac{1}{2\pi},$$

and defines an equilibrium for Eq.(3.23) since $R = 0$ at ρ_0.

The stationary states of the continuity equation (3.23) are the steady solutions that we have seen in the previous section. The stationarity of Eq.(3.23) implies that

$$\rho v = C(\omega), \tag{3.25}$$

and if $C(\omega) \neq 0$, we recover the stationary density (3.13) that has been derived intuitively for the drifting oscillators. On the other hand if $C(\omega) = 0$ the density function ρ must be a delta function in θ.

The order parameter (3.4) can be alternatively expressed in terms of the density as

$$Re^{i\psi} = \int_0^{2\pi} d\theta \int_{-\infty}^{\infty} e^{i\theta}\rho(\theta, \omega, t)g(\omega)d\omega. \tag{3.26}$$

The density function $\rho(\theta, t, \omega)$ is 2π-periodic in θ and therefore it admits the Fourier expansion

$$\rho(\theta, \omega, t) = \sum_{l=-\infty}^{l=\infty} \rho_l(\omega, t)e^{il\theta}, \tag{3.27}$$

with coefficients $\rho_{-l} = \rho_{-l}^*$ since the density function is real. An important observation to be done is that the purely sinusoidal coupling allows to express the order parameter exclusively in terms of the first Fourier mode. Indeed, substituting (3.27) into the order parameter (3.4) yields

$$Re^{i\psi} = 2\pi \int_{-\infty}^{\infty} \rho_1^*(\omega, t)g(\omega)d\omega, \tag{3.28}$$

and so

$$\begin{aligned} -R\sin(\theta_i - \psi) =& 2\pi \mathrm{Im}\left[\left(\int_{-\infty}^{\infty} \rho_1^*(\omega, t)g(\omega)d\omega\right)e^{-i\theta}\right] \\ =& i\pi\left(\int_{-\infty}^{\infty} \rho_1(\omega, t)g(\omega)d\omega\right)e^{i\theta} + \text{c.c.}, \end{aligned} \tag{3.29}$$

where c.c. denotes the complex conjugate of the preceding term.

The continuity equation (3.23) and the order parameter can be combined to yield the equation for the evolution of the density ρ

$$\frac{\partial \rho(\theta,\omega,t)}{\partial t} = -\frac{\partial}{\partial \theta}\left[\rho(\theta,\omega,t)\left(\omega + Ki\pi\left(\int_{-\infty}^{\infty}\rho_1(\omega',t)g(\omega')d\omega'\right)e^{i\theta} + \text{c.c.}\right)\right].$$

This equation provides a continuum description of the oscillator population for which issues of stability and bifurcations can be analyzed in detail. It is equivalent to the following infinite system of integro-differential equations for the Fourier modes

$$\begin{aligned}\frac{\partial \rho_l(\omega,t)}{\partial t} = -i\omega l\rho_l(\omega,t) + lK\pi\rho_{l-1}(\omega,t)\int_{-\infty}^{\infty}\rho_1(\omega',t)g(\omega')d\omega' \\ - lK\pi\rho_{l+1}(\omega,t)\int_{-\infty}^{\infty}\rho_1^*(\omega',t)g(\omega')d\omega'.\end{aligned} \tag{3.30}$$

Note that equations corresponding to the negative modes are just the complex conjugate to the equations for the positive modes.

3.2.2 Linear stability analysis of the incoherent state

First note that the homogeneous distribution of the phases where all the Fourier modes -except ρ_0- vanish, is a solution of the system (3.30). Next, we study the evolution of a small perturbation of the incoherent state ρ_0. This corresponds to

$$\begin{aligned}\rho_l &= O(\epsilon) \quad \forall l \neq 0; \\ \rho_0 &= 1/2\pi,\end{aligned}$$

where $\epsilon \ll 1$. Thus from Eqs. (3.30) it can be easily checked that all the modes have the form

$$\frac{\partial \rho_l(\omega,t)}{\partial t} = -il\omega\rho_l(\omega,t) + O(\epsilon^2)$$

except the modes $l = 1$ and $l = -1$. The equation corresponding to the mode $l = 1$ up to first order in ϵ is

$$\frac{\partial \rho_1(\omega,t)}{\partial t} = -i\omega\rho_1(\omega,t) + \frac{K}{2}\int_{-\infty}^{\infty}\rho_1(\omega',t)g(\omega')d\omega' \tag{3.31}$$

and the equation for the $l = -1$ is just the complex conjugate of Eq.(3.31). Therefore only these modes contribute to the linear stability of the incoherent state ρ_0. Then the coherence $R(t)$ is determined at this order by ρ_1 via Eq.(3.31). In particular, if ρ_1 grows exponentially, so does $R(t)$.

Equation (3.31) reflects the mean-field character of the Kuramoto model: for any given ω, the evolution of $\rho_1(\omega,t)$ depends on all the other frequencies through

the integrals in the right-hand side of Eq.(3.31). However, this dependence is the same for all frequencies because the integral is independent of ω.

The right-hand side of Eq.(3.31) defines the following linear operator $\mathcal{L}$

$$\mathcal{L}\rho_1(\omega,t) = -i\omega\rho_1(\omega,t) + \frac{K}{2}\int_{\infty}^{\infty}\rho_1(\omega',t)g(\omega')d\omega' \tag{3.32}$$

that has both, a continuous and a discrete spectrum. We concentrate the discussion on the discrete part since it is the only one that is relevant for our purposes.

The linear problem (3.31) has the solution

$$\rho_1(\omega,t) = b(\omega)e^{\lambda t},$$

that implies

$$\lambda b(\omega) = -i\omega b(\omega) + \frac{K}{2}\int_{-\infty}^{\infty} b(\omega')g(\omega')d\omega'. \tag{3.33}$$

Here, the integral in the right-hand side is just a real constant to be determined self-consistently. Therefore the function $b(\omega)$ must satisfy

$$b(\omega) = \frac{1}{\lambda + i\omega}\frac{K}{2}\int_{-\infty}^{\infty} b(\omega')g(\omega')d\omega',$$

that can be substituted back to Eq.(3.33) in order to obtain the following condition

$$1 = \frac{K}{2}\int_{-\infty}^{\infty}\frac{1}{\lambda + i\omega}g(\omega)d\omega, \tag{3.34}$$

to be satisfied by the eigenvalues λ. Note that until now we have not made assumptions of any kind about the shape of the frequency distribution $g(\omega)$ nor about the type of solutions that we expect. Eq.(3.34) gives the discrete spectrum of the system (3.31) that determines the linear stability properties of the incoherent state ρ_0, in contrast to the Kuramoto analysis. In particular Eq.(3.34) also permits to calculate the critical coupling K_c for which synchronization takes place for a given frequency distribution.

Eq.(3.34) can be alternatively written as

$$1 = \frac{K}{2}\left(\int_{-\infty}^{\infty}\frac{\lambda^*}{|\lambda|^2 + \omega^2 - 2\omega\mathrm{Im}(\lambda)}g(\omega)d\omega - \int_{-\infty}^{\infty}\frac{i\omega}{|\lambda|^2 + \omega^2 - 2\omega\mathrm{Im}(\lambda)}g(\omega)d\omega\right), \tag{3.35}$$

This equation can be simplified making two assumptions about $g(\omega)$:

- The function $g(\omega)$ is an even function, i.e. $g(\omega) = g(-\omega)$. As we have already discussed in previous section, in virtue of the reflection symmetry of the Kuramoto model it is always possible to go into a rotating frame moving with frequency $\bar{\omega}$ the mean of $g(\omega)$. Therefore this condition holds for symmetric unimodal and bimodal frequency distributions.

- $g(\omega)$ is assumed to be nonincreasing on $[0, \infty)$, in the sense that $g(\omega) \leq g(\omega')$ for all $\omega \geq \omega'$. Of course this property only holds for unimodal frequency distributions.

If these two assumptions are fulfilled one can prove that Eq. (3.31) has at most one solution for λ, and if such solution exists, it is necessarily real (Mirollo and Strogatz, 1990). Then the second integral of the r.h.s vanishes exactly since its integrand is an odd function of ω. Thus Eq.(3.34) reduces to

$$1 = \frac{K}{2} \int_{-\infty}^{\infty} \frac{\lambda}{\lambda^2 + \omega^2} g(\omega) d\omega. \tag{3.36}$$

This result is very interesting: It shows that the eigenvalue λ must be a positive number, since otherwise the right-hand side of Eq. (3.36) is negative or zero. Hence, the fundamental mode $l = 1$ is never linearly stable (Strogatz and Mirollo, 1991).

Now it is possible to calculate the critical coupling K_c of synchronization by letting $\lambda \to 0^+$ on Eq.(3.36). Noting that

$$\lim_{\lambda \to 0^+} \frac{\lambda}{\lambda^2 + \omega^2} = \pi \delta(\omega),$$

Eq. (3.36) implies that

$$K_c = \frac{2}{\pi g(\omega)},$$

which is the critical coupling (3.16) found by Kuramoto. However, note that this is a demonstration that the *the incoherent state becomes unstable at* K_c.

3.3 Ensemble of Landau-Stuart oscillators

In the following we study the synchronization in an ensemble of globally coupled Landau-Stuart oscillators. The system is the following

$$\dot{z}_i = z_i[1 + i(\omega_i + q) - (1 + iq) z_i z_i^*] - \frac{K}{N} \sum_{j=1}^{N} (z_i - z_j) \tag{3.37}$$

where the natural frequencies ω_i are assumed to be randomly selected from a frequency distribution $g(\omega)$. As usual it can be assumed that the sample mean of ω is zero: if the mean of ω is $\bar{\omega}$, $\bar{\omega} \neq 0$, we can go into a rotating frame defining $z_i' = z_i e^{-i\bar{\omega}t}$ and then the equations for z_i' are identical to Eqs.(3.37) with zero mean frequency. We assume that $g(\omega)$ is symmetric and non-increasing on $[0, \infty)$.

If we use the order parameter (3.4), then Eq.(3.37) becomes

$$\dot{z}_i = z_i[1 + i(\omega_i + q) - (1 + iq) z_i z_i^*] - K(z_i - Z) \tag{3.38}$$

A simple stability analysis can be carried out under the assumption that for a large difference in the natural frequencies the phases of the individual oscillators are randomly distributed, while the amplitudes rearrange themselves around a given mean value, so that the value of the averaged position is close to zero $Z \approx 0$. It is then useful to rewrite Eq.(3.38) in the following way:

$$\begin{aligned} \dot{z}_i &= z_i[1 + i(\omega_i + q) - (1 + iq)z_i z_i^*] - K(z_i - Z) \\ &\approx z_i[1 - K + i(\omega_i + q) - (1 + iq)z_i z_i^*]. \end{aligned} \tag{3.39}$$

The eigenvalues of the origin in Eq.(3.39) are $1-K \pm i(\omega_i+q)$ and therefore, as soon as $K > 1$, the origin becomes attracting. This phenomenon is known as *oscillation death* (Mirollo and Strogatz, 1990).

Next we reduce Eqs. (3.38) to their corresponding phase equations (in the limit of weak coupling K and narrowly distributed frequencies), as we made in Chapter 2 in the case of two coupled Landau-Stuart oscillators. We start by rewriting the Eqs. (3.38) in polar coordinates

$$\begin{aligned} \dot{r_i} &= r_i(1 - r_i^2) + K[R\cos(\theta_i - \psi) - r_i] \\ \dot{\theta}_i &= \omega_i + q(1 - r_i^2) - \frac{KR}{r_i}\sin(\theta_i - \psi). \end{aligned} \tag{3.40}$$

In the incoherent state, the differential equations for the radial part of Eqs. (3.40) reduce to

$$1 - r_i^2 = K[1 - \frac{R}{r_i}\cos(\theta_i - \psi)],$$

since $\dot{r}_i \approx 0$ for all i. This can be substituted into the angular component of Eq.(3.40), and hence the angular part of Eqs. (3.40) reduce to

$$\dot{\theta}_i = \omega_i + qK - KR[\sin(\theta_i - \psi) + q\cos(\theta_i - \psi)]. \tag{3.41}$$

This result confirms that any population of weakly and diffusively coupled limit cycles close to a Hopf bifurcation can be generically expressed in the form of Eqs. (3.41). Note that in the case of isochronous oscillators, $q = 0$, Eqs. (3.41) reduce to the Kuramoto model (3.2). We have written phase equations were the effect of the frequency response to the small perturbation is taken into account through the terms proportional to the nonisochronicity q.

The transformation $\alpha \equiv \tan^{-1} q$ leaves the system

$$\dot{\theta}_i = \omega_i + K\tan\alpha - \frac{K}{\cos\alpha}\sin(\theta_i - \theta_j + \alpha), \tag{3.42}$$

which is very similar to the model presented in Section 3.1.1. However, in the present case the coupling has a direct effect on the distribution of natural frequencies in the incoherent state due to the presence of nonisochronicity. This first effect

of α (realized by the factor $K \tan \alpha$ in Eq.(3.42)) is the most relevant effect of the nonisochronicity far from the synchronization transition, i.e. for small coupling. The study of such effects in more general systems will be the subject of Chapter 4. On the other hand, close to the synchronization transition the angular terms in Eqs. (3.42) are fundamental: In this regime Eqs. (3.42) behave essentially as the Eqs. (3.19) studied Section 3.1.1. Therefore the nonisochronicity also breaks the symmetry imposed through the distribution of frequencies. In the Chapter 5 we investigate the influence of such effects in the transition to synchronization of two coupled populations of a Landau-Stuart type (3.42).

Chapter 4

Anomalous synchronization

In this Chapter the concept of anomalous synchronization is described. Whereas in the previous Chapter the analysis of synchronization has been restricted to Landau-Stuart and phase oscillators, here synchronization is studied in a broader class of systems. However, the phase approximation described, described in Chapter 2, is still of validity since we consider weakly coupled and nearly identical oscillators.

The phenomenon described here arises when the nonisochronicity of each oscillator in the ensemble is related with its natural frequency. As it was shown in Chapter 3, the heterogeneity in the ensemble is usually taken into account considering that the oscillators have natural frequencies according to a certain distribution. However, here we show that there are new collective phenomena emerging if there is disorder in other characteristics of the individual oscillators. Besides the natural frequency, the next relevant parameter in synchronization theory is the nonisochroncity.

The outline of this Chapter is as follows: first, in Section 4.1, we define the type of systems under investigation as an interacting ensemble of limit cycle systems or chaotic oscillators. Further we review some basic properties of phase synchronization in chaotic systems. Next, we use these methods to numerically explore the transition to phase synchronization in spatially extended ecological systems with oscillating dynamics. This will lead us to the phenomenon of anomalous synchronization. In the following Section 4.2 we present analytic arguments which demonstrate the origin of these effects and provide an exact criteria that permits to know when anomalous effects are to be expected. In order to show that anomalous synchronization appears universally, in Section 4.3 an ensemble of weakly nonlinear Van-der-Pol oscillators is analyzed and the theoretical results show effectively that the previously developed techniques are useful. The last Section is devoted to the study of anomalous synchronization in the Landau-Stuart model. This equations are specially convenient because the natural frequency and the nonisochronicity

appear as independent parameters. This fact allows to apply the analytical techniques developed in Chapter 3 in order to calculate the synchronization threshold. The results obtained in this Chapter are summarized in (Blasius et al., 2003; Montbrió and Blasius, 2003), and the last section will be published in (Montbrió et al., 2004a).

4.1 Numerical results for general systems

In this Section the systems under investigation consist in N-coupled nonidentical oscillators of the following form

$$\dot{\mathbf{x}}_\mathbf{i} = \mathbf{F}(\mathbf{x}_\mathbf{i}; \chi_i) + \frac{K}{N} C \sum_{j=1}^{N} (\mathbf{x}_\mathbf{j} - \mathbf{x}_\mathbf{i}), \quad i = 1 \dots N. \tag{4.1}$$

To be more specific, Eqs. (4.1) have the following properties:

- In the absence of coupling each oscillator follows its own local dynamics $\dot{\mathbf{x}} = F(\mathbf{x}, \chi)$ where $\mathbf{x}$ belongs to R^n. All oscillators have the same functional form but depend on a set of l control parameters $\chi = (a, b..)$. It is always assumed that each oscillator is parameterized either on a limit cycle or on a regime with phase coherent chaos. Thus every, possibly chaotic, oscillator is characterized by a well defined natural frequency which is given by the long term average of phase velocity, $\omega = \overline{\dot{\theta}}(t)$ (Pikovsky et al., 2001).

- Disorder or quenched noise is imposed onto the system by assigning to each oscillator i an independent value for every control parameter out of the set χ_i, usually taken from a statistical distribution. Here, a uniform distribution is always used. However our results remain valid if different distributions such as a Gaussian are used. In general, the control parameters affect the natural or unperturbed frequency of each oscillator, $\omega_i = \omega(\chi_i)$. Therefore, the natural disorder in control parameters leads to a frequency mismatch between the oscillators which it is also referred to as frequency disorder.

- Each oscillator is coupled with strength K to a predefined set of m neighbors $\{j\}$. In this Chapter, only two cases are considered: either coupling to next neighbors in a one or two dimensional lattice or global coupling. However we have obtained similar results with different coupling topologies. $C = \mathrm{diag}(c_1, c_2..., c_n)$ is a diagonal matrix which indicates the strength of the interaction in each component of the state vector $\mathbf{x}$. We also assume that even with the onset of coupling each oscillator is still rotating uniformly. This means especially that we don't allow for situations with oscillation death (Aronson et al., 1990; Mirollo and Strogatz, 1990). In practice, this can

always be realized if the coupling is restricted to be small enough and the variance of the inhomogeneities in the ensemble parameters is not large.

Synchronization arises as an interplay between the interaction and the frequency mismatch of the oscillators. Thereby, in general, the frequency of each oscillator will be detuned

$$\Omega_i = \Omega_i(K). \tag{4.2}$$

The process of synchronization between two mutually coupled phase oscillators has been described in Chapter 2. Interestingly, these ideas can directly be extended to systems with self sustained chaotic dynamics (Rosenblum et al., 1996). For these aims it is necessary to extend the concepts of phase and frequency to the case of a chaotic attractor. This is well established in phase coherent chaotic systems. Let us take for example the Rössler system (Rössler, 1976)

$$\begin{aligned} \dot{x} &= -by - z, \\ \dot{y} &= bx + ay, \\ \dot{z} &= 0.4 + (x - 8.5)z. \end{aligned} \tag{4.3}$$

In the parameter range $a \approx 0.15$ and $b \approx 1$ the motion shows phase coherent dynamics (see also Fig.4.3). In this regime a phase can be defined as an angle in (x, y)-phase plane or via the Hilbert-transform (Rosenblum et al., 1996). In this work, the phase of chaotic systems is always estimated by counting successive maxima, e.g. the times t_n of the n'th local maxima of the y-variable are located. We define that the phase increases by 2π between two successive maxima and interpolate linearly in between (Pikovsky et al., 2001)

$$\phi(t) = 2\pi \frac{t - t_n}{t_{n+1} - t_n} + 2\pi n, \qquad t_n < t < t_{n+1}. \tag{4.4}$$

Next we explore the transition to synchronization in two mutually coupled Rössler systems (see Fig. 4.1). The oscillators are nonidentical and vary in the value of parameter b. Both oscillators are diffusively coupled in the y variable with strength K (i.e. by adding the term $K(y_{2,1} - y_{1,2})$ in the equation of $\dot{y}_{1,2}$). As can be seen in Fig.4.1, despite the chaotic amplitudes the transition to the synchronized state is very similar to the case of two coupled phase oscillators. Due to the interaction both oscillators are detuned and the frequencies approach each other. As a result the frequency difference, $\Delta\Omega(K)$ decreases monotonically until it becomes zero in the synchronized state. In the following we study how these ideas generalize to an ensemble of many interacting Rössler systems (Osipov et al., 1997)

$$\begin{aligned} \dot{x_i} &= -b_i y_i - z_i \\ \dot{y_i} &= b_i x_i + a y_i + \tfrac{K}{m} \textstyle\sum_j (y_j - y_i) \\ \dot{z_i} &= 0.4 + (x_i - 8.5) z_i. \end{aligned} \tag{4.5}$$

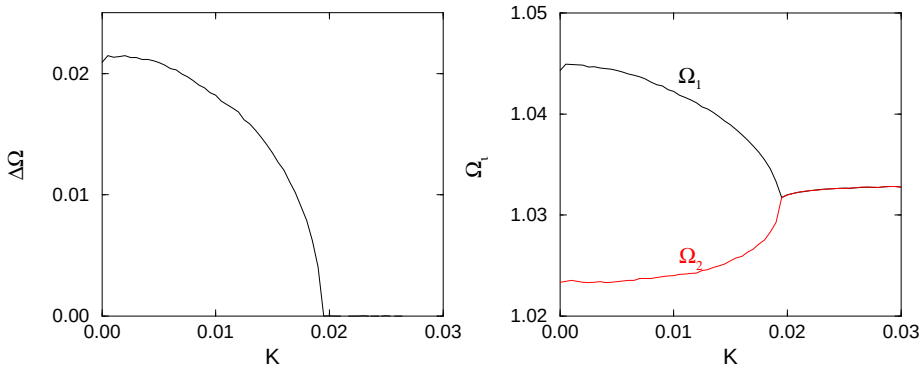

Figure 4.1: Transition to synchronization in two coupled Rössler systems (4.3). Plotted is the frequency difference $\Delta\Omega(K)$ (left) and the individual frequencies of each oscillator, $\Omega_{12}(K)$ (right) as a function of coupling strength. Parameter values $a = 0.15$, $b_{1,2} = 1.0 \pm 0.01$.

Here, all Rössler oscillators are nonidentical. The disorder is realized by taking the parameters b_i for each oscillator from a uniform distribution and thereby assigning it its own frequency $\omega_i \approx b_i$. In Fig. 4.2 we plot the numerical results in a ring of 10 locally coupled Rössler oscillators. With the onset of coupling the frequencies of all oscillators move towards each other forming synchronized clusters. At a certain coupling strength only one cluster is left and the ensemble reaches the synchronized state.

In this Chapter we introduce another measure for detecting synchronization. In Chapter 3 the complex order parameter (3.4) was defined in order to measure the phase coherence in the ensemble. However, in this Chapter we are also interested in the behavior of the frequencies, and hence another measure for synchronization is required. The frequency synchronization in the ensemble can be revealed by measuring the standard deviation of the frequencies (4.2), $\sigma(K)$. As is shown in Fig.4.2, $\sigma(K)$ is a decreasing function of coupling strength. Global phase synchronization is achieved when $\sigma(K > K_c) = 0$ and all oscillators rotate with the same frequency. By comparing Fig. 4.2 with Fig. 4.1 it follows that in interacting oscillator systems the standard deviation $\sigma(K)$ takes over the role of $\Delta\Omega(K)$ in the case of two coupled oscillators.

To summarize, in order to measure the transition to synchronization in a system of interacting oscillators (4.1) we identify the frequency of each oscillator in dependence of the coupling strength, $\omega_i(K)$. For phase coherent chaotic dynamics this is done by counting the number of local maxima of a chosen variable. We define the frequency disorder as the standard deviation of all oscillator frequencies $\sigma(K)$. Then synchronization is given by the single criterion that $\sigma(K) = 0$.

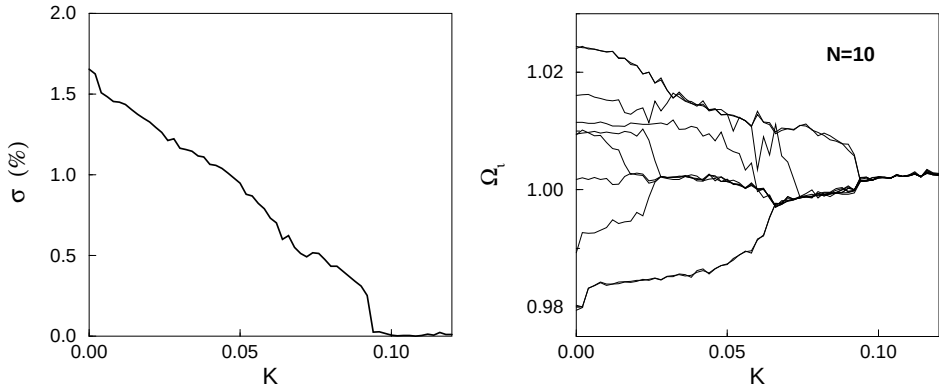

Figure 4.2: Transition to synchronization in a ring of ten diffusively coupled Rössler systems (4.5) with periodic boundary conditions. Plotted is the standard deviation $\sigma(K)$ of all oscillator frequencies in percent (left) and the individual oscillator frequencies Ω_i (right) as a function of coupling strength K. Parameters are taken randomly in the range $b_i = 0.97 \pm 0.025$ and $a = 0.15$.

Occasionally, we also use the the complex order parameter $R(K)$ to characterize the synchrony in the ensemble which then is always compared to our usual measure.

4.1.1 Anomalous synchronization in ecological models

The question arises whether the simple transition to synchronization as exemplified in Figs. 4.1 and 4.2 is universal, e.g. whether the frequency disorder $\sigma(K)$ is always a monotonically decreasing function of coupling strength. To explore this case we turn to spatially extended ecological systems which are examples for spatio-temporal synchronization in natural systems (Heino et al., 1997). Maybe the most intriguing example is Ecology's well known Canadian hare-lynx cycle with hare and lynx populations synchronizing in phase to a collective 10-year cycle over vast regions in Canada (Blasius et al., 1999; Elton and Nicholson, 1942; Schwartz et al., 2002).

In order to describe such phenomenon the following model was proposed (Blasius et al., 1999; Blasius and Stone, 2000)

$$\begin{array}{lllll} \dot{x_i} = & a\,(x_i - x_0) & -\alpha_1 x_i y_i & & \\ \dot{y_i} = & -b_i(y_i - y_0) & +\alpha_1 x_i y_i & -\alpha_2 y_i z_i + \frac{K}{m}\sum_j (y_j - y_i) & \\ \dot{z_i} = & -c\,(z_i - z_0) & & +\alpha_2 y_i z_i. & \end{array} \tag{4.6}$$

This model describes a three level "vertical" food chain where the vegetation x is consumed by herbivores y which themselves are preyed upon by the top predator z. In the absence of interspecific interactions the dynamics is linearly expanded

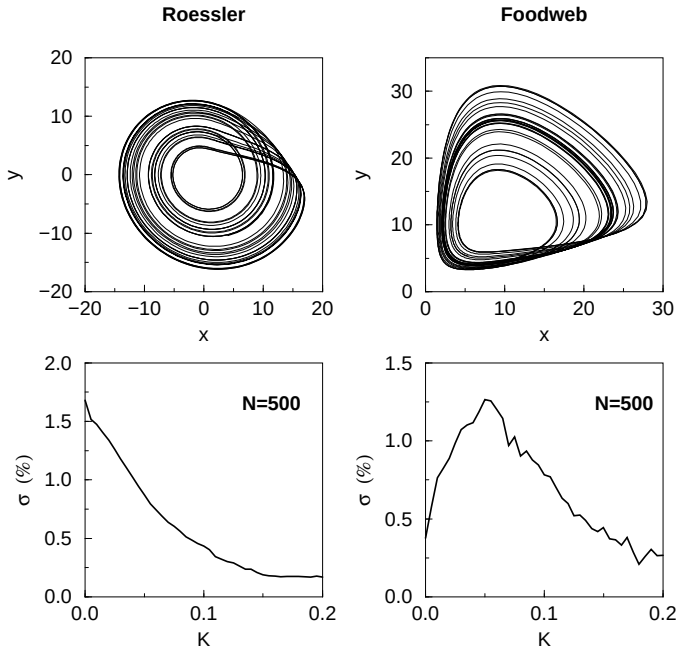

Figure 4.3: Comparison of the transition to synchronization in a chain of 500 locally coupled Rössler systems (4.5) (left) and foodweb models (4.6) (right). Oscillators have been coupled in the y-variable with strength K to next neighbors in a ring with periodic boundary conditions. Initial values were set randomly. Top: attractor projection of the uncoupled system in the (x, y)-plane. Bottom: standard deviation of frequencies, $\sigma(K)$, as a function of coupling strength. Parameter values: Rössler system $a = 0.15$; Foodweb model $x_0 = 1.5, y_0 = 0, z_0 = 0.1, \alpha_1 = 0.1, \alpha_2 = 0.6, a = 1, c = 10$. Parameters b_i are taken in both systems as uniformly distributed random numbers in the range $b_i = 0.97 \pm 0.025$.

around the steady state (x_0, y_0, z_0) with coefficients a, b and c that represent the respective net growth and death rates of each species. Predator-prey interactions are introduced via Lotka-Volterra terms with strength α_1 and α_2.

Despite their minimal structure, the equations are able to capture complex dynamics which matches real data for example in the Canadian hare-lynx cycle (Blasius and Stone, 2000; Blasius et al., 1999; Vandermeer et al., 2001; Schwartz et al., 2002). In this parameter range the model shows phase coherent chaotic dynamics, where the trajectory rotates with nearly constant frequency in the (x, y)-plane but with chaotic dynamics that appear as irregular spikes in the top predator z [Fig.4.3]. This behavior of the foodweb model is reminiscent to the Rössler system and therefore one might expect similar synchronization properties in both systems. To explore this in more detail, in Fig.4.3 we compare the transition to synchronization in coupled chains of Rössler and foodweb systems. Quenched disorder is

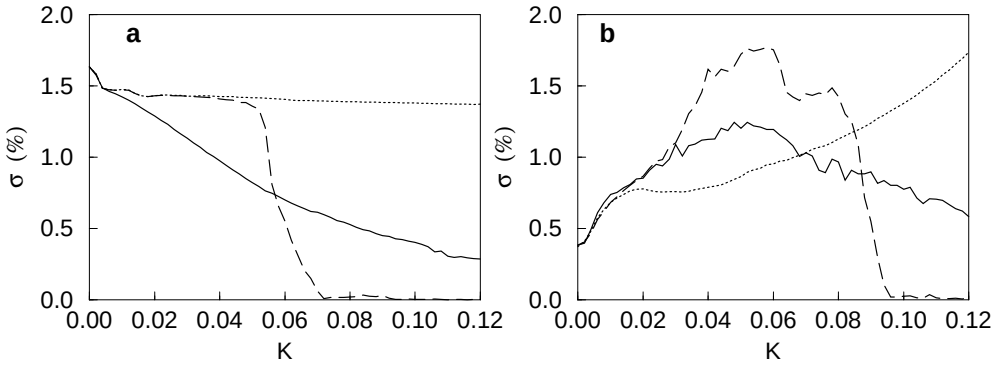

Figure 4.4: Onset of synchronization in a chain of 500 nonidentical Rössler systems (4.5) (left) and foodweb models (4.6) (right) for different coupling topologies. Plotted is the standard deviation of frequencies, $\sigma(K)$. Oscillators are coupled in the y-variable with strength K either in a ring with next neighbor coupling (solid lines), with global coupling (dashed lines) or using the approximation of independent oscillators (4.12) (dotted lines). Parameters and methods otherwise as in Fig.4.3.

introduced by taking b_i for each oscillator from the same statistical distribution. Despite the fact that both systems have very similar attractor topology we find fundamental differences in their response to the interaction. For the ensemble of Rössler systems the onset of synchronization is as expected and $\sigma(K)$ decreases monotonically with increasing coupling strength, in accordance to the above theory. In contrast, the ensemble of foodweb models shows a totally different behavior. Here, with increasing coupling the frequency disorder is first amplified leading to a maximal decoherence for intermediate levels of coupling. Only for much larger coupling strength frequency disorder is reduced again and synchronization sets in. We denote this unusual increase of disorder with coupling strength as *anomalous transition to phase synchronization* (Blasius et al., 2003).

We have tested the robustness of anomalous synchronization in a large number of numerical simulations. We have always found that the long term behavior is independent of initial conditions, which usually are set randomly for each oscillator (in the foodweb model initial conditions have to be taken out of the domain of attraction of the phase coherent attractor). Our results are numerically robust to the network topology. We have numerically checked simulations in 1 and 2-dimensional lattices with different sizes and also in systems with global coupling. In all cases we have found large parameter ranges in which the ecological model exhibits anomalous synchronization (see Fig. 4.4). In general, the strength of anomalous synchronization, measured as the maximal gain of frequency disorder, increases with the number of next neighbors and is most pronounced with global coupling. Furthermore, we have found anomalous synchronization when disorder

is realized by different statistical distributions and it retains also in chains with linearly increasing control parameters b_i. Anomalous synchronization appears already in two coupled chaotic foodweb models, albeit not as pronounced as in large ensembles. In general we find that the effect of anomalous synchronization appears independently of the number of oscillators, with a tendency to be more distinct in large systems. Note, that the strength of anomalous synchronization in general depends also on the choice of control parameters and may appear only in certain regimes in parameter space.

To gain more insight into the strikingly different behavior of Rössler and foodweb systems in Fig.4.5 the frequency detuning of individual oscillators in a globally coupled ensemble is depicted. In the Rössler system synchronization appears in the usual way. For small coupling levels the oscillator frequencies are not much affected and fall down slightly with coupling strength. When coupling reaches a critical level all oscillator frequencies are rapidly attracted towards each other and synchronize to a common frequency. In the foodweb model the transition to the synchronized state is totally different. Compared to the Rössler system the average decrease of oscillator frequencies is much stronger. Simultaneously, the interaction leads to a repelling of frequencies where the whole ensemble deviation is enlarged. In this way $\sigma(K)$ can reach values which are four times larger than the natural frequency disorder $\sigma(0)$. This picture is further complicated due to the appearance of clustering. Therefore, Fig.4.5 also includes a plot of the order parameter $R(K)$. In the Rössler system for small coupling levels $R(K)$ remains nearly zero. At the critical level, $K = K_{th}$, cluster formation sets in and all oscillators fastly synchronize to one final cluster. This is reflected in the sudden increase of the order parameter $R(K)$ which appears in the same coupling range as the rapid drop of $\sigma(K)$. In contrast, in the foodweb model clustering sets in already for small coupling levels where the oscillators start to form one main cluster at the high frequency range. This process is accompanied by a slow increase of $R(K)$ and, simultaneously, by a rise of the frequency disorder $\sigma(K)$. With increasing coupling strength the cluster is able to catch more and more oscillators until finally all frequencies become identical for $K > K_c$.

The simultaneous increase of order parameter and frequency disorder with coupling as exemplified here in the foodweb model is rather unusual in the sense that both measures for synchronization lead to different results. Whereas the increase of $R(K)$ signifies the onset of synchronization it is evident from the increase of $\sigma(K)$ that the frequencies are driven away from each other. This apparent paradox can be explained by the fact that while the cluster is able to attract frequencies in close range, at the same instant oscillators with a bigger frequency distance from it are repelled off even stronger. As will be shown later anomalous synchronization does not always go together with such complications and it is also possible that the oscillator frequencies simply split apart without simultaneous onset of clustering.

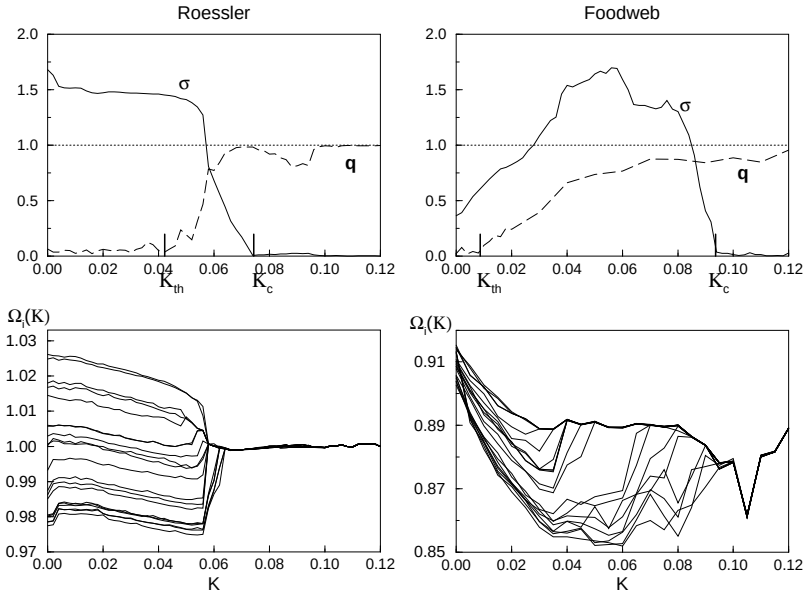

Figure 4.5: Top: Frequency disorder $\sigma(K)$ and order parameter $R(K)$ as function of coupling in an ensemble of 500 globally coupled Rössler systems (4.5) (left) and foodweb models (4.6) (right). Additionally the frequencies $\Omega_i(K)$ of 20 randomly selected oscillators are indicated as well (bottom). Parameters and methods otherwise as in Fig.4.3.

We now explore whether chaotic dynamics is a necessary ingredient in order to obtain anomalous synchronization. To this end we take again an example from Ecology and study an interacting ensemble of Lotka-Volterra systems (May, 1973) which can be thought of as a limit cycle counterpart to the more complicated chaotic system (4.6)

$$\begin{aligned} \dot{x_i} &= ax_i(1-\frac{x_i}{K}) - k\frac{x_i y_i}{1+\kappa x_i} + \frac{K_x}{2}\sum_j (x_j - x_i) \\ \dot{y_i} &= -b_i y_i + k\frac{x_i y_i}{1+\kappa x_i} + \frac{K_y}{2}\sum_j (y_j - y_i). \end{aligned} \tag{4.7}$$

Here, x denotes the prey and y the predator species, a and b are the birth and death rates, K is the prey carrying capacity, k the predation rate and κ the half saturation constant of the functional response. Without coupling system (4.7) is well known to exhibit limit cycle oscillations with a frequency roughly determined by $\omega = \sqrt{ab}$ (May, 1973).

We now take a disordered ensemble of such foodweb models, introduce disorder as usual in the death rates b_i and explore the transition to synchronization (see Fig.4.6). The foodwebs are globally coupled with strength K_x and K_y. We

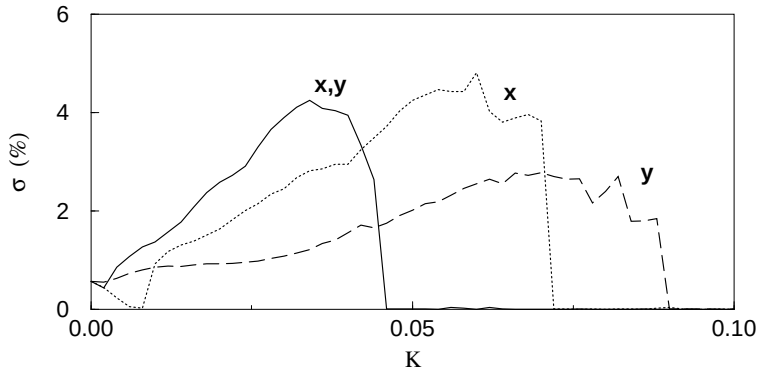

Figure 4.6: Anomalous synchronization in limit cycle systems. Plotted is the transition to synchronization in an ensemble of globally coupled Lotka-Volterra systems (4.7). Parameter values $a = 1$, $k = 3$, $K = 3$ $\kappa = 1$. Parameters b_i are taken from a uniform distribution in the range 1 ± 0.025. Coupling has been introduced either in both x and y-variable (solid line), solely in the x-variable (dotted line) or in the y-variable (dashed line).

distinguish between three different coupling schemes: a) only prey migrate, b) only predators migrate and c) both prey and predators migrate. In all three cases we observe strong anomalous synchronization. However, the exact form of the transition depends on the coupling type. Thus, we conclude that anomalous synchronization can arise in limit cycle systems and therefore the effect does not rely on chaotic dynamics. Interestingly it is again an ecological model, here with limit cycle dynamics, which shows anomalous synchronization. Summarizing, in the classic theory the introduction of coupling leads to synchronization via a monotonical decrease of frequency disorder $\sigma(K)$. In contrast, in both ecological foodweb models which have been studied here the transition to synchronization is strongly modified. In these models we find that $\sigma(K)$ increases with K, reaches a maximal decoherence for intermediate coupling strength and synchronization sets in only for larger levels of K. Thus we observe a counterintuitive effect of coupling which leads to a desynchronization of the oscillators and to an enlargement of the frequency disorder. Lacking a better terminology we call this phenomenon anomalous phase synchronization. To our knowledge such an anomalous onset of synchronization has never before been noted in the literature. The rest of this Chapter is dedicated to a detailed study of this phenomenon.

4.2 Analytical treatment

In this section we start with an analytical treatment and estimate the oscillator frequencies in the regime of weak coupling to gain some insight into the origin of

anomalous synchronization. The aim is to derive exact criteria which determine the conditions when anomalous effects are to be expected.

4.2.1 Approximation as uncoupled oscillators

To explain the basic method we start with the examples of the Rössler and food-web models of the previous section. Later these results will be put into a more general framework. Take again the interacting ensemble of Rössler systems (4.5) and rewrite the equation for the y variable in the following way

$$\dot{y_i} = b_i x_i + a y_i + \frac{K}{m}\sum_{j=1}^{m}(y_j - y_i) = b_i x_i + (a-K)y_i + K\langle y_j\rangle. \tag{4.8}$$

Here, $\langle y_j\rangle = \frac{1}{m}\sum_j y_j$ denotes the average of the y-variable over all oscillators in a coupling neighborhood of oscillator i. For small coupling we can assume that the oscillators are nearly independent and therefore we can safely replace the ensemble average $\langle y_j\rangle$ by the time average of the uncoupled oscillator $\bar{y}_i$. As a result, in the limit of very small coupling the interacting system essentially behaves as a system of independent oscillators with modified dynamics

$$\begin{aligned}\dot{x_i} &= -b_i y_i - z_i \\ \dot{y_i} &= b_i x_i + (a-K)y_i + K\bar{y}_i \\ \dot{z_i} &= 0.4 + (x_i - 8.5)z_i.\end{aligned} \tag{4.9}$$

Here, in the case of the Rössler system we can approximate the constant $\bar{y}_i \approx 0$. Therefore, the only effect of weak coupling is to introduce a small damping into the dynamics of each oscillator which is seen as an effective reduction of parameter $a \to a - K$. To test this approximation of independent oscillators we have included in Fig. 4.4 a plot of the frequency disorder calculated for system (4.9). Indeed, in the range of small coupling the approximated frequency disorder closely follows the numerical results of the full system. Using equation (4.9) it is possible in principle to calculate the frequency detuning of each oscillator in the ensemble as a function of coupling strength $\Omega_i(K)$. In order to proceed further we need to estimate the average rotating frequency of the chaotic system. As a crude approximation here we simply use the imaginary part of the eigenvalues in a linear expansion around the unstable fixed point. To simplify the algebra even more we make use of the fact that in the Rössler system the dynamics takes place mainly in $z = 0$ plane and set $z \approx 0$. Putting all this together leads to

$$\Omega_i(K) \approx \sqrt{b_i^2 - \frac{1}{4}(a-K)^2} \approx \omega_i + \frac{a}{4\omega_i}K, \tag{4.10}$$

where the natural frequency of the Rössler system has been approximated by $\omega_i = \sqrt{b_i^2 - \frac{1}{4}a^2}$.

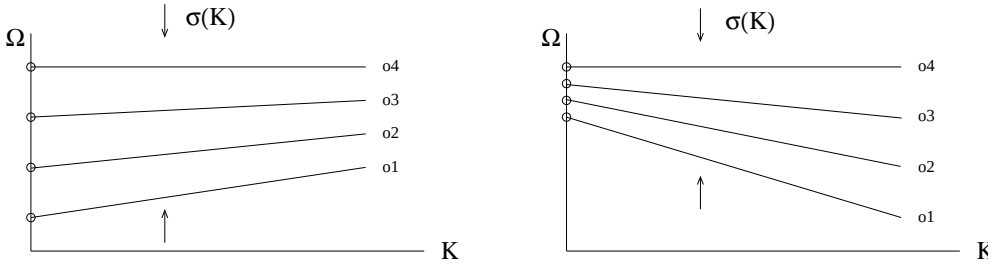

Figure 4.7: Frequency detuning here schematically indicated for 4 oscillators as a function of coupling strength, $\Omega_i(K) = \omega_i + K\kappa_i$. Left: the slope of each line, κ_i, decreases with ω_i. Therefore, frequency disorder $\sigma(K)$ is reduced leading to synchronization enhancement. Right: anomalous synchronization when κ_i increases with ω_i.

Eq. (4.10) tells that the mean frequency at the first order in K is a linear increasing function of coupling strength with a slope $\kappa_i = \frac{a}{4\omega_i}$ that depends on the natural frequency of this unperturbed oscillator (see Fig. 4.7). In the usual parameter range the detuning is very small, $\kappa \approx 0.04$, which corresponds very well with Fig. 4.5 where for small coupling ranges the frequencies are nearly unaffected by coupling.

From this analysis (4.10) it is also clear that the Rössler systems in the form (4.5) cannot exhibit anomalous synchronization (see Fig.4.7). The simple reason is that for every oscillator the slope κ_i is decreasing with the natural frequency, $\kappa_i \sim 1/\omega_i$. Therefore, in oscillators which start out with higher natural frequency ω_i, the oscillating frequency $\Omega_i(K)$ is changing less with coupling than in oscillators with smaller ω_i. By this mechanism all frequencies $\Omega_i(K)$ are attracted together with coupling, which finally confirms the usual synchronization transition of the interacting Rössler systems.

We now proceed in a similar way for the ensemble of coupled foodweb models (4.6). Recall that this system shows an anomalous enlargement of the natural frequency disorder and therefore behaves exactly in the opposite way as the Rössler system. In analogy to (4.9) we replace the interacting ensemble with the following system of uncoupled oscillators

$$\begin{array}{lllll} \dot{x_i} = & a\,(x_i - x_0) & -\alpha_1 x_i y_i & & \\ \dot{y_i} = & -(b_i + K)y_i + b_i y_0 & +\alpha_1 x_i y_i & -\alpha_2 y_i z_i + K\bar{y}_i & \\ \dot{z_i} = & -c\,(z_i - z_0) & & +\alpha_2 y_i z_i. & \end{array} \tag{4.11}$$

From inspection of Fig.4 it is clear that in our parameter range $\bar{y} \approx 10$ and therefore the time average cannot be set to zero as in the Rössler system. Probably for this reason the simple scheme (4.10) is not applicable to estimate the average rotating frequency of the model (4.11). When calculating the imaginary parts of the eigenvalue of the unstable fixed point and setting $z = 0$ we obtain a bad estimate of

$\Omega_i(K)$. Despite these analytical difficulties, the numerically evaluated frequencies of model (4.11) agree perfectly with the behavior of the full model as long as $K \ll K_c$. The same holds for the frequency disorder of the uncoupled system, $\sigma(K)$, which is plotted in Fig. 4.4b and shows similar anomalous synchronization effects. Thus again, for weak coupling the approximation of uncoupled oscillators (4.11) provides an excellent description for the full system dynamics.

The origin of this anomalous increase in $\sigma(K)$ can be understood from Fig. 4.6 which depicts the frequencies $\Omega_i(K)$ for each oscillator. We find that in the foodweb model the frequencies are a nearly linear decreasing function of K with slope $\kappa_i \approx -2$. Careful inspection of Fig. 4.6 reveals that for different oscillators the slope κ_i increases with the natural frequency ω_i. Note, that this is just the opposite trend as exhibited in the Rössler system. As a result, in contrast to the Rössler system here the frequency disorder effectively can be enlarged with coupling strength. Schematically this situation is sketched in Fig. 4.7b which in this way gives a visualization of the basic mechanism underlying anomalous synchronization.

4.2.2 General approach

In the previous examples we have demonstrated how the frequency detuning can be estimated in the weak coupling regime. Now we generalize the approach to gain deeper theoretical understanding about the parameter regimes where anomalous synchronization appears. Take again the general system of interacting oscillators (4.1). Without coupling the system is quasiperiodic and all oscillators are rotating independently from each other on a N-torus. Now suppose that weak coupling is switched on. As long as the coupling is very weak, $K \ll K_c$, it is reasonable to assume that the system remains quasiperiodic and therefore is still filling the N-torus. In this limit we can replace the average over the coupling neighborhood of oscillator i with the time average of the single oscillator. Thus for weak coupling the interacting system (4.1) can be treated as a system of N uncoupled oscillators with modified dynamics (as in (4.9) and (4.11)),

$$\dot{\mathbf{x}}_\mathbf{i} = \mathbf{F}(\mathbf{x}_\mathbf{i}; \chi_i) + C\frac{K}{m}\sum_{j=1}^{m}(\mathbf{x}_\mathbf{j} - \mathbf{x}_\mathbf{i}) \approx \mathbf{F}(\mathbf{x}_\mathbf{i}; \chi_i) - CK(\mathbf{x}_\mathbf{i} - \bar{\mathbf{x}}_\mathbf{i}). \tag{4.12}$$

Here, $\bar{\mathbf{x}}_\mathbf{i}$ indicates the temporal average of each uncoupled oscillator. With the new term $-CK(\mathbf{x_i} - \bar{\mathbf{x}}_\mathbf{i})$ effectively a damping proportional to the coupling strength has been introduced. In our numerical simulations we have always found that (4.12) is a very good approximation as long as the coupling strength remains small enough. This is demonstrated for example in Fig. 4.4 where we have plotted $\sigma(K)$ for the Rössler and foodweb systems using approximation (4.12).

In the uncoupled system (4.12) the frequency of each oscillator depends only on its individual parameters and on coupling strength, but is independent of the

other oscillators, $\Omega_i = \Omega_i(\chi_i, K)$. If this expression is developed as a Taylor series in K we can write the frequency detuning in first order as follows

$$\Omega_i \approx \Omega(\chi_i, K) \approx \omega(\chi_i) + \kappa(\chi_i)\ K. \tag{4.13}$$

Here $\omega(\chi_i)$ represents the natural frequency of each oscillator i in the absence of coupling. $\kappa(\chi_i)$ describes the frequency response of the system to the interaction. Similar to the natural frequency it is a characteristic of the unperturbed system dynamics and, as will be shown later, it is closely related to the nonisochronicity of oscillation. Both functions $\omega(\chi_i)$ and $\kappa(\chi_i)$ depend only on the control parameters χ_i of each system i and, in principle, can be determined by various techniques. For example in the previous section we used a linearization about the unstable fixed point in order to estimate $\Omega(\chi_i, K)$ for the Rössler system (4.10). Other more rigorous approaches include for example normal form expansions or averaging methods (see Section 4.3).

Note that relation (4.13) does not depend on the fact whether the system dynamics is a limit cycle or phase coherent chaos. An alternative way to derive formula (4.13) in the case of nearly identical oscillators goes back to the representation of phase equations. Again assuming independently rotating oscillators for $K << K_c$ the frequency response $\kappa(\chi_i)$ can be calculated as an average over the interaction function

$$\kappa(\chi_i) = \frac{1}{m}\sum_{j=1}^{m}\frac{1}{2\pi}\int_0^{2\pi}\Gamma_{ij}(\Delta\theta_{ij})d\Delta\theta_{ij}. \tag{4.14}$$

Once $\omega(\chi_i)$ and $\kappa(\chi_i)$ are known for every oscillator it is straightforward to calculate ensemble magnitudes. The mean frequency Ω is simply given by

$$\langle\Omega_i\rangle = \langle\omega_i\rangle + \langle\kappa_i\rangle\ K. \tag{4.15}$$

Similar, the standard deviation of the ensemble frequencies up to first order in K is

$$\sigma(K) = \sqrt{\sigma_\omega^2 + 2\mathrm{Cov}(\omega_i, \kappa_i)K} \approx \sigma_\omega + \frac{K}{\sigma_\omega}\mathrm{Cov}(\omega_i, \kappa_i). \tag{4.16}$$

Here σ_ω represents the standard deviation of the natural frequencies ω_i. Therefore, the appearance of anomalous effects depends on the the covariance

$$\mathrm{Cov}(\omega_i, \kappa_i) = \langle(\omega_i - \langle\omega_i\rangle)(\kappa_i - \langle\kappa_i\rangle)\rangle \tag{4.17}$$

between the values ω_i and κ_i of all oscillators in the ensemble. Note, that this corresponds to the schematic representation in Fig. 4.7. If $\mathrm{Cov}(\omega_i, \kappa_i) > 0$ then the κ_i increase on average with the natural frequencies ω_i and thus the frequency disorder spreads out with increasing coupling strength.

Eq. (4.16) is our analytic expression for the frequency disorder of an interacting oscillator system. It provides a general criterion to decide under which conditions anomalous synchronization can be observed. Anomalous enlargement of frequency disorder appears if $\mathrm{Cov}(\omega, \kappa) > 0$ in the whole parameter range of the system. On the other hand if the covariance is negative then synchronization is enhanced. In other words in order to achieve anomalous synchronization ω and κ must *both* be on average increasing or decreasing functions of the parameters χ_i.

Thus, if we want to observe anomalous synchronization in a specific system it is fundamental to know the regions in the parameter space where the correlation function is positive. More formally this can be phrased in the following terms. In order to calculate $\sigma(K)$ we need to know the characteristics ω_i and κ_i for all oscillators. They are determined for each oscillator by the value of the l control parameters $\chi_i = (a_i, b_i, ..)$. Let us denote the parameter space for each individual oscillator by $\Sigma \subseteq R^l$. Then we are interested in the function

$$F : \Sigma \to R^2, \qquad \chi_i \mapsto (\omega(\chi_i), \kappa(\chi_i)) \,. \tag{4.18}$$

In the whole disordered ensemble the parameters are determined by a subset $S \subset \Sigma$. The mathematical problem now is to find an appropriate parameter set S so that $\mathrm{Cov}(F(S)) > 0$. Furthermore we have to take care that the region in parameter space which can physically be realized in a given system usually is much smaller than the size of the full parameter space Σ.

In the remainder of this section we provide some simple criteria which allow to determine appropriate parameter sets. For simplicity, assume that system parameters are uniformly distributed continuous variables. Different oscillators are identified by the value of their control parameter. We first discuss the simplest case $l = 1$ where the oscillators differ only in one control parameter b. Then (4.13) takes the form

$$\Omega_i \approx \Omega(b, K) \approx \omega(b) + \kappa(b)\ K.$$

It is straightforward to write down the conditions that the functions $\omega(b)$ and $\kappa(b)$ have to fulfill in order that anomalous synchronization can be observed. Using either (4.16) or simply from inspection of Fig. 4.7 ω and κ must simultaneously be increasing or decreasing functions of the system parameter b. Therefore, a sufficient condition for anomalous synchronization can be written as

$$\frac{d\kappa}{d\omega} > 0. \tag{4.19}$$

If this relation is fulfilled over the whole parameter range S of the interacting ensemble anomalous synchronization will be achieved. In this case we call S an 'anomalous (parameter) set'. Similarly if over the whole parameter range $\frac{d\kappa}{d\omega} < 0$ then $\sigma(K)$ is a decreasing function of coupling and synchronization is enhanced.

So far the disorder has always been introduced only in one parameter. Now we extend the analysis to the case $l = 2$ when the disorder is distributed between two control parameters a and b (the same ideas can then easily be generalized to a larger number of control parameters). In this case (4.13) takes the form

$$\Omega_i \approx \Omega_i(a, b, K) \approx \omega(a, b) + \kappa(a, b)\ K. \tag{4.20}$$

Now we cannot simply use condition (4.19) because it involves the differentials of a and b. Instead, in the case of several independently varying parameters a sufficient condition for anomalous frequency enlargement is given by

$$\boldsymbol{\nabla}\omega \cdot \boldsymbol{\nabla}\kappa > 0. \tag{4.21}$$

Relation (4.21) defines regions in the parameter space where the angle between the two gradients is smaller than $\frac{\pi}{2}$. In these regions ω and κ are simultaneously increasing or decreasing functions of the parameters a, b and as a result these regions are anomalous. Similar we find for synchronization enhancement

$$\boldsymbol{\nabla}\omega \cdot \boldsymbol{\nabla}\kappa < 0. \tag{4.22}$$

From this we conclude that even in systems where no anomalous set can be found with $l = 1$, there is still a high chance to achieve anomalous synchronization when two parameters are varied simultaneously.

One particularly interesting case arises if different oscillators are parameterized along a one dimensional trajectory in Σ in such a way that both functions ω and κ are simultaneously increasing with the path length. This possibility depends on the determinant of the Jacobian matrix of F in (4.18),

$$J = \left| \frac{\partial(\omega, \kappa)}{\partial(a, b)} \right|. \tag{4.23}$$

If $J = 0$ then the two functions $\omega(a, b)$ and $\kappa(a, b)$ are functionally related and the sign of condition (4.19) cannot easily be controlled. However, if $J \neq 0$ the system (4.18) is invertible,

$$a = a(\omega, \kappa), \quad b = b(\omega, \kappa). \tag{4.24}$$

In this case any relation between ω and κ can be realized by simply plugging $\kappa = \kappa(\omega)$ into (4.24) and calculating the values of a and b in a certain range of frequencies ω. In this way it is possible to systematically find parameter sets so that our anomalous criteria (4.19) can be fulfilled. Such a parameter set corresponds to a trajectory in the parameter space Σ. Of course in practice one has to take care that this trajectory in Σ intersects with the subset of parameters which can be realized physically.

4.2.3 Anomalous synchronization in the Rössler system

Above we have demonstrated how anomalous effects may be achieved in a given system by simultaneous variation of two parameters. In order to demonstrate how all this works we now apply these ideas to the Rössler model. We have already calculated an estimate for the frequency detuning (4.10) by linearizing the system around its fixed point

$$\omega = \sqrt{b^2 - a^2/4}, \qquad \kappa = \frac{a}{4\sqrt{b^2 - a^2/4}}. \tag{4.25}$$

For our purposes this crude approximation gives all information that is needed to check for the presence of anomalous synchronization. First we check for anomalous behavior when, as usual, only one parameter b is varied. This corresponds to the case $l = 1$. Application of criteria (4.19) yields $\frac{d\kappa}{d\omega} = a - 4b^2/a > 0$. This is fulfilled for positive parameters only if $4b^2 < a^2$. However in this regime the Rössler system does not exhibit phase coherent chaos. This again confirms our simulation results that Rössler systems cannot show anomalous synchronization if the oscillators vary only in parameter b.

However, as mentioned above it might still be possible to observe anomalous synchronization when a functional dependence between two system parameters can be achieved. Using (4.25) we find for the Rössler system that the Jacobian $J \neq 0$ and therefore the function F in (4.18) is invertible. The inverted system is given by

$$a = 4\kappa\omega, \qquad b = \omega\sqrt{1 + 4\kappa^2}. \tag{4.26}$$

Now, following the above outlined scheme, the procedure to achieve anomalous synchronization in the Rössler system is as follows: take a certain distribution of frequencies $\{\omega\}$, choose some appropriate values of $\{\kappa(\omega)\}$ and, finally, use (4.26) to calculate the resulting set of control parameters $\{(a, b)\}$. Usually we are considering nearly identical oscillators and therefore our parameter range is very small. Then the relation $\kappa(\omega)$ can be linearized $\kappa(\omega) = c\omega + c_0$. Of course anomalous behavior relies on a choice of $c > 0$. For practical purposes we can use an even more simple scheme. Instead of implying a linear relation in (ω, κ) space we can also linearize directly in Σ. Thus we demand that parameters a and b are taken from a straight line with slope k in parameter space. This can be realized with a 'test' function $a - \langle a\rangle = k(b - \langle b\rangle)$ where parameters b are uniformly distributed in the range $b = \langle b\rangle \pm \delta$. To check for anomalous effects we have to find the projected gradients of both functions $\kappa(a, b)$ and $\omega(a, b)$ in all possible directions k. This is measured by the scalar product of each gradient with the unit vector $\hat{k} = \frac{1}{\sqrt{1+k^2}}(k, 1)$, i.e. by taking the directional derivative in all k directions $D_{\hat{k}}$. In this way we can determine the directions in parameter space where condition (4.21) is fulfilled. In this scheme the criterion for anomalous behavior becomes

$$D_{\hat{k}}\omega \, D_{\hat{k}}\kappa > 0. \tag{4.27}$$

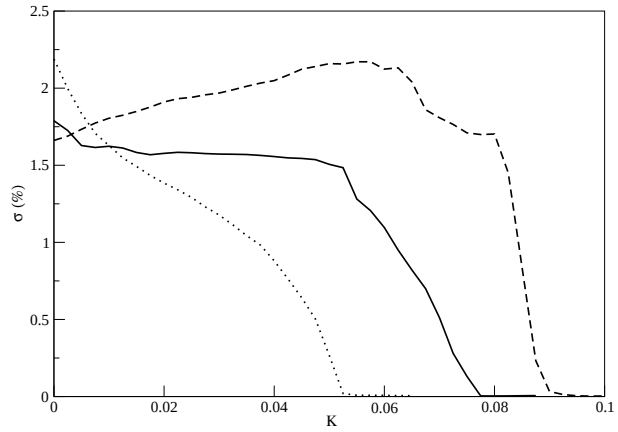

Figure 4.8: Possibility of anomalous behavior in the Rössler system which is achieved by simultaneously varying two parameters. Plotted is the frequency disorder $\sigma(K)$ as a function of coupling strength K in an ensemble of 300 globally coupled Rössler oscillators. Parameter values are taken as $a = k(b - \langle b \rangle) + \langle a \rangle$ with δ=0.025, $\langle b \rangle$=0.97 and $\langle a \rangle$=0.15. We observe anomalous synchronization for $k = 2$ (dashed line), usual synchronization for $k = 0$ (solid line) and enhanced synchronization for $k = -2$ (dotted line).

In the Rössler system this can be calculated with the help of (4.25) where, as usual, we take the natural frequencies in the range $b \approx 1$. As a result positive anomaly is present when parameter a is simultaneously verifying $a < k$ and $a < 1/k$. These two conditions can be fulfilled for instance when $k = 2$. Indeed for this choice of k we have achieved our goal and the ensemble of Rössler systems shows anomalous behavior (see Fig. 4.8). Similar if $k = 0$ and parameter a is constant in the ensemble the conditions cannot be fulfilled and synchronization anomalies are absent. By reversing our criterion (4.27) we can identify the region for synchronization enhancement in the Rössler system. For example, this is fulfilled for a choice of $k = -2$ which agrees perfectly with the simulation results in Fig.4.8.

4.3 Ensemble of Van-der-Pol oscillators

We now demonstrate how the methods of the previous section can be practically applied in a weakly nonlinear system. As an illustrative example we use an ensemble of nonidentical Van-der-Pol oscillators which are coupled in the x and y variables

$$\begin{aligned} \dot{x_i} &= y_i + \frac{K}{N}\sum_j^N (x_j - x_i) \\ \dot{y_i} &= a_i(1 - x_i^2)y_i - b_i^2 x_i + \frac{K}{N}\sum_j^N (y_j - y_i). \end{aligned} \tag{4.28}$$

Here a is the nonlinearity or stiffness of the system and b is the harmonic frequency of oscillation. In the following we use frequencies in the range $b \approx 1$ and further assume weak nonlinearity, $a << 1$. Our main goal now is to express the oscillation frequency as a function of coupling strength. This can be achieved with the help of perturbation techniques. Here we use a normal form expansion up to third order in a (Kahn and Zarmi, 1998) and find for the radial and the angular equations

$$\begin{aligned} \dot{r}_i &= \frac{1}{2}a_i r(1-\frac{1}{4}r^2) - rK + O(a_i^3) \\ \dot{\theta}_i &= b_i - \frac{a_i^2}{b_i}(\frac{1}{8} - \frac{3}{16}r^2 + \frac{11}{256}r^4) + O(a_i^4). \end{aligned} \tag{4.29}$$

Note, that in the Van-der-Pol oscillator non-isochronicities appear only with the second order in the nonlinearity a. The coupling term in the radial equation has been calculated assuming that $\dot{r} = 0$ after relaxation, and thus has a single stable equilibrium $r^{*2} = 4\left(1 - \frac{2K}{a}\right)$. Plugging this into the angular equation we obtain the mean frequency in first order in K

$$\Omega_i(K) = b_i - \frac{a_i^2}{16b_i} + \frac{5a_i}{4b_i}K. \tag{4.30}$$

With this the system of Van-der-Pol oscillators has been brought into the general form (4.13) with

$$\omega(a,b) = b - \frac{a^2}{16b}, \qquad \kappa(a,b) = \frac{5a}{4b}. \tag{4.31}$$

4.3.1 Functional dependence between control parameters

At this point we have to specify how the disorder is realized in the control parameters a and b. The simplest possibility would be to introduce disorder only in the harmonic frequencies b. In this case $\omega(b)$ and $\kappa(b)$ in (4.31) are functions of only one parameter b. It is straightforward to see that in this form it is not possible to obtain anomalous desynchronization since inequality (4.19) can then only be fulfilled if $a < 0$. However Van-der-Pol systems are not defined for negative values of the nonlinearity. Therefore, ensembles of Van der Pol oscillators do not show anomalous enlargement of frequency disorder if the oscillators are varying only in their harmonic frequencies b.

However we have already demonstrated that, in general, it is possible to achieve anomalous synchronization if some functional dependence between control parameters can be maintained. This means that the disorder necessarily must be affecting both parameters a and b. Here we show that anomalous synchronization can be obtained if we have the possibility to adjust the parameters of each oscillator in the ensemble. To this aim we take parameters b from a uniform distribution with center $\langle b \rangle$=1 and width $\delta = 0.5$ and adjust the system parameters in such a way

that the nonlinearity or stiffness of each oscillator is a function of the harmonic frequency, $a = a(b)$. If the range or spread of parameters δ is small enough the functional dependence is essentially linear,

$$a = kb - k_0. \tag{4.32}$$

Here, the value of k determines the strength of correlation between nonlinearity and natural frequency. Note, that the absolute value k_0 has to be chosen in such a way that in the whole range parameters a are always positive.

When the parameters are fixed (4.32) we can use (4.30) to calculate the standard deviation $\sigma(K)$

$$\sigma(K) = \frac{5}{4}\sigma_b[\frac{3}{4} + (k-1)(K - \frac{1}{10})]. \tag{4.33}$$

Here σ_b represents the standard deviation of the uniformly distributed natural frequencies b, i.e. $\sigma_b = \frac{\delta}{\sqrt{12}}$. With this result (4.33) we have calculated an approximation for the frequency disorder of an ensemble of weakly nonlinear Van-der-Pol oscillators in the regime of small coupling.

To check our results in Fig. 4.9 we compare formula (4.33) with a direct simulation in an ensemble of 800 globally coupled Van-der-Pol oscillators for different functional dependencies of the control parameters. Take first the case $k = 0$ when the nonlinearity a is independent of b and it is a constant for all oscillators in the ensemble. As mentioned above, in this case synchronization arises in the usual way and $\sigma(K)$ is a decreasing function of K. However, from (4.33) when nonlinearity increases sufficiently with the natural frequency and $k > 1$, $\sigma(K)$ increases with K and anomalous synchronization is achieved. This is plotted in Fig. 4.9 for $k = 3$. In the opposite case when $k < 1$ we find that synchronization is enhanced (depicted as $k = -3$ in Fig. 4.9). Note the good agreement of numerical results and analytics (4.33) in the regime of small coupling. As has been demonstrated already in Fig.4.5, it is quite possible that cluster formation starts immediately after the onset of coupling and therefore $\sigma(K)$ provides only partial information about the amount of synchronization in the system. To obtain more information about the transition to synchronization we include in Fig.4.9 a plot of the order parameter as function of coupling strength, $R(K)$. Again, we observe that anomalous synchronization has large consequences also in the higher coupling regime. Inspection of Fig.4.9 reveals that the synchronization threshold is lifted up to higher coupling values in both measures with increasing levels of k. In consequence the synchronization threshold can be controlled through parameter k. It is interesting to note that coupling induced changes in the frequency disorder (i.e. anomalous effects) are not detectable with the complex order parameter which is already nearly zero for small coupling levels.

We want to stress that in order to compare the synchronization thresholds in Fig.4.9 for different k, one must take into account that by the way in which k

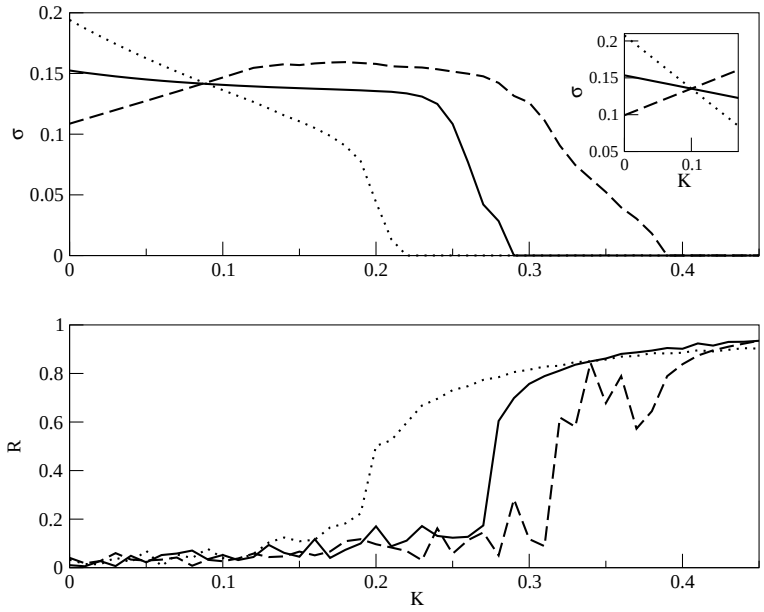

Figure 4.9: Standard deviation $\sigma(K)$ (top) and order parameter amplitudes $R(K)$ (bottom) as a function of coupling strength K in 800 globally coupled Van-der-Pol oscillators (4.28). Natural frequencies are taken from a uniform distribution with $\delta = 0.5$, $\langle b \rangle = 1$ and related to nonlinearities with $a = k(b - \langle b \rangle) + \langle b \rangle$. Plotted are results for $k = 3$ (dashed line), $k = 0$ (solid line) and $k = -3$ (dotted line). Inset: analytical results Eq. (4.33).

has been introduced in (4.32) any change of k simultaneously affects the natural frequency disorder $\sigma(0)$ of the ensemble. Therefore by increasing the value of k automatically the system disorder is reduced. This is seen as the different heights of $\sigma(0)$ for different values of k in Fig.4.9. In order to have a 'fair' comparison between different functional dependencies of parameters a and b one would have to rescale the overall system disorder to equal starting values. Nevertheless, even without this procedure we observe that higher level of k can increase the synchronization threshold despite the fact that the overall disorder has effectively reduced. For example in Fig.4.9 the synchronization threshold has been increased by a factor of around 100

4.3.2 Correlation between system parameters

In the previous section we have demonstrated how anomalous synchronization can be achieved in ensembles of Van-der-Pol oscillators if there is some functional dependence (4.32) between the control parameters. However, such a tight relation might not always be possible to realize in a practical situation. In this section we study a more general situation in which the two control parameters are ran-

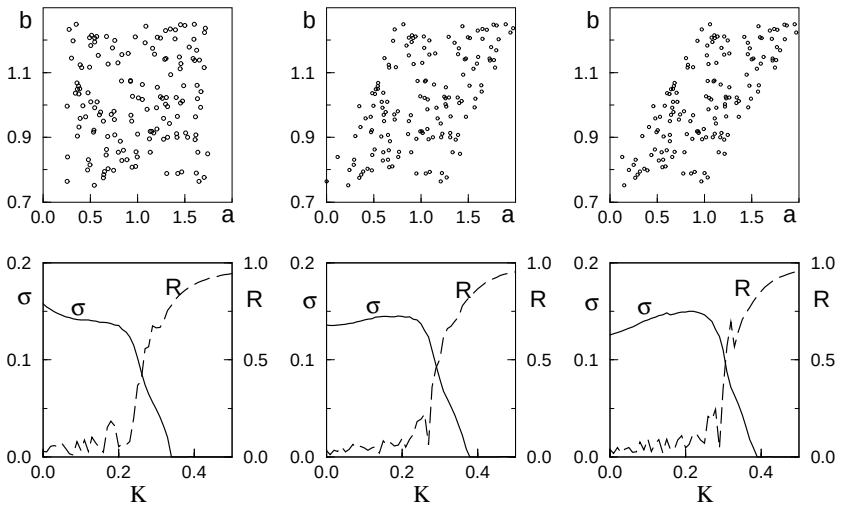

Figure 4.10: Transition to synchronization in an ensemble of 800 globally coupled Van-der-Pol oscillators (4.28) with correlated parameter values, $\mathrm{Corr}(a_i, b_i) = r$. The distribution of control parameters is based on two series, $\tilde{a}_i$ and $\tilde{b}_i$, of uniformly distributed random numbers in the range $[-\delta, \delta]$ that are correlated with coefficient r. Then, parameter values are taken as $b_i = \langle b \rangle + \tilde{b}_i$, and $a_i = \langle a \rangle + k\,\tilde{a}_i$, for $k = 3$, $\delta = 0.25$, $\langle a \rangle = \langle b \rangle = 1$ and $r = 0$ (left), $r = 0.5$ (center), $r = 0.7$ (right). Top) Subset of 100 parameter pairs, $\{a_i, b_i\}$, in the parameter space. Bottom) Numerical results of standard deviation $\sigma(K)$ and order parameter amplitude $R(K)$.

dom numbers that are correlated to a certain degree. The question arises if it is still possible to achieve anomalous synchronization effects in a such more realistic scenario.

Let us start with a calculation of the synchronization regimes when disorder is distributed independently in both parameters a and b. By using condition (4.21) we obtain the following inequality

$$\boldsymbol{\nabla}\omega(a,b) \cdot \boldsymbol{\nabla}\kappa(a,b) = -\frac{5}{32}\frac{a}{b^2}(9 + \frac{1}{2}\frac{a^2}{b^2}) > 0. \tag{4.34}$$

The solution of this inequality is the unphysical region $a < 0$, and therefore we find no anomalous parameter sets with two independently varying parameters. In the physical region $a > 0$, however, inequality (4.22) is always fulfilled and therefore synchronization is enhanced. This result can be observed in a numerical simulation (see Fig.4.10, left) where in the small coupling regime the standard deviation decreases with increasing coupling strength. Now we explore how this situation is changed when some correlation has been imposed upon the control parameters of the Van-der-Pol oscillators. Suppose that parameters a and b are generated to be random numbers with a certain correlation coefficient r which still

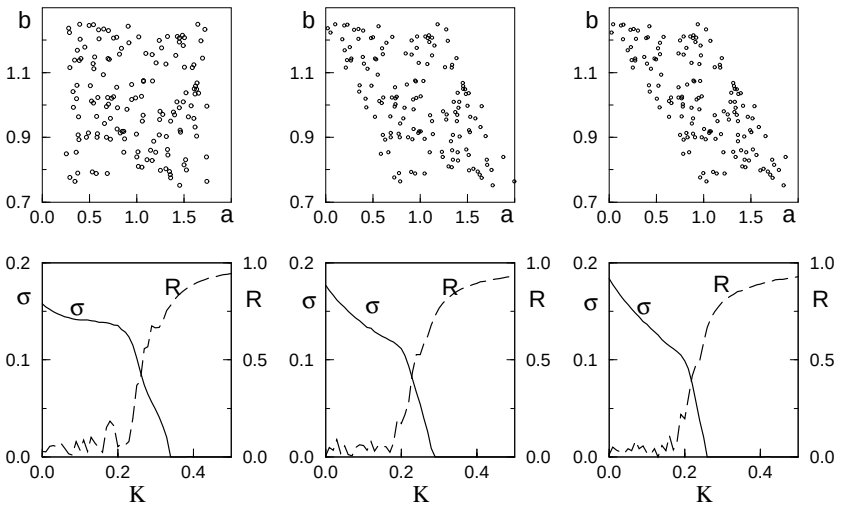

Figure 4.11: Same as Fig.4.10 with $k = -3$ and $r = 0$ (left), $r = -0.5$ (center), $r = -0.7$ (right). Increasing anticorrelation between a and b leads to anomalous enhancement of synchronization.

have a linear functional dependences as in the previous subsection: $k = 3$ and $k = -3$. Figs. 4.10 and 4.11 show the corresponding subsets in parameter space (a, b) for different values of r and the numerical simulation results for $\sigma(K)$ and $R(K)$.

When the correlation coefficient $r = 0$ then a and b are independent control parameters and all oscillator parameters are uniformly distributed in the region [0.25,1.75]×[0.75,1.25]. Figs. 4.10 and 4.11 show the emergence of anomalous synchronization ($k = 3$) and fast synchronization ($k = -3$) with increasing levels of $|r|$. Note that in both cases even if parameters are correlated only with 70%, $|r| = 0.7$, the synchronization transition is already significantly modified compared to the case $r = 0$ where a and b are uncorrelated. To summarize, it is sufficient that two control parameters are related only 'on average' in order to achieve anomalous synchronization effects.

4.4 Anomalous synchronization in the Landau-Stuart model

As we have discussed in the Chapter 2, the Landau-Stuart model has two independent parameters that represent exactly the natural frequency and the non-isochronicity. Thus, anomalous synchronization is expected to occur by establishing functional dependences between the system's parameters. As we will see, this fact

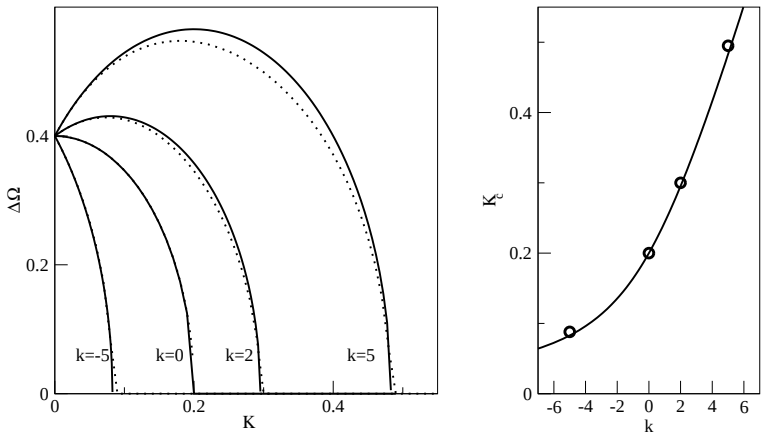

Figure 4.12: Left: Frequency difference of two coupled Landau-Stuart oscillators (see Chapter 2 for details) with $\Delta q = k\Delta\omega$ as a function of coupling strength for different values of k (ω_1=1.2, ω_2=0.8). Plotted are the simulation results (dotted lines) and the analytical result from Eq. (4.36) (solid lines). Right: Synchronization threshold, K_c, as a function of k. Solid line: analytical result from Eq. (4.36) by making $\Delta\Omega = 0$, circles: numerical results.

makes this model especially indicated for studying the phenomenon of anomalous synchronization analytically.

4.4.1 Two coupled oscillators

So far our analytic treatment of anomalous synchronization effects has been restricted to very small coupling levels, $K \ll K_c$, so that we could use the assumption of independently rotating oscillators. Now we show that in the case of two coupled Landau-Stuart oscillators (2.25) the full transition to synchronization can be described analytically. Using the phase equations (4.45) with $N = 2$ we obtain for the phase difference $\phi = \theta_2 - \theta_1$

$$\dot{\phi} = \Delta\omega - K[2\sin\phi + \Delta q(\cos\phi - 1)], \tag{4.35}$$

with $\Delta\omega = \omega_2 - \omega_1$ and $\Delta q = q_2 - q_1$. It is straightforward to solve this equation for $\phi(t)$. The beat frequency can be analytically calculated as it has been shown in Chapter 2. Integration leads for the mean frequency difference, $\Delta\Omega = 2\pi/T$, to

$$\Delta\Omega(K) = \sqrt{\Delta\omega^2 + 2K\Delta\omega\Delta q - 4K^2}. \tag{4.36}$$

With this expression the transition to synchronization of two coupled nearly identical, weakly nonlinear oscillators has been described in the full coupling range. Note, that our criterion (4.16) here simplifies to the product $\Delta\omega\Delta q$. For $\Delta q = 0$ expression (4.36) reduces to the well known beat frequency of two coupled isochronous

phase oscillators. In general however, $\Delta q \neq 0$ and we can write $\Delta q = k\Delta\omega$. Fig. 4.12 shows the results for different correlations between $\Delta\omega$ and Δq. We observe a good agreement of the analytical result (4.36) with the numerical simulations as long as both oscillators differ not too much. In particular, for positive values of k we find anomalous synchronization, whereas negative values of k lead to an enhancement of synchronization, as expected. Note that anomalous synchronization is effective not only at the onset of coupling but has important consequences also in the regime of larger coupling levels. This can be observed for example in the synchronization threshold K_c which is shifted substantially by increasing levels of $|\Delta q|$.

As a consequence, anomalous synchronization is also reflected in the Arnold tongue structure of the system. Here, the idea is to indicate the synchronization region in the $(\Delta\omega, K)$-plane (see Fig. 4.13). This region typically has the form of vertical (Arnold-)tongues. In our case the Arnold tongue is easily obtained by setting $\Delta\Omega(K) = 0$ in (4.36). If $\Delta q = 0$ we recover the usual result for two coupled phase oscillators that the border of the tongues are the two straight lines $K = |\Delta\omega|/2$.

When both oscillators differ in their respective value of nonisochronicity, $\Delta q \neq 0$, the Arnold tongue becomes asymmetrical with respect the $\Delta\omega$ axis. A simple calculation shows that the border of the tongue is still given by a straight line, but with a modified slope which is scaled by a factor ξ and ξ^{-1} on the right and left side, respectively. Thus, the anomalous synchronization borders are given by

$$K = \begin{cases} \frac{\Delta\omega}{2}\,\xi(\frac{\Delta q}{2}), & \Delta\omega > 0 \\ -\frac{\Delta\omega}{2}\,\frac{1}{\xi(\frac{\Delta q}{2})}, & \Delta\omega < 0 \end{cases} \tag{4.37}$$

or in a more compact form

$$K = \frac{|\Delta\omega|}{2}\,\left[\xi\left(\frac{\Delta q}{2}\right)\right]^{\mathrm{sign}(\Delta\omega)}. \tag{4.38}$$

Here, the function $\xi(x)$ defines the modification of the slope in dependence on the difference in nonisochronicity, $2x = \Delta q$, and is given by

$$\xi(x) = x + \sqrt{x^2 + 1}. \tag{4.39}$$

Note, the special property $\xi(x) = 1/\xi(-x)$. Fig. 4.13 shows the Arnold tongue of the system for a given value of $\Delta q > 0$. In concord to our above discussion we find that on the right side of Fig. 4.13a where there is a positive correlation between nonisochronicity and natural frequency, $\Delta\omega\Delta q > 0$, synchronization is largely inhibited, whereas on the left side with negative covariance the synchronization regime is enlarged.

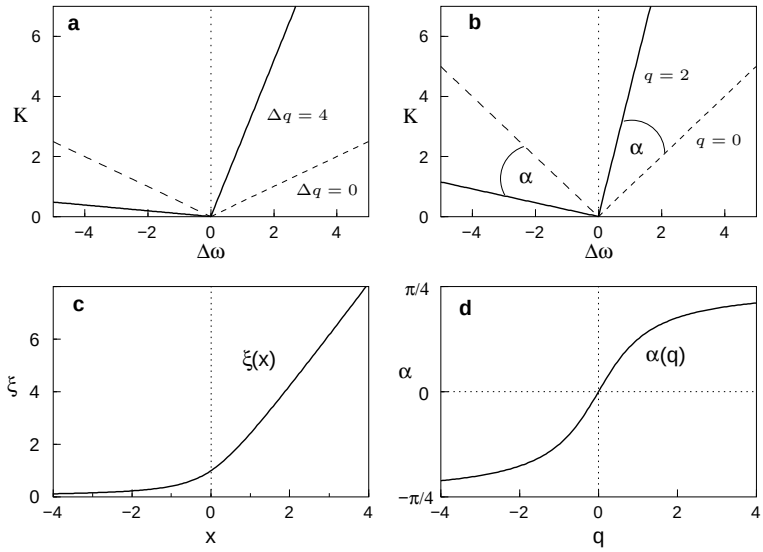

Figure 4.13: Deformation of the Arnold tongues in the presence of nonisochronicity. a) Comparison between the Arnold tongues in a system of two coupled Landau-Stuart oscillators (4.35) with identical nonisochronicity $\Delta q = 0$ (dashed line) and with $\Delta q = 4$ (solid line). If both oscillators differ in nonisochronicity, on the right hand side where $\Delta\omega\Delta q > 0$ the entrainment requires a higher coupling and the slope of the border of the tongue is enlarged by a factor $\xi(\Delta q/2)$. In contrast, on the left side where $\Delta\omega\Delta q < 0$ synchronization is enhanced and the slope is reduced by a factor $1/\xi$ (4.38). b) Arnold tongue of an externally forced phase oscillator 4.42) without nonisochronicity, $q = 0$ (dashed line) and with $q = 2$ (solid line). In the nonisochronous oscillator there is a similar deformation of the Arnold tongue (4.43) and effectively results in a rotation by an angle α (4.44). c) Plot of the function $\xi(x) = x + \sqrt{x^2 + 1}$ (4.39). d) Rotation angle, α, of the Arnold tongue in b) as a function of nonisochronicity.

We want to stress that assuming different values of ω and q in both oscillators we always observe anomalous effects, either inhibiting or enhancing synchronization. Since the Landau-Stuart model is a very general way to describe any oscillator of type (4.1) near its Hopf bifurcation we can say that the effects which we are describing are *always* present in the synchronization transition of two non-identical oscillators which vary in both natural frequency and non-isochronicity.

4.4.2 Asymmetric coupling and periodically forced oscillator

In the previous sections we have discussed how anomalous effects can emerge when there is a correlation between two system characteristics such as nonisochronicity and natural frequency. In this section we show that similar effects arise even when the oscillators have identical nonisochronicity, q, if the coupling between the oscillators is asymmetrical. For simplicity, we restrict us to the case of two coupled

oscillators (2.25), where oscillators z_1 and z_2 are coupled with strength K_1 and K_2, respectively. In this case of asymmetrical coupling we find for the phase difference in a analogy to (4.35)

$$\dot{\phi} = \Delta\omega - (K_2 + K_1)\sin\phi - (K_2 - K_1)q(\cos\phi - 1). \tag{4.40}$$

Proceeding as in the previous section the observed frequency difference yields

$$\Delta\Omega(K) = \sqrt{\Delta\omega^2 + 2q\Delta\omega(K_2 - K_1) - (K_1 + K_2)^2}. \tag{4.41}$$

By comparison with (4.36) it is immediately evident that we find anomalous enlargement when the product $q\Delta\omega\Delta K > 0$ and anomalous synchronization enhancement if $q\Delta\omega\Delta K < 0$. Thus, if the oscillators are nonisochronous the asymmetry of coupling is reflected through an asymmetry of the synchronization regime and the Arnold tongue.

It is especially important the limiting case of an externally forced oscillator which arises when we set $K_1 = 0$. In this case (4.40) goes over to (for simplicity we denote $K_2 = K$)

$$\dot{\phi} = \Delta\omega - K[\sin\phi + q(\cos\phi - 1)]. \tag{4.42}$$

This equation describes the evolution of the phase difference between a single nonisochronous oscillator and a periodically driving force, where the natural frequency of the oscillator and the driving frequency have a frequency mismatch of $\Delta\omega$.

We now analyze the synchronization threshold and the geometry of the Arnold tongue in dependence of the nonisochronicity q. If $q = 0$ the border of the Arnold tongue is given by the two lines $K = |\Delta\omega|$ (see Fig. 4.13b). However, if $q \neq 0$ the slope of the lines is scaled similar to (4.38)

$$K = |\Delta\omega| \ [\xi(q)]^{\mathrm{sign}(\Delta\omega)}. \tag{4.43}$$

Thus, the whole synchronization transition depends on the sign of $\Delta\omega$. If $q > 0$ and the natural frequency of oscillation is larger than the driving frequency, then the synchronization threshold is enlarged. Otherwise, the synchronization threshold is reduced. Indeed, here in the case of an externally forced phase oscillator it turns out that the Arnold tongue is simply rotated due to the presence of nonisochronicity. The rotation angle α is given by

$$\tan(2\alpha) = q. \tag{4.44}$$

In the limit of infinite large nonisochronicity the Arnold tongue is rotated by 90^0 degrees. In other words the rotation angle of the Arnold tongue is a measurement

for the nonisochronicity of oscillation (see Fig. 4.13b). Similar asymmetric Arnold tongues are well known from many experimental data (Pikovsky et al., 2001). In these cases a simple measurement of the position and asymmetry of the Arnold tongue can reveal valuable information about the dynamics of the observed oscillator.

4.4.3 Ensemble of phase oscillators of Landau-Stuart type

In the following we generalize our discussion to an ensemble of phase oscillators of Landau-Stuart type. It is important to stress that since in the Landau-Stuart model the parameters ω and q are independent, in order to observe anomalous synchronization one must take *correlated distributions*.

As it has been shown in Chapter 3 the phase equations corresponding to the Landau-Stuart model are

$$\dot{\theta}_i = \omega_i - \frac{K}{N}\sum_{j=1}^{N}\left[\sin(\theta_i - \theta_j) + q_i(1 - \cos(\theta_i - \theta_j)\right]. \tag{4.45}$$

For small coupling levels, $K \ll K_c$, the oscillators are rotating nearly independently and the trigonometric functions

$$\sum_{j=1}^{N}\sin(\theta_i - \theta_j) \approx \sum_{j=1}^{N}\cos(\theta_i - \theta_j) \approx 0$$

and thus the system transforms into an ensemble of independent oscillators

$$\dot{\theta}_i(K) = \omega_i + q_i K. \tag{4.46}$$

Note, that this equation can also be obtained by using (4.14) and averaging over the interaction function in (4.45).

With Eq.(4.46), the frequency of the system of interacting Landau-Stuart oscillators becomes fully described in the range of small coupling where it takes a very simple form. The physical interpretation is straightforward. Due to the interaction the oscillators are perturbed off their limit cycle. On average this leads to a radial contraction of each limit cycle which produces a shift of the angular velocity proportional to the value of the shear term q_i.

Note that formula (4.46) corresponds exactly to (4.13), and the nonisochronicity q_i takes over the role of the κ_i in the general system. Obviously in Landau Stuart systems the functions ω and q are directly the independent control parameters. In this respect system (4.45) is especially interesting for our studies since we don't have to consider the roundabouts of mapping F (4.18) of the previous section.

Now assume again a disordered system where the oscillators differ in their respective values of ω_i and q_i. If the 'faster' oscillators (with higher natural frequency,

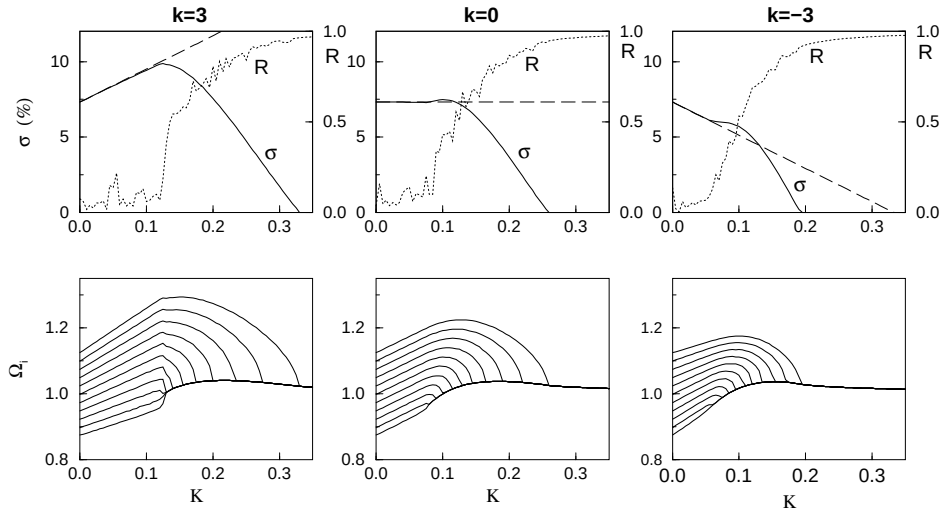

Figure 4.14: Ensemble of 500 globally coupled Landau Stuart oscillators (4.45) with $q = k(\omega - \langle\omega\rangle) + \langle\omega\rangle$. Natural frequencies are linearly increasing in the range $\delta = 0.25$, $\langle\omega\rangle$=1. Left) $k = 3$: anomalous synchronization; center) $k = 0$: usual synchronization; right) $k = -3$ enhanced synchronization. Top) Standard deviation of the ensemble frequencies $\sigma(K)$; numerical simulation (solid line) and analytical result using 4.48) (dashed line). Further indicated is the order parameter $R(K)$ (dotted line). Bottom) Frequencies $\Omega_i(K)$ of 11 equally spaced oscillators as a function of coupling strength K.

ω_i) have a stronger shear of phase flow (higher value of q_i) compared to the 'slower' ones, then small coupling leads to an enlargement of the frequency difference between the 'faster' and the 'slower' oscillators (see Fig.4.7). Therefore, if the ω_i covary with q_i then small coupling tends to desynchronize the oscillators. In fact, this is nothing else but our previous result (4.16) that anomalous effects arise only if the nonisochronicity of oscillation covaries with the natural frequency.

Suppose now that the nonisochronicity of each oscillator depends in some specific way on the natural frequency $q = q(\omega)$. If the width of the distribution of ω is small in the spirit of the previous section we can develop this dependence in first order as

$$q(\omega) = k\omega + q_0. \tag{4.47}$$

Then it is straightforward to calculate the standard deviation of the ensemble frequencies. Up to first order we find

$$\sigma(K) = (1 + kK)\sigma_\omega. \tag{4.48}$$

Thus, the standard deviation is an increasing function of coupling strength when $k > 0$ and a decreasing function when $k < 0$. When $k = 0$ we are only varying the natural frequency and the correlation term in Eq. (4.16) is zero. We have

tested these results in a direct simulation of 500 globally coupled Landau Stuart systems for different values of k (see Fig. 4.14). Again, we find a perfect agreement between our theory and the numerical simulations. Note that $\sigma(0)$ does not change with k, or equivalently with q. This means that by increasing $|k|$, i.e. by making the ensemble more 'non-identical', $\sigma(0)$ remains constant and the ensemble has apparently the same 'disorder'. Only when $K \neq 0$ coupling is able to reduce the mean oscillation amplitudes and non-isochronicity effects begin to play a role.

4.4.4 Linear stability analysis

It is possible to apply the techniques developed in Chapter 3 in order to determine the synchronization threshold in the phase equations of Landau-Stuart type (4.45).

The analytic treatment is similar to the one performed in Section 3.2. Thus, if we define an order parameter as in (3.4) the system (4.45) writes

$$\dot{\theta}_i = \omega_i - KR\left[\sin(\theta_i - \theta_j) + q_i(1 - \cos(\theta_i - \theta_j)\right]. \tag{4.49}$$

where now the parameters ω and q are *both* distributed according to the two distributions $g(\omega)$ and $h(\omega)$, respectively. In order to proceed, we follow the following strategy: In the thermodynamic limit it is possible to define a density function $\rho(\theta, \omega, t)$ that evolves according to the continuity equation (3.23). If we consider the evolution of a small disturbance from the incoherent solution it is possible to linearize the continuity equation around the incoherent solution ρ_0, and from this to determine when the stability of ρ_0 is lost, i.e. the value of the synchronization threshold K_c.

Since the function $\rho(\theta, \omega, t)$ is 2π periodic (and real) it can be developed in Fourier series. This permits to write the linearized problem for the first Fourier mode as follows

$$\frac{\partial \rho_1}{\partial t} = -i(\omega + qK)\rho_1 + \frac{K}{2}(1 + iq)\int_{-\infty}^{\infty}\int_{-\infty}^{\infty} \rho_1(t, \omega', q')\ g(\omega')h(q')d\omega' dq', \tag{4.50}$$

and the same complex conjugate equation for the mode -1. The right-hand of (4.50) defines a linear operator that has both continuous and discrete parts. Let

$$\rho_1(t, \omega, q) = b(\omega, q)e^{\lambda t},$$

and hence Eq.(4.50) becomes

$$\lambda b = -i(\omega + qK)b + \frac{K}{2}(1 + iq)\int_{-\infty}^{\infty}\int_{-\infty}^{\infty} b(\omega', q')\ g(\omega')h(q')d\omega' dq', \tag{4.51}$$

where the average integral in the right-hand side of Eq. (4.51) is just a real constant B to be determined self-consistently. Hence solving (4.51) for $b(\omega, q)$ yields

$$b(\omega, q) = \frac{K}{2}\frac{(1 + iq)}{\lambda + i(\omega + qK)}B. \tag{4.52}$$

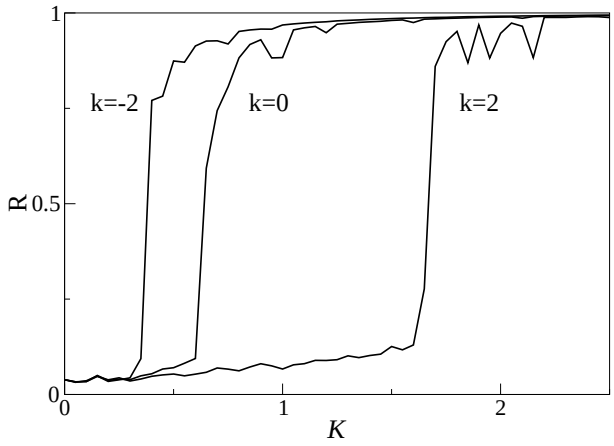

Figure 4.15: Transition to synchronization of 500 oscillators with uniform frequency distribution ($g(\omega) = (2\gamma)^{-1}$) with $\gamma = 0.5$ and with $q = k\omega$ for k=-2 (enhanced synchronization), k=0 and k=2 (anomalous synchronization).

Now invoking self-consistency and without considering the trivial solution $b = 0$, Eq. (4.52) gives

$$1 = \frac{K}{2}\int_{-\infty}^{\infty}\int_{-\infty}^{\infty}\frac{1+iq}{\lambda + i(\omega + qK)}\; g(\omega)h(q)d\omega dq. \tag{4.53}$$

Equation (4.53) can alternatively be written, separating real and imaginary parts, as

$$0 = \int_{-\infty}^{\infty}\int_{-\infty}^{\infty}\frac{q\mathrm{Re}(\lambda) - \omega - \mathrm{Im}(\lambda) - qK}{\mathrm{Re}(\lambda)^2 + (\mathrm{Im}(\lambda) + \omega + qK)^2}\; g(\omega)h(q)d\omega dq \tag{4.54}$$

$$\frac{2}{K} = \int_{-\infty}^{\infty}\int_{-\infty}^{\infty}\frac{\mathrm{Re}(\lambda) + q(\omega + \mathrm{Im}(\lambda) + qK)}{\mathrm{Re}(\lambda)^2 + (\mathrm{Im}(\lambda) + \omega + qK)^2}\; g(\omega)h(q)d\omega dq \tag{4.55}$$

Combining the last two equations, the Eq. (4.55) can be also written as

$$\frac{2}{K} = \int_{-\infty}^{\infty}\int_{-\infty}^{\infty}\frac{\mathrm{Re}(\lambda)(1+q^2)}{\mathrm{Re}(\lambda)^2 + (\mathrm{Im}(\lambda) + \omega + qK)^2}\; g(\omega)h(q)d\omega dq. \tag{4.56}$$

The synchronization threshold K_c can be determined form Eq.(4.56) by performing the limit $\mathrm{Re}(\lambda) \to 0$ which yields

$$K_c = \frac{2}{\pi}\left(\int_{-\infty}^{\infty}\int_{-\infty}^{\infty}\delta(\omega + \mathrm{Im}(\lambda) + qK)(1+q^2)\; g(\omega)h(q)d\omega dq\right)^{-1} \tag{4.57}$$

using the fact that $\mathrm{Re}(\lambda)/(\mathrm{Re}(\lambda)^2 + x^2) \to \pi\delta(x)$ as $\mathrm{Re}(\lambda) \to 0$. This equation has to be calculated once $\mathrm{Im}(\lambda)$ is known through the equation (4.54)

$$\begin{aligned}\int_{-\infty}^{\infty}\int_{-\infty}^{\infty} q\ \delta(\omega + \mathrm{Im}(\lambda) + qK)\ g(\omega)h(q)d\omega dq \\ = \frac{1}{\pi}\int_{-\infty}^{\infty}\int_{-\infty}^{\infty} \frac{1}{\omega + \mathrm{Im}(\lambda) + qK}\ g(\omega)h(q)d\omega dq\end{aligned} \tag{4.58}$$

Let us now suppose that the nonisochronicity and the natural frequency are functionally related, for instance considering $q = k\omega$. Then assuming that $g(\omega)$ is symmetric, the integrals (4.57) and (4.58) can be straightforwardly calculated. Thus, the synchronization threshold yields

$$K_c = \frac{2}{\pi g(0) - k}. \tag{4.59}$$

The Fig. 4.15 shows a numerical simulation of an ensemble of phase oscillators showing anomalous synchronization and enhanced synchronization in good agreement with the critical coupling (4.59).

Chapter 5

Synchronization between populations of phase oscillators

In this Chapter we investigate the possible routes to synchronization taking place between two populations of phase oscillators. Therefore we now combine the phenomenon of mutual synchronization taking place between two single oscillators (studied in Chapter 2) with that of macroscopic mutual entrainment (described in Chapter 3). The results presented here are summarized in (Montbrió et al., 2004b).

The two ensembles are composed of phase oscillators of a Landau-Stuart type. In contrast with Chapter 4 here the inhomogeneities in the populations are only taken into account through a distribution of natural frequencies. Thus, we restrict our study to the phase equations given by (3.19), since the other terms introduced by the nonisochronicities into the phase equations have the trivial effect of rescaling the coupling strength, and shifting the distributions of natural frequencies (see Eq.3.42). Additionally, the model (3.19) is also of interest because it appears naturally in the phase reduction of an array of superconducting Josephson junctions (Wiensenfeld and Swift, 1995; Wiesenfeld et al., 1996). It also has been proved to be useful in modeling information concerning the synaptic connections in a neural network (Hoppensteadt and Izhikevich, 1998) and time delays (Izhikevich, 1998).

5.1 The model

The system under study is

$$\begin{aligned}\dot{\theta}_i^{(1,2)} =& \omega_i^{(1,2)} - \frac{K_p}{N}\sum_{j=1}^{N}\sin(\theta_i^{(1,2)} - \theta_j^{(1,2)} + \alpha) \\ & - \frac{K}{N}\sum_{j=1}^{N}\sin(\theta_i^{(1,2)} - \theta_j^{(2,1)} + \alpha),\end{aligned} \tag{5.1}$$

where $|\alpha| < \pi/2$ and $i = 1, \ldots, N \gg 1$. Here, $\theta_i^{(1,2)}$ describes the phase of the ith oscillator in population 1 or 2, respectively. Both populations have the same size N and are coupled internally with intra-population coupling strength K_p, whereas the inter-population coupling is determined by K. The oscillators within each population have randomly distributed natural frequencies $\omega_i^{(1,2)}$ according to a density $g^{(1,2)}(\omega)$ of width γ that is assumed to be symmetric about the mean $\bar{\omega}^{(1,2)}$ and unimodal. From now on we assume that $\Delta\omega \equiv \bar{\omega}^{(1)} - \bar{\omega}^{(2)} > 0$ and $0 \leq \alpha < \pi/2$.

The phase coherence within each population is described by the two complex order parameters (3.4),

$$R^{(1,2)} e^{i\psi^{(1,2)}} = \frac{1}{N} \sum_{j=1}^{N} e^{i\theta_j^{(1,2)}}, \tag{5.2}$$

for each population, which permits to write system (5.1) in terms of the mean field quantities $R^{(1,2)}$ and $\psi^{(1,2)}$

$$\begin{aligned} \dot{\theta}_i^{(1,2)} =& \omega_i^{(1,2)} - K_p\, R^{(1,2)} \sin(\theta_i^{(1,2)} - \psi^{(1,2)} + \alpha) \\ & - K\, R^{(2,1)} \sin(\theta_i^{(1,2)} - \psi^{(2,1)} + \alpha). \end{aligned} \tag{5.3}$$

If the populations are uncoupled, i.e. $K = 0$, each of them reduces to the well known Kuramoto model with a phase shift α in the coupling function (3.42) studied in Chapter 3. For a given K_p this model exhibits a phase transition at a critical value of the frequency dispersal γ_c. For $\gamma > \gamma_c$ the oscillators rotate with their natural frequencies and $R^{(1,2)} \sim O(\sqrt{1/N})$, but for $\gamma < \gamma_c$ mutual entrainment occurs among a small fraction of oscillators giving rise to a finite value of the order parameter $R^{(1,2)}$. Thus, a cluster of locked oscillators emerges through a Hopf-bifurcation of frequency $\Omega^{(1,2)}$ that, in general ($\alpha \neq 0$), depends on the overall shape of $g^{(1,2)}(\omega)$. The drifting oscillators arrange in a stationary distribution that does not contribute to the order parameters.

On the other hand, in the limit of identical oscillators $\gamma = 0$, the oscillators within each population are all identical and therefore they are able to synchronize in-phase (all the oscillator in each population have exactly the same phase for all times, i.e. $R^{(1,2)} = 1$) for arbitrary small K_p, and hence each population may act exactly as a single oscillator. Note that in this case the observed frequency is $\Omega^{(1,2)} = \bar{\omega}^{(1,2)} - K_p \sin\alpha$, that therefore deviates from $\bar{\omega}^{(1,2)}$ because of $\alpha \neq 0$, as we have seen in Chapter 2.

When $K > 0$ the two locked clusters begin to interact. If this interaction is similar to the frequency adjustment between two coupled oscillators, one expects mutual locking between these two clusters to occur in a saddle-node bifurcation at some critical value $K = K_c$, as we have seen in Chapter 2. Especially, for $\gamma = 0$, synchronization should arise at

$$K_c = \frac{\Delta\omega}{2\cos\alpha}. \tag{5.4}$$

5.2 Linear stability analysis of the incoherent states

In the following we investigate the dynamics of (5.3) in the full (K, γ)-parameter plane. We proceed as in Chapter 3: In the thermodynamic limit a density function can be defined so that $\rho^{(1,2)}(\theta, t, \omega)d\omega d\theta$ describes the number of oscillators with natural frequencies in $[\omega, \omega + d\omega]$ and phase in $[\theta, \theta + d\theta]$ at time t. For fixed ω the distribution $\rho^{(1,2)}(\theta, t, \omega)$ of the phases θ is normalized to unity. The evolution of $\rho^{(1,2)}(\theta, t, \omega)$ obeys the continuity equation $\partial\rho^{(1,2)}/\partial t = -\partial(\rho^{(1,2)}\dot{\theta}^{(1,2)})/\partial\theta$, for which the incoherent state $\rho_0 = (2\pi)^{-1}$ is always a trivial solution. The function $\rho^{(1,2)}(\theta, t, \omega)$ is real and 2π-periodic in θ and therefore admits the Fourier expansion

$$\rho^{(1,2)}(\theta, t, \omega) = \sum_{l=-\infty}^{\infty} \rho_l^{(1,2)}(t, \omega)e^{il\theta}. \tag{5.5}$$

where $\rho_{-l}^{(1,2)} = \rho_l^{*(1,2)}$. Using (5.2) and (5.5) the order parameter can be written in terms of the Fourier components as $R^{(1,2)}e^{i\psi^{(1,2)}} = 2\pi \left\langle \rho_1^{(1,2)*} \right\rangle$ (we use $\left\langle f^{(1,2)}(\omega) \right\rangle$ to denote frequency-average weighted with $g^{(1,2)}(\omega)$, respectively). Now, after inserting (5.3) into the continuity equation, we obtain an infinite system of integro-differential equations for the Fourier modes

$$\begin{aligned} \dot{\rho}_l^{(1,2)} = &- i\omega l\rho_l^{(1,2)} + \\ &l\rho_{l-1}^{(1,2)}\pi e^{i\alpha}\left(K_p\left\langle \rho_1^{(1,2)} \right\rangle + K\left\langle \rho_1^{(2,1)} \right\rangle\right) - \\ &l\rho_{l+1}^{(1,2)}\pi e^{-i\alpha}\left(K_p\left\langle \rho_1^{*(1,2)} \right\rangle + K\left\langle \rho_1^{*(2,1)} \right\rangle\right). \end{aligned} \tag{5.6}$$

The stability of ρ_0 can be analyzed by studying the evolution of a perturbed state $\rho^{(1,2)}(\theta, t, \omega)$ close to ρ_0 (note that $\rho_l^{(1,2)}$ are then small quantities). Linearization of (5.6) reveals that the only potentially unstable modes are $l = \pm 1$ and hence $l = 1$ has solution $\rho_1^{(1,2)}(t, \omega) = b^{(1,2)}(\omega)e^{\lambda t} + O(|\rho_l|^2)$. This leads to

$$b^{(1,2)}(\omega) = \left(K_p\left\langle b^{(1,2)}(\omega) \right\rangle + K\left\langle b^{(2,1)}(\omega) \right\rangle\right)\frac{e^{i\alpha}/2}{\lambda + i\omega}. \tag{5.7}$$

the self-consistent problem (5.7) can be solved analytically. Eq (5.7) can be written as

$$2\left\langle b^{(1,2)}(\omega) \right\rangle e^{-i\alpha} = \left(K_p\left\langle b^{(1,2)}(\omega) \right\rangle + K\left\langle b^{(2,1)}(\omega) \right\rangle\right)\int_{-\infty}^{\infty}\frac{1}{\lambda + i\omega}g^{(1,2)}(\omega)d\omega. \tag{5.8}$$

If the distribution of frequencies is considered to be of Lorentzian type, $g^{(1,2)}(\omega) = (\gamma/\pi)[\gamma^2 + (\omega - \bar{\omega}^{(1,2)})^2]^{-1}$, then the integral in the right hand of Eq.(5.8) can be solved analytically. First, the integrand is extended to the complex plane

$$\int_{-\infty}^{\infty}\frac{1}{\lambda + i\omega}g^{(1,2)}(\omega)d\omega = \frac{-i\gamma}{\pi}\oint_C \frac{dz}{(z - i\lambda)(z - (\bar{\omega}^{(1,2)} + i\gamma))(z - (\bar{\omega}^{(1,2)} - i\gamma))},$$

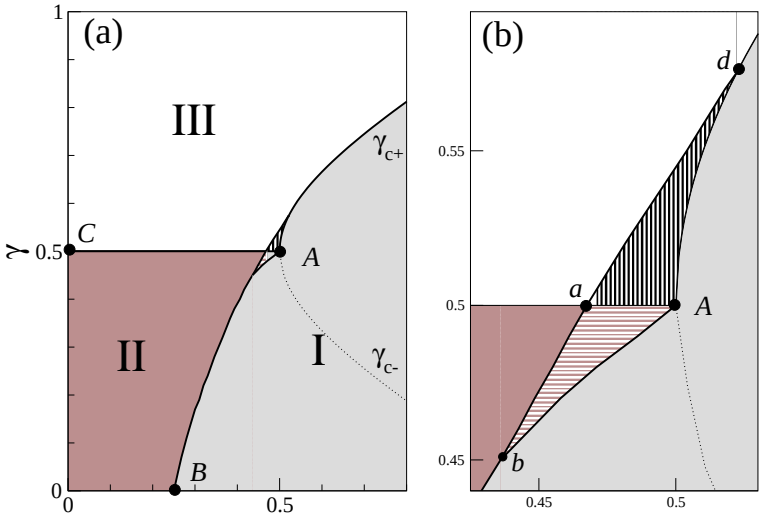

Figure 5.1: (K, γ) phase diagram of system (5.1) assuming Lorentzian frequency distributions, $\Delta\omega = 1/2$, $K_p = 1$ and for $\alpha = 0$. Fig.(b) in an enlarged region of Fig.(a). Numerical stability boundaries ($N = 1000$) are indicated as solid lines. The dotted line represents the analytical stability boundaries γ_{c-} obtained from (5.9) whereas the boundary γ_{c+} fully overlaps with numerical results. Region I: synchronization. Region II: coexistence. Region III: incoherence. (b) Enlarged region where bistability between states I and II (horizontal dashed) and between states III and I (vertical dashed) is observed.

where the real axis has been extended to the closed contour C by attaching a half-circle in the upper half-plane. The integrand has two simple poles, at $z = i\lambda$ and $z = \bar{\omega}^{(1,2)} + i\gamma$, and thus using the residue theorem the integral gives

$$\begin{aligned}\int_{-\infty}^{\infty} \frac{1}{\lambda + i\omega} g^{(1,2)}(\omega) d\omega &= \frac{2\gamma}{(i\lambda - (\bar{\omega}^{(1,2)} - i\gamma))(i\lambda - (\bar{\omega}^{(1,2)} + i\gamma))} \\ &\quad - \frac{i}{(\bar{\omega}^{(1,2)} + i\gamma - i\lambda)} = \\ &= \frac{\gamma - \lambda - i\bar{\omega}^{(1,2)}}{\gamma^2 + (\bar{\omega}^{(1,2)} - i\lambda)^2}.\end{aligned}$$

Substituting the previous result into Eq. (5.8), this equation can be solved for λ and gives

$$\lambda_{\pm} = -\gamma + \frac{K_p e^{i\alpha}}{2} \pm \frac{1}{2}\sqrt{K^2 e^{i2\alpha} - \Delta\omega^2} - i\bar{\omega}, \tag{5.9}$$

with $\bar{\omega} \equiv (\bar{\omega}^{(1)} + \bar{\omega}^{(2)})/2$. Thus the stability of the incoherent state ρ_0 is described by the two complex eigenvalues (5.9) for mode $l = 1$, and the complex conjugate for $l = -1$.

Imposing $\mathrm{Re}(\lambda_{\pm}) = 0$ defines explicitly the two critical curves $\gamma_{c\pm}(K)$ (see Figs. 5.1, 5.5 and 5.9 where the stability boundaries in the γ-K parameter space

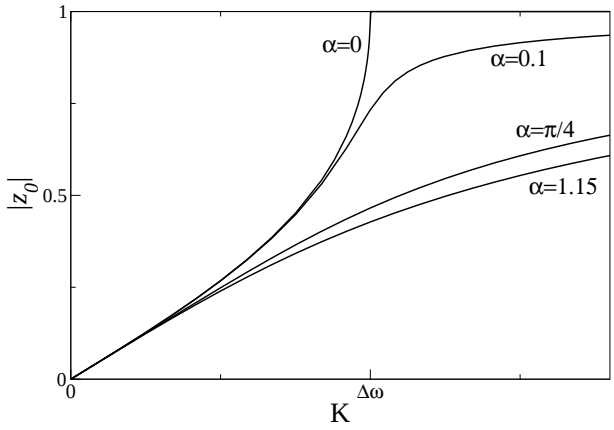

Figure 5.2: Complex modulus of the function z_0 (Eq.(5.11)), for different values of the parameter α (in rad.).

are depicted for increasing values of α). Each curve represents a Hopf bifurcation with frequency given by $\Omega_\pm \equiv -\mathrm{Im}(\lambda_\pm)$. The largest eigenvalue determines the stability of the incoherent state (III), and therefore the curve $\max(\gamma_{c+}, \gamma_{c-}) = \gamma_{c+}$ separates the region where the incoherent solution III is stable from the unstable regions, marked as I and II in the stability diagrams.

The eigenmodes $\left\langle \rho^{(1,2)}(\theta, t, \omega) \right\rangle$ near criticality are

$$\begin{pmatrix} \langle \rho^{(1)} \rangle \\ \langle \rho^{(2)} \rangle \end{pmatrix} = \begin{pmatrix} 1/2\pi \\ 1/2\pi \end{pmatrix} + Z_+(t) \begin{pmatrix} -iz_0 \\ 1 \end{pmatrix} e^{i(\theta - \Omega_+ t)} + \text{c.c.} + \\ Z_-(t) \begin{pmatrix} 1 \\ iz_0 \end{pmatrix} e^{i(\theta - \Omega_- t)} + \text{c.c.} + O(|Z|^2), \tag{5.10}$$

where $Z_\pm(t) \equiv e^{\mathrm{Re}(\lambda_\pm)t}$ and c.c. denotes the complex conjugate of the preceding term. The modulus of the number

$$z_0 \equiv \frac{e^{-i\alpha}}{K}(\Delta\omega - \sqrt{\Delta\omega^2 - e^{i2\alpha}K^2}), \tag{5.11}$$

is a weight for the fraction frequencies Ω_+ and Ω_- in populations 1 and 2, respectively. The function $|z_0|$ as a function of K is depicted in Fig.5.2 for different values of α.

5.3 The symmetric case, $\alpha = 0$

The first important result is that our results coincide with those of Okuda and Kuramoto (1991) when the width of the frequency distribution is substituted by

the intensity of the noise. The eigenvalues in this case are simply

$$\lambda_{\pm} = -\gamma + \frac{K_p}{2} \pm \frac{1}{2}\sqrt{K^2 - \Delta\omega^2} - i\bar{\omega}, \tag{5.12}$$

From the eigenvalues (5.12) the state III can become unstable in two different ways, depending on the sign of $(K - \Delta\omega)$:

- When $K > \Delta\omega$ the transition III-I takes place through a single Hopf bifurcation and both populations synchronize to the same frequency $\Omega = \bar{\omega}$. The presence of a single macroscopic oscillation is denoted as *region I*.

- When $K < \Delta\omega$ the instability is through a *degenerated* Hopf bifurcation. Both (λ_+, λ_+^*) and (λ_-, λ_-^*) cross simultaneously the imaginary axis at $\gamma_{c\pm} = \gamma_c = K_p/2$ (line $\overline{CA}$) and two macroscopic oscillations with frequencies

  $$\Omega_{\pm} = \mp\frac{1}{2}\sqrt{\Delta\omega^2 - K^2} + \bar{\omega}, \tag{5.13}$$

  emerge. The region of coexistence of two different macroscopic fields is labeled as *region II*. Note that this result is a consequence of the reflectional symmetry of the model (5.1) [1].

  Observe that when $K = 0$ the amplitudes are $|z_0| = 0$ in (5.10), and hence, if $\gamma < \gamma_c$, the phase of the order parameters evolves uniformly, i.e. $\psi^{(1)} = \Omega_- t$ and $\psi^{(2)} = \Omega_+ t$. On the other hand, when $\Delta\omega = K$ then the function is $|z_0| = 1$, indicating synchronization of the order parameters.

The coupling-modified frequencies of the individual oscillators, provide a useful measure of synchronization: when $K = 0$ the frequency-locked oscillators form a single plateau that is the only contribution to the fields (5.2), as it it shown in Fig.5.3(a). Thus, the phase of each order parameter evolves linearly in time according to $\psi^{(1)} = \bar{\omega}^{(1)}/t$ and $\psi^{(2)} = \bar{\omega}^{(2)}/t$, i.e. the phase difference of the order parameters also grows uniformly as $\Delta\psi(t) = \psi^{(1)}(t) - \psi^{(2)}(t)$. The time evolution of the order parameter of population 1 is depicted in Fig.5.4(a) (the population 2 behaves as population 1 due to the reflection symmetry, and therefore we show only the order parameters corresponding to the first population).

With further increases in K, some of the oscillators in populations 1 and 2 begin to lock in a second plateau at Ω_+ and Ω_-, respectively, in accord to (5.10) (see Fig.5.3(b)). Hence, $R^{(1,2)}$ begin to oscillate with frequency $\Delta\Omega = \Omega_- - \Omega_+$ (Fig.5.4(b)). With further increases in K the system approaches the saddle node

[1] When $\alpha = 0$, a reflection ($\theta_i^{(1,2)} \to -\theta_i^{(1,2)}$ and $\omega_i^{(1,2)} \to -\omega_i^{(1,2)}$) in the rotating frame moving with frequency $(\bar{\omega}^{(1)} + \bar{\omega}^{(2)})/2$ leaves the system (5.1) invariant. Otherwise the system in invariant under the transformation ($\theta_i^{(1,2)} \to -\theta_i^{(1,2)}$, $\omega_i^{(1,2)} \to -\omega_i^{(1,2)}$, $\alpha \to -\alpha$).

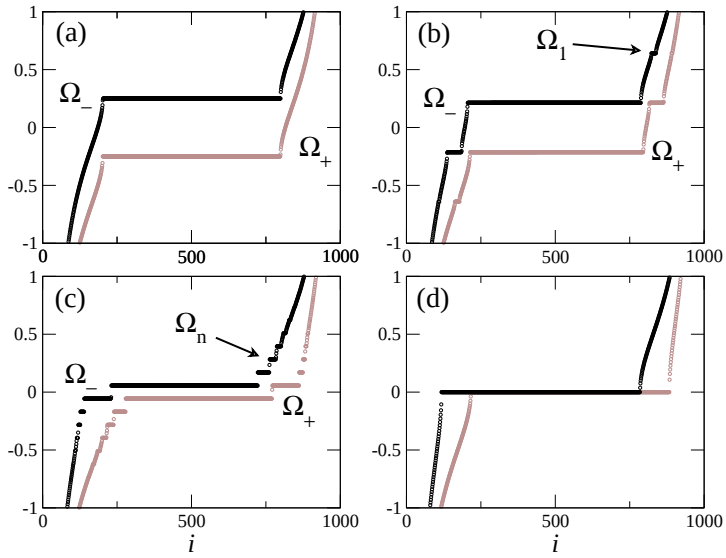

Figure 5.3: Coupling-modified frequencies $\tilde{\omega}_i$ of populations 1(:black) and 2(:grey) as a function of the oscillator's index i: oscillator i has natural frequency $\omega_i^{(1,2)} = \bar{\omega}^{(1,2)} + \gamma \tan\left[(\pi/2)(2i - N - 1)/(N + 1)\right]$ (Lorentzian) $\alpha = 0$, $\gamma = 0.4$ and (a) $K = 0$, (b) $K = 0.2$, (c) $K = 0.4$, (d) $K = 0.41$. ($\Delta\omega = 1/2$, $\bar{\omega} = 0$, $K_p = 1$ $N = 1000$).

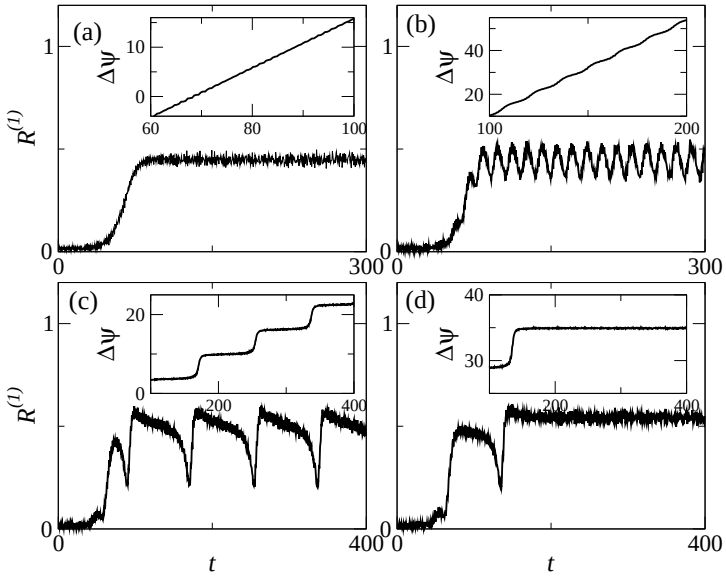

Figure 5.4: Time evolution of the order parameter of population 1 from a random initial condition to the state I (Figs. (a,b,c)) or II (Fig.(c)) ($\alpha = 0$, $K_p = 1$, $\gamma = 0.4$, Lorentzian distributions) for (a) $K = 0$, (b) $K = 0.2$,(c) $K = 0.4$, (d) $K = 0.41$. The population size is $N = 1000$ and the state of the system at time $t = 0$ random initial conditions

line $\overline{Ba}$ (see Figs 5.3(c) and 5.4(c)) from the region II. At this line the synchronized state is reached, $\delta\Omega = 0$, and the populations become synchronized (see Figs 5.3(d) and 5.4(d)).

Note that our analysis gives

$$T = 2\pi/\Delta\Omega \sim 1/\sqrt{\Delta\omega^2 - K^2}, \tag{5.14}$$

and hence the saddle-node bifurcation should take place at $K_c = \Delta\omega$ for all $\gamma < \gamma_c$ which deviates from the numerical line $\overline{Ba}$ even for $\gamma = \gamma_c$. The inset of Fig.5.1(a) shows how the saddle-node line $\overline{bad}$ crosses the degenerated Hopf line γ_c at point a, and joins the Hopf curve γ_{c+} at the codimension-2 point d. Consequently the Hopf bifurcation is supercritical all along the curve γ_{c+}, except in the vicinity of point A (line $\overline{aAd}$) where it is subcritical and therefore a small region of bistability between states III/I and II/I is observed.

5.3.1 Higher-order entrainment

In the Chapter 3 we have discussed how the drifting oscillators behave in the presence of a cluster of mutually entrained elements in the ensemble. In particular, the drifting oscillators form a stationary distribution which do not contribute to the coherence, and each individual oscillator behaves exactly as if it was forced by an external periodic field, independently from all the other drifting oscillators. In the present study, the situation is different: The drifting oscillators are coupled to two distinct fields with different effective coupling strengths $K_p R^{(1,2)}$ and $K R^{(2,1)}$. In this section we investigate such effects over the drifting oscillators.

From Figs.5.3 we can see that there is an important contribution to the order parameters which has not been taken into account by the linear theory developed in the previous section. In Figs.5.3(b) and 5.3(c) we observe clusters of frequency-synchronized oscillators with mean frequencies that are not the frequencies Ω_+ and Ω_-. Specifically, these frequencies do not appear in the the eigenmodes (5.10): It is obvious that the new locked oscillators must generate a coherent field that will sum up together with the contributions of the main clusters, and hence it should be included in the equations describing the mean fields of populations 1 and 2.

On the other hand, the Figs.5.3 show that the number of new plateaus as well as their size grows as the system approaches the saddle-node bifurcation $\overline{Ba}$ from the region of coexistence II. Therefore the new contribution to the order parameters must be also increasingly significant close to the bifurcating line $\overline{Ba}$ (within region II). At this line the synchronized state I is reached, so $\Delta\Omega = 0$, and the steps disappear abruptly, as it can be seen in Fig.5.3(c). We will see in the next section that in the asymmetric case the new clusters can even provoke synchronization of the populations within region II.

From our numerics we observe that the new clusters emerge due to mutual entrainment of the drifting oscillators having frequencies $\tilde{\omega}_i^{(1,2)}$ close to

$$\Omega_n = \Omega_- + n\Delta\Omega, \quad \text{where} \quad n = 1, \pm 2, \pm 3.... \tag{5.15}$$

In the following we discuss the dynamics of the drifting oscillators: If we start with initial conditions corresponding to the incoherent state, the linear stability analysis indicates that the first thing to occur is the emergence of the two clusters of frequencies Ω_+ and Ω_-. As we have seen, the degenerated Hopf bifurcation leading to region II is supercritical except in a small region close to point A (see diagram 5.5). Therefore the amplitude of the emergent fields is small close to criticality and the solutions (5.10) are of validity.

Consequently, a drifting oscillator is actually forced by the two mean fields (5.10) not far -in the parameter space- from the incoherent state. Thus its dynamical equation is given by Eq.(5.3) with the mean fields near criticality (5.10). Moreover, exploiting the rotational symmetry of the model (5.3) it is always possible to go into a rotating frame such that in the new coordinates $\bar{\omega} = 0$ (see Chapter (3). After this the system is symmetric with respect reflections and therefore $R \equiv R^{(1)} = R^{(2)}$ and $\psi \equiv \psi^{(1)} = -\psi^{(2)}$. This allows us to write without loss of generality the Eq.(5.3) for the drifting oscillators in population 1 as

$$\dot{\theta}_i^{(1)} = \omega_i^{(1)} - R[(K + K_p)\sin\theta_i^{(1)}\cos\psi + (K - K_p)\cos\theta_i^{(1)}\sin\psi], \tag{5.16}$$

where $R(t)$ is a time-periodic function given by Eq.(5.10) (with period T and given by Eq.(5.14)), and ψ is a monotonically increasing function of t with slope Ω_-.

In order to simplify the analysis let us assume that $K_p = K$, i.e. a bimodal frequency distribution. Then Eq.(5.16) becomes

$$\dot{\theta}_i^{(1)} = \omega_i^{(1)} - f(t)\sin\theta_i^{(1)}, \tag{5.17}$$

where

$$f(t) \equiv 2KR(t)\cos\psi(t),$$

is a periodic function, with period given by $2T$. The function $R(t)$ is positive and has its minimum exactly when $\psi = \pi/2$. Therefore we can consider that the drifting oscillators are governed by the Adler equation (2.18) with a time periodic coupling. Such system produces similar higher order entrainment as the one observed in Figs 5.3.

The observation of similar clusters was reported by Sakaguchi (1988) in an externally periodically forced population of nonidentical phase oscillators, even though their origin was not explained. Additionally similar locking plateaus appear in when an external periodic forcing is applied to a single phase oscillator (for a derivation for a weakly nonlinear Van der Pol oscillator under a general

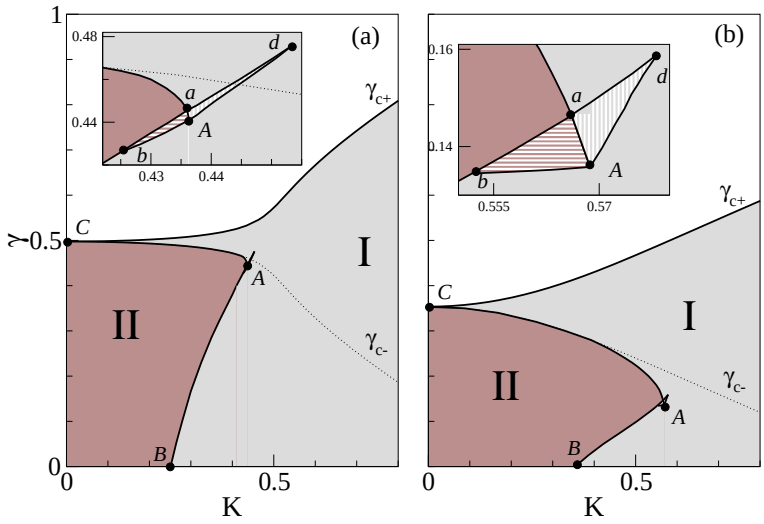

Figure 5.5: (K, γ) phase diagram of system (5.1) assuming Lorentzian frequency distributions, $\Delta\omega = 1/2$, $K_p = 1$, and for different values of α (in rad.): (a) $\alpha = 0.1$ and (b) $\alpha = \pi/4$. Numerical stability boundaries ($N = 1000$) are indicated as solid lines. Dotted lines represent analytical stability boundaries $\gamma_{c\pm}$ obtained from (5.9). Note that γ_{c+} fully overlaps with numerical results. Region I: synchronization. Region II: coexistence. Region III: incoherence. Insets: bistability in the dashed regions around A (see text).

external periodic forcing see Landa (1996)). In such case the emergent plateaus are known as *Shapiro steps* (Shapiro, 1963; Shapiro et al., 1964), and it has been shown that their effect over a population of nonidentical oscillators with randomly distributed coupling strengths leads to periodic synchronization (Choi et al., 1994).

5.4 The asymmetric case, $\alpha > 0$

As α is increased from zero the bifurcating lines γ_{c+} and γ_{c-} split due to the breaking of symmetry. Interestingly, the eigenmodes (5.10) do not reflect the asymmetry through the amplitudes $|z_0|$, but only through the different exponential growths $Z_\pm(t)$. Figs.5.6 show the modified frequencies of the oscillators for $\alpha = \pi/4$ (Fig.5.5(b)), keeping K constant and decreasing γ continuously from region III.

We find that incoherence (Fig.5.6(a)) only goes unstable through a single Hopf bifurcation γ_{c+} (at Ω_+ in Fig.5.6(b)) and hence nucleation first takes place *mainly* within population 2.

The second Hopf bifurcation (at Ω_- in Fig.5.6(c)) follows γ_{c-} as far as the system is close enough to the incoherent state III. Fig.5.7(a) shows the order parameters of the populations in the region II close to the bifurcating line γ_{c-}.As γ is decreased further the system approaches the saddle-node bifurcation, $\overline{Bd}$, and an

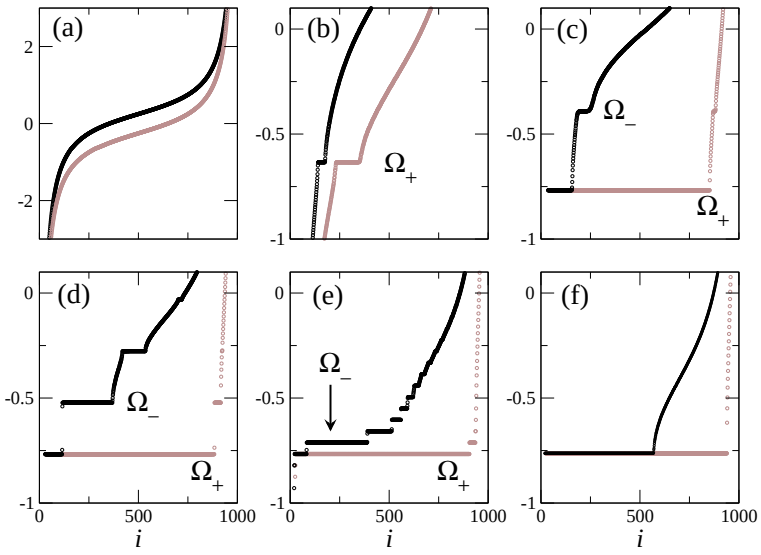

Figure 5.6: Coupling-modified frequencies $\bar{\omega}_i$ of populations 1(:black) and 2(:grey) as a function of the oscillator's index i: oscillator i has natural frequency $\omega_i^{(1,2)} = \bar{\omega}^{(1,2)} + \gamma \tan\left[(\pi/2)(2i - N - 1)/(N + 1)\right]$ (Lorentzian), for $\alpha = \pi/4$, $K = 0.53$ and (a) $\gamma = 0.5$, (b) $\gamma = 0.47$, (c) $\gamma = 0.187$, (d) $\gamma = 0.15$, (e) $\gamma = 0.13$, (f) $\gamma = 0.118$. ($\Delta\omega = 1/2$, $\bar{\omega} = 0$, $K_p = 1$ and $N = 1000$).

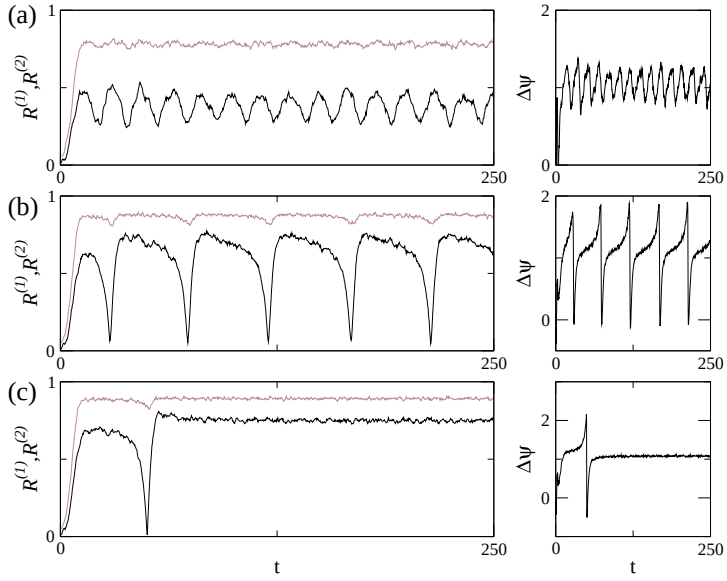

Figure 5.7: Order parameters $R^{(1)}$ (black) and $R^{(2)}$ (grey) and phase difference $\Delta\psi$ as a function of time for $\alpha = \pi/4$, $K = 0.53$ $N = 1000$, $\Delta\omega = 0.5$, $\bar{\omega} = 0$, $K_p = 1$. At $t = 0$ the phases were randomly distributed in $(0, 2\pi]$. Plots (a) $\gamma = 0.187$ (Fig.5.6(c)) and (b) $\gamma = 0.13$ (Fig.5.6(e)) correspond to parameter values within the region of coexistence II. Plot (c) $\gamma = 0.118$ (Fig.5.6(f)) corresponds to the synchronized region I.

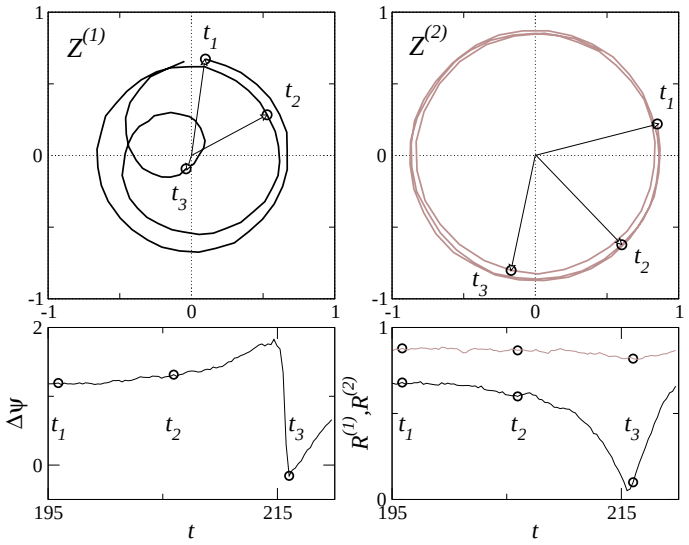

Figure 5.8: Characteristic population dynamics during a short period of time in the region of coexistence II, close to the saddle-node bifurcation for $\alpha = \pi/4$ (see diagram 5.5(b)). The parameters have been set as in Fig.5.7(b) and Fig.5.6(e) ($K = 0.53$, $\gamma = 0.13$, $\Delta\omega = 0.5$, $\bar{\omega} = 0$, $K_p = 1$, $N = 1000$, Lorentzian distribution). In the first row the complex order parameters $Z^{(1)}$ and $Z^{(2)}$ are shown for $t : [195, 220]$ an well as the order parameters at three different times t_1, $t_2 = t_1 + \Delta t$ and $t_3 = t_1 + 2\Delta t$. In the second row the phase difference $\Delta\psi$ (in rad.) (right) and the order parameters $R^{(1)}$ and $R^{(2)}$ (left) in the corresponding time interval are shown.

increasing number of oscillators in population 1 become entrained to the frequencies given by (5.15) (see Figs.5.6(d,e)). In consequence the order parameter $R^{(1)}(t)$ oscillates with frequency $\Delta\Omega$ with a large amplitude whereas $R^{(2)}(t)$ remains almost constant (Fig.5.7(b)). The phase difference between the order parameters $\Delta\psi(t) \equiv \psi^{(1)} - \psi^{(2)}$ reveals the presence of such clusters (see Fig. 5.8): $\Delta\psi(t)$ (Figs.5.7(a,b)) is bounded despite the fact that the populations are not locked in frequency (Fig.5.6(c,e)).

The bistability regions - enlarged in the insets of Figs.5.5(a,b) - are located near the intersection a of the Hopf line $\overline{CA}$ with the saddle-node line $\overline{Bd}$. Within the region enclosed by Aba the states I and II coexist, as in the $\alpha = 0$ case. In contrast, the region enclosed byAad is surrounded only by the region I and bistability between a small and a large amplitude of the synchronized oscillation in population 1 is observed.

With increase in α, the synchronization regions I and II become gradually smaller because as $\alpha \to \pi/2$ synchronization is increasingly inhibited due to frustration (Daido, 1987; Bonilla et al., 1993). At the same time, the number $|z_0|$ decreases indicating a lower degree of synchronization between the populations.

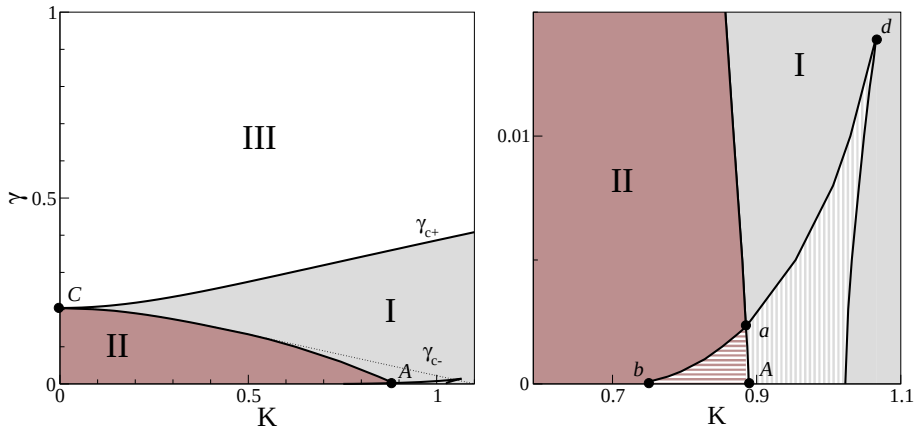

Figure 5.9: (K, γ) phase diagram of system (5.1) assuming Lorentzian frequency distributions, $\Delta\omega = 1/2$, $K_p = 1$, and $\alpha = 1.15$. Numerical stability boundaries ($N = 1000$) are indicated as solid lines. Dotted lines represent analytical stability boundaries $\gamma_{c\pm}$ obtained from (5.9). Note that γ_{c+} fully overlaps with numerical results. Region I: synchronization. Region II: coexistence. Region III: incoherence. Left panel: regions of bistability in the dashed regions around A (see text).

This is in qualitative agreement with the approaching of the saddle node line to the $\gamma = 0$ axis (see Figs. 5.5). At the critical value $\alpha = \alpha^*$ the saddle-node line collides with the $\gamma = 0$ axis and disappears, as it is shown in Fig. 5.9. Note also that the regions of bistability spread in a larger region around the end of the Hopf line A. Therefore, for $\alpha > \alpha^*$ synchronization between the populations *always* occurs when the oscillation of frequency Ω_- dies in the Hopf bifurcation γ_-.

5.5 The limit $\gamma = 0$

The limit identical oscillators in each population $\gamma = 0$ is of special interest. First note that the transition point B simply follows Eq.(5.4) as far as $\alpha < \alpha^*$. Since the oscillators within each population are identical, they synchronize in-phase, $R^{(1,2)} = 1$, and the population's dynamics reduce to that of a system of two identical oscillators. However, for $\alpha > \alpha^*$ the synchronization transition occurs via a Hopf bifurcation A, and thus the behavior in each population is of higher complexity (see Fig.5.10).

As soon as α reaches the critical value α^* (point P), the curve K_c splits in two bifurcating lines, K_c^I and K_c^{II}, that enclose the new regions II' and I' where the order parameters are not synchronized (Fig.5.11) and synchronized (Fig.5.12), respectively. Within those regions the oscillators in population 1 are not in-phase synchronized and hence $R^{(1)}(t) < 1$, whereas the population 2 shows perfect in-phase entrainment $R^{(2)}(t) = 1$. We point out that $R^{(1)}(t)$ strongly depends on the

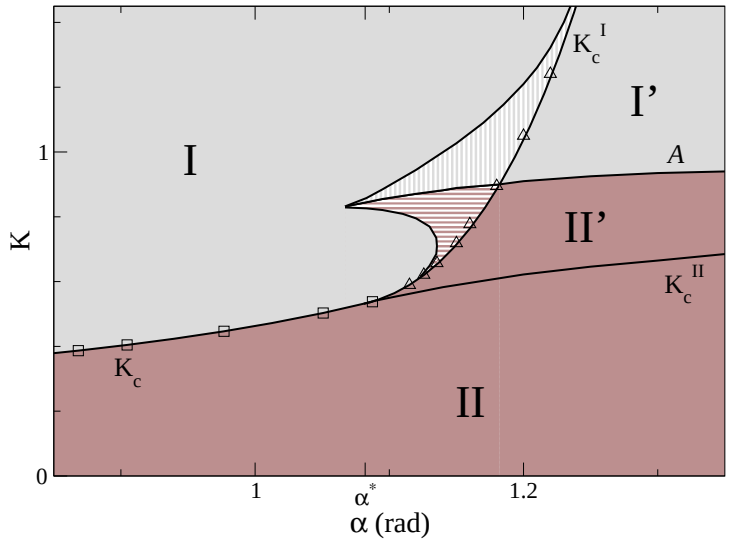

Figure 5.10: Phase diagram (α, K) for $\gamma = 0$. Boundaries K_c and K_c^I are obtained analytically from Eqs.(5.4) and (5.18), respectively, whereas the symbols correspond to numerical results. All other boundaries are determined numerically. Regions I (synchronization) and II (drift) characterized by $R^{(1,2)} = 1$. Within regions I' ($\Delta\psi(t)$ bounded) and II' ($\Delta\psi(t)$ not bounded) $R^{(1)} < 1$ whereas $R^{(2)} = 1$ (see text). Dashed regions present bistability between states I and II' (horizontal) and between I and I' (vertical).

initial conditions whereas $\Delta\psi(t)$ and $R^{(2)}(t)$ not, as it can be seen by in Figs. 5.11 (region II') and Figs .5.12 (region I').

5.5.1 Linear stability analysis of the 2-oscillator locked state

Finally we outline the linear stability analysis of the in-phase synchronized state in population 1 when the populations are locked (region I).

As we have seen in Chapter 2 the phase difference of two synchronized non-identical phase oscillators yields $\Delta\psi = \arcsin \Delta\omega/(2K\cos\alpha)$, and hence this also holds for the two in-phase synchronized populations in state I. Then linearization of (5.1) results in a simple Jacobi matrix with one eigenvalue $N-1$ eigenvalues μ_+ and $N-1$ eigenvalues μ_- characterizing the stability of the in-phase state of populations 1 and 2, respectively

$$\mu\pm = K_p \cos\alpha + K\cos(\pm\Delta\psi + \alpha) < 0, \tag{5.18}$$

and two eigenvalues $\mu_0 = 0$ and $\mu_c = -2K\cos\alpha\cos\Delta\psi$ [2]. Since $\pi/2 > \Delta\psi > 0$, the condition (5.18) is only violated for the population 1, and hence $\mu_+ = 0$ determines the boundary K_c^I and thus, the point P in very good agreement to numerics (Fig.5.10).

[2]Note that $\mu_c = 0$ leads to Eq.(5.4)

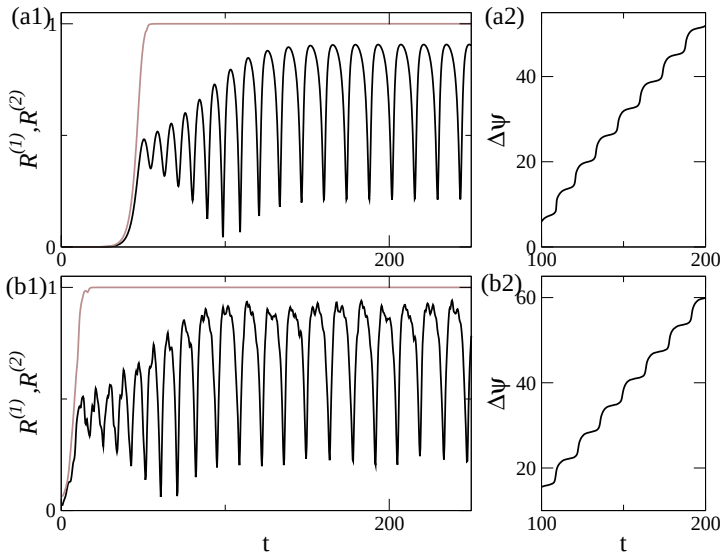

Figure 5.11: Order parameters $R^{(1)}$ (black) and $R^{(2)}$ (grey) and phase difference $\Delta\psi$ as a function of time ($N = 1000$, $\Delta\omega = 0.5$, $\bar{\omega} = 0$, $K_p = 1$). At $t = 0$ the phases were *equally spaced* in $(0, 2\pi]$. corresponding to parameter values in region II' ($\alpha = 1.2$, $K = 0.8$), (see Fig.5.10).

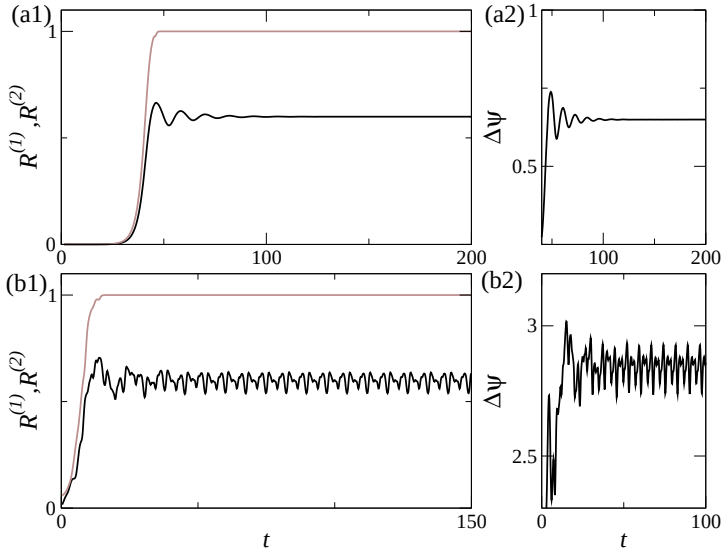

Figure 5.12: Order parameters $R^{(1)}$ (black) and $R^{(2)}$ (grey) and phase difference $\Delta\psi$ as a function of time ($N = 1000$, $\Delta\omega = 0.5$, $\bar{\omega} = 0$, $K_p = 1$). At $t = 0$ the phases *randomly distributed* in $(0, 2\pi]$. (a) corresponds to parameter values within region I' ($\alpha = 1.2$, $K = 1.05$), (see Fig.5.10).

Notice that with $K = 0$ we recover the in-phase stability condition for a single population, $K_p \cos\alpha > 0$. For $|\alpha| > \pi/2$ this state becomes unstable and reaches a new (splay) state, which is neutrally stable. The splay state has been the subject of intense theoretical work due to the applications in devices consisting of superconducting Josephson Junctions (Wiensenfeld and Swift, 1995; Watanabe and Strogatz, 1993). In the present case, however, even for $|\alpha| < \pi/2$ the in-phase state in one population can be destabilized (population 1) or overstabilized (population 2) due to the interaction with the other population. The global stability properties of the states I' and II' are interesting directions of further study.

Chapter 6

Conclusion

This work was devoted to an investigation of synchronization in large ensembles of nonidentical oscillators, with special emphasis on the effects that nonisochronicity bears upon the synchronization process.

The work presented in this thesis has been focused on two particular problems:

- A *population of oscillators with inherent disorder in the nonisochronicities, in addition to the disorder in the natural frequencies.* In this context the new phenomenon of 'anomalous synchronization' has been discovered, in which small coupling is able to increase the frequency disorder, inducing a spread of the oscillator frequencies. It has been demonstrated that occurs naturally in groups of globally and locally coupled oscillatory systems of different types: phase oscillators, limit cycles and chaotic oscillators (Blasius et al., 2003; Montbrió and Blasius, 2003; Montbrió et al., 2004a) [1].

- A study of the routes leading to synchronization between *two populations of globally coupled oscillators* (Montbrió et al., 2004b). The systems that have been used are phase oscillators of a Landau-Stuart type. In this case the inhomogeneity in the ensemble has been introduced simply through the natural frequencies whereas the nonisochronicity has been considered to be constant for all the elements in the ensembles. However, it has been demonstrated that the presence of nonisochronicity plays a significant role, because it induces a breaking of the reflectional symmetry properties of the purely isochronous system.

Altogether these results stress the importance of considering the presence of nonisochronicity in the synchronization theory.

[1] Additionally, anomalous synchronization has been recently observed in coupled spatially extended systems of a Ginzburg-Landau type (Bragard et al., 2003, 2004), and also experimentally in coupled Chua's circuits (Dana et al., 2004).

6.1 Results

6.1.1 Anomalous synchronization

In the Chapter 4 of this thesis anomalous synchronization has been described analytically in the regime of weak coupling and the validity of these results has been numerically confirmed for a number of different models. It has been demonstrated that the effect emerges because the interaction perturbs the oscillators away from their attractors. This brings the nonisochronicity of the oscillation into play. Disorder enlargement occurs if nonisochronicity has positive covariance with the natural frequency of oscillation. As such, it is a universal effect and generically appears when inherent disorder is affecting more than one characteristics of the system. Among all known coupling-induced effects anomalous synchronization stands out, since the effect sets in without a threshold, whereas usually coupling-induced instabilities arise only when the coupling level is larger than a critical threshold.

On the other hand, it has been shown that anomalous synchronization effects have consequences for the large coupling regime. In particular, they strongly control the synchronization threshold. Therefore anomalous synchronization might have important applications for the synchronization and control of large ensembles of coupled oscillators. With appropriate choice of system parameters it is possible to change the synchronization transition of the system, and in this way either to increase or decrease the onset of synchronization. This was particularly clear in the case of ensembles of globally coupled phase oscillators, for which an analytical expression for the synchronization threshold was obtained (Montbrió et al., 2004a). For more general systems, the control of the onset of synchronization was achieved when different parameters of the system were simultaneously affected by the disorder. On the other hand, it was shown that there are also classes of oscillators, like for example predator-prey systems, for which this is automatically achieved by distributing only one parameter.

Anomalous synchronization has implications for biological systems which are typically characterized by large amounts of inherent disorder. In many cases strong synchronization is desirable for biological reasons. Therefore, it is quite possible that evolution has made use of this effect by selecting organisms with (anti)correlated system parameters in such a way as to speed up synchronization and by this to compensate the natural heterogeneity of all living environments.

On the other hand there are situations where synchronization is regarded as dangerous. For example, it is known that synchronization of fluctuating population numbers is strongly connected to the risk of global species extinction (Heino et al., 1997; Earn et al., 2000). Such synchronization effects are now understood to be critical in controlling the regional extinction rates of endangered species. This is because asynchrony between a set of patch populations makes it possible to 'spread the risk' of survival in a fluctuating environment and increases the chances

of global persistence. Synchronization, on the other hand, tends to increase the extinction probability. In this context, the above findings of the presence of anomalous synchronization in typical ecological models obtain a particular importance. Because of the presence of the anomaly spatially extended ecological systems are not synchronized for levels of coupling which otherwise would have led to collective, and therefore dangerous, cycles. In this respect the anomalous synchrony inhibiting effect of coupling, which we find in ecological predator-prey models, may have important consequences for conservation ecology.

6.1.2 Synchronization between populations of oscillators

In Chapter 5 the presence of nonisochronicity has been proved to be important in the transition to synchronization of two globally coupled populations of nonidentical phase oscillators of a Landau-Stuart type. The isochronicity in the phase equations is modelized simply by introducing a phase shift α in the coupling function of the usual Kuramoto model.

The system has been investigated numerically in a broad region of its parameter space. Additionally analytical results were provided close to the onset of synchronization, studying the linear stability analysis of the incoherent states (or desynchronized states) of the ensembles. Altogether, the analytical and the numerical results, have been presented in several bifurcating diagrams, whereas the parameter regions with more interesting dynamical behavior have been analyzed in detail.

The analysis has been organized in two different sections in order to understand the effect the nonisochronicity in the system:

- *The isochronous case*:
  - We have found that the incoherent state can become unstable in two different ways: Either through a *single* or through a *degenerated* Hopf bifurcation. The analytical stability boundaries show good agreement with the numerics. The nonisochronous system possesses a reflectional symmetry, that produces identical behavior in both populations. This symmetry is reflected in the degeneracy of the Hopf bifurcating line, that leads to similar nucleation within each population.
  - The synchronization between the macroscopic fields occurs *always* via a saddle-node bifurcation, as in the synchronization of two single oscillators. Around the intersection of the saddle-node with the Hopf bifurcations, *bistability* is observed.
  - The coupling-modified frequencies show *higher-order entrainment* in the region of coexistence of the oscillations. The effect of the new synchronized clusters on the order parameters is relevant when the systems are

close to the saddle-node bifurcation. This phenomenon is not explained by the critical eigenvectors. However, it can be understood considering that the drifting oscillators are forced by two order parameters (one from each population).

- *The nonisochronous case*:

  - The main effect due to the presence of nonisochronicity in the systems is the *breaking of the reflectional symmetry of the model*: The degeneracy of the Hopf lines is broken. Due to this fact the incoherent state becomes unstable either via a single Hopf bifurcation or via *two different Hopf bifurcations* (with different eigenvalues): This difference is the origin of the dissimilar behavior shown by the two ensembles. The analytical results show good agreement with the numerics as far as the system remains close enough to the incoherent state. On the other hand, the bistability regions are located at the intersection of the saddle-node line with the second Hopf bifurcation.

  - The behavior of the two populations is clearly asymmetric, as shown by the coupling-modified frequencies and the order parameters. In some parameter regions (large values of K_p) the two order parameters are locked in phase , even though the individual oscillators within the populations van possess very different frequencies. This phenomenon can be explained taking into account the contribution of many oscillators entrained to higher order frequencies.

  - As the nonisochronicity is increased further, the saddle-node line approaches and collides with the $\gamma = 0$ axis. This establishes a critical value α^* of the nonisochronicity above which *the synchronization between the two populations always takes place through a Hopf bifurcation*, in contrast to what happens for two single oscillators. Moreover, the bistability region spreads in a larger region around the end of the second Hopf line.

  - It has been shown that the limit of *identical oscillators* in each population presents interesting stability properties for $\alpha > \alpha^*$ since the identical oscillators within one of the populations leave being in-phase synchronized. The linear stability analysis of the in-phase synchronized populations has confirmed the breakdown of the '2-oscillator dynamics' in this limiting case. The global stability properties of this problem are interesting directions of further study, since they seem to be related with the neutral stability of an splay state (Watanabe and Strogatz, 1993; Wiensenfeld and Swift, 1995).

6.2 Outlook

A number of interesting questions arise from the present level of understanding reached in this thesis, pointing to possible promising directions for future investigations in this field.

All realistic oscillatory systems are nonisochronous, and hence it is worth to study synchronization phenomena in the presence of nonisochonicity. Our study has been restricted to weakly coupled systems, in which the amplitude degrees of freedom of the oscillators have been neglected. However, we showed that some important effects of the nonisochronicity could be included in the phase equations and thus the problem of synchronization in the presence of nonisochronicity could be significantly simplified. Nevertheless, when amplitude variations are not negligible, a number of intriguing new phenomena can occur. For instance, the simplest possibility is amplitude death, that is a coupling induced stabilization of the origin arising typically in presence of both large parameter mismatch and strong coupling (Yamaguchi and Shimizu, 1984; Bar-Eli, 1985; Mirollo and Strogatz, 1990; Reddy et al., 1999). Besides, it has been shown that isochronous Landau-Stuart oscillators present a plethora of nonsteady regimes, ranging from quasiperiodicity to high dimensional chaos, whose description require in general a higher number of effective degrees of freedom (Matthews et al., 1991; Hakim and Rappel, 1992). Additionally, Aronson et al. (1990) showed that the nonisochronicity terms greatly complicate the dynamics in systems of two coupled oscillators. We have demonstrated that two populations of nonisochronous phase oscillators show already very complex dynamics (Montbrió et al., 2004b). However, one natural question would be whether the inclusion of the amplitude terms can have interesting dynamical effects.

On the other hand, the mean field model studied in Chapter 5 is one of the simplest models of coupled populations of nonidentical oscillators. Beyond its importance for theory of synchronization, oscillating systems consisting in asymmetrically interacting subunits are common in neuroscience (Gray et al., 1989) and are likely to be found in nature (Winfree, 1980). Moreover, the study of two coupled populations of oscillators is a first step in order to understand synchronization in complex networks (Strogatz, 2001; Albert and Barabási, 2002). Therefore, we believe that considering more realistic models would be an interesting direction for further study. Such models would incorporate features such as different population sizes, temporal delays, noise and the consideration of heterogeneity in more that one parameter of the system (Montbrió and Blasius, 2003).

Acknowledgment

The completion of this thesis would not have been possible without the help of many people. In particular I want to express my thanks to:

Dr Bernd Blasius, my main supervisor, who tirelessly provided advice and a critical atmosphere. I would also like to acknowledge Prof Dr Jürgen Kurths, who as my second supervisor provided constructive comments during my studies. It was a pleasure for me to complete this thesis under their supervision. I am also grateful for their financial support.

All my colleagues at the AGNLD group for the friendly atmosphere. Particularly Birgit Nader for her friendness and help and Jörg-Uwe Tessmer for the perfectly running computer network and his support in all technical problems.

Dr Grigory Osipov, Dr Damián Zanette and Dr Michael Zaks for fruitful stimulating discussions. I also would like to thank Dr Manuel Matías for stimulating discussions and for his warm hospitality during my stay at the research center IMEDEA in Mallorca.

All the people with whom I have spent my time with in Potsdam. Especially Jürgen Schmidt for the stimulating and useful discussions, Marcus Gellert, Gustavo Rodrigues, Suso Kraut, and Douglas Maraun, for creating a really warm and friendly atmosphere in our office. I also thank Miodrag Sremcevic, Ralf Steuer and Daniel Kubas for making my stay at the university more pleasant, as well as Diego Pazó, who helped me a great deal during my initial period in Potsdam.

Antonio Gámez, for his helpfulness and encouragement, and for bringing a bit of humor and good gastronomy into my daily routine. I am also grateful to Mamen Romano and to Marco Thiel, who kindly helped me with the many administrative and linguistic difficulties I have had with the University.

Finally, last but not least, I would like to thank my mother and my sister, for their continuing encouragement. I am also especially grateful to Àngels Badal, Daniel

Martí and Matteo Rini for helping me throughout my four years in Germany.

Bibliography

Acebrón, J. A., Bonilla, L. L., De Leo, S., and Springler, R. (1998). Breaking the symmetry in bimodal frequency distributions of globally coupled oscillators. *Phys. Rev. E*, 57:5287–5290.

Acebrón, J. A., Perales, A., and Springler, R. (2001). Bifurcations and global stability of synchronized stationary states in the kuramoto model for oscillator populations. *Phys. Rev. E*, 64:016218.

Albert, R. and Barabási, A. L. (2002). Statistical mechanics of complex networks. *Rev. Mod. Phys.*, 74:47–97.

Aronson, D. G., Ermentrout, G. B., and Kopell, N. (1990). Amplitude response of coupled oscillators. *Physica D*, 41:403–449.

Bar-Eli, K. (1985). On the stability of coupled chemical oscillators. *Physica D*, 14:242–252.

Blasius, B., Huppert, A., and Stone, L. (1999). Complex dynamics and phase synchronization in spatially extended ecological systems. *Nature*, 399:354–359.

Blasius, B., Montbrió, E., and Kurths, J. (2003). Anomalous phase synchonization in populations of nonidentical oscillators. *Phys. Rev. E*, 67:035204.

Blasius, B. and Stone, L. (2000). Chaos and phase synchronization in ecological systems. *Int. J. Bif. and Chaos*, 10:2361.

Bonilla, L. L., Neu, J. C., and Springler, R. (1992). Nonlinear stability of incoherence and collective synchronization in a population of coupled oscillators. *J. Stat. Phys.*, 67:313–330.

Bonilla, L. L., Pérez Vicente, C. J., and Rubí, J. M. (1993). Glassy synchronization in a population of coupled oscillators. *J. Stat. Phys.*, 70:921–937.

Bragard, J., Boccaletti, S., and Mancini, H. (2003). Asymmetric coupling effects in the synchronization of spatially extended chaotic systems. *Phys. Rev. Lett.*, 61:064103.

Bragard, J., Montbrió, E., Mendoza, C., Boccaletti, S., and Blasius, B. (2004). Defect enhanced anomaly in frequency synchronization of asymmetrically coupled spatially extended systems. *submitted to Phys Rev. Lett.*

Buck, J. and Buck, E. (1968). Mechanism of rhythmic synchronous flashing of fireflies. *Science*, 159:1319–1327.

Choi, M. Y., Kim, Y. W., and Hong, D. C. (1994). Periodic synchronization in a driven system of coupled oscillators. *Phys. Rev. E*, 49:3825–3832.

Crawford, J. D. (1994). Amplitude expansions for instabilities in populations of globally-coupled oscillators. *J. Stat. Phys.*, 74:1047–1084.

Daido, H. (1987). Population dynamics of randomly interacting self-oscillators, i. *Prog. Theor. Phys.*, 77:622–634.

Dana, S. K., Blasius, B., and Kurths, J. (2004). Experimental observation of anomalous phase synchronization in coupled Chua's oscillators. *Preprint.*

Dano, S., Sorensen, P. G., and Hynne, F. (2001). Sustained oscillations in living cells. *Nature*, 402:320–322.

Earn, D. J. D., Levin, S. A., and Rohani, P. (2000). Coherence and conservation. *Science*, 290:1360.

Eckhorn, R., Bauer, R., Jordan, W., M., B., W., K., Munk, M., and Reitboeck, H. J. (1988). Coherent oscillations: A mechanism of feature linking in the visual cortex?. *Biol. Cybern*, 60:121–130.

Elton, C. and Nicholson, M. (1942). The ten year cycle in numbers of canadian lynx. *J. Anim. Ecol.*, 11:215–244.

Engel, J. and Pedley, T. A. (1975). *Epilepsy, a comprehensive textbook.* Lippincott-Raven, Philadelphia.

Ertl, G. (1991). Oscillatory kinetics and spatio-temporal self-organization in reactions at solid surfaces. *Science.*, 254:1750–1755.

Garcia-Ojalvo, J., Casademont, J., Torrent, M. C., Mirasso, C. R., and Sancho, J. M. (1999). Coherence and synchronization in diode-laser arrays with delayed global coupling. *Int. J. Bif. Chaos.*, 9:2225–2229.

Garcia-Ojalvo, J. and Roy, R. (2001). Spatiotemporal communication with synchronized optical chaos. *Phys. Rev. Lett.*, 86:5204.

Glass, L. and Mackey, M. C. (1988). *From clocks to chaos: The rhythms of life.* Princeton University Press, Princeton, New Jersey.

Gray, C. M., König, P., Engel, A. K., and Singer, W. (1989). Oscillatory responses in cat visual cortex exhibit inter-columnar synchronization which reflects global stimulus properties. *Nature*, 338:334–337.

Gray, J. (1928). *Ciliary movement.* New York: MacMillan.

Guckenheimer, J. and Holmes, P. (1996). *Nonlinear oscillations, dynamical systems and bifurcations of vector fields.* Springer, New York.

Hakim, V. and Rappel, W. J. (1992). Dynamics of the globally coupled complex ginzburg-landau equation. *Phys. Rev. A*, 46:7347–7350.

Han, S. K., Kurrer, C., and Kuramoto, Y. (1995). Dephasing and bursting in coupled neural oscillators. *Phys. Rev. Lett.*, 75:3190.

Heino, M., Kaitala, V., Ranta, E., and J, L. (1997). Synchronous dynamics and rates of extinction in spatially structured populations. *Proc. R. Soc. Lond. B*, 264:481.

Hoppensteadt, F. C. and Izhikevich, E. M. (1998). *Weakly connected neural networks.* Springer-Verlag New York Inc.

Hoppensteadt, F. C. and Izhikevich, E. M. (1999). Oscillatory neurocomputers and dynamics connectivity. *Phys. Rev. Lett.*, 82:2983.

Hoppensteadt, F. C. and Izhikevich, E. M. (2000). Synchronization of laser oscillators, associative memory, and optical neurocomputing. *Phys. Rev. E*, 62:4010–4013.

Izhikevich, E. M. (1998). Phase models with explicit time delays. *Phys. Rev. E*, 58:905–908.

Kahn, P. B. and Zarmi, Y. (1998). *Nonlinear dynamics. Exploration through normal forms.* Wiley, New York.

Kiss, I. Z., Zhai, Y., and Hudson, J. L. (2002). Emerging coherence in a population of chemical oscillators. *Science*, 296:1676–1678.

Koshiya, N. and Smith, J. C. (1999). Neuronal pacemaker for breathing visualized. *Nature*, 400:360–363.

Kuramoto, Y. (1974). *Chemical oscillations, waves, and turbulence.* Springer-Verlag, Berlin.

Kurrer, C. (1997). Synchronization and desynchronization of weakly coupled oscillators. *Phys. Rev. E*, 56:3799–3802.

Landa, P. S. (1996). *Nonlinear oscillations and waves in dynamical systems.* Kluwer Academic Publishers, Dordrecht-Boston-London.

Landau, L. D. (1944). On the problem of turbulence. *C. R. Dokl. Acad. Sci. URSS*, 44:311.

Matthews, P. C., Mirollo, R. E., and Strogatz, S. H. (1991). Dynamics of a large system of coupled nonlinear oscillators. *Physica D*, 52:293–331.

May, R. (1973). *Stability and complexity in model ecosystems.* Princeton University Press, Princeton, 1973.

Mikhailov, A. S. and Loskutov, A. Y. (1996). *Foundations of synergetics II: Chaos and Noise.* Springer, Berlin.

Mirollo, R. E. and Strogatz, S. H. (1990). Amplitude death in an array of limit cycle oscillators. *J. Stat. Phys.*, 60:245–262.

Montbrió, E. and Blasius, B. (2003). Using nonisochronicity to control synchronization in ensembles of nonidentical oscillators. *Chaos*, 13:291–308.

Montbrió, E., Kurths, J., , and Blasius, B. (2004a). Synchronization in populations of nonisochronous phase oscillators. *In preparation.*

Montbrió, E., Kurths, J., and Blasius, B. (2004b). Synchronization between nonidentical populations of phase oscillators. *submitted to Phys. Rev. Lett.*

Néda, Z. ans Ravasz, E., Brechet, Y., and Barabási, A. L. (2000). Tumultuous applause can transform itself into waves of synchronized clapping. *Nature*, 403:849–850.

Okuda, K. and Kuramoto, Y. (1991). Mutual entrainment between populations of coupled oscillators. *Prog. Theor. Phys.*, 86:1159–1176.

Oliva, R. and Strogatz, S. H. (2001). Dynamics of a large array of globaly coupled lasers with distributed frequencies. *Int. J. Bif. Chaos.*, 11:2359–2374.

Osipov, G., Pikovsky, A. S., Rosenblum, M. G., and Kurths, J. (1997). Phase synchronization effects in a lattice of nonidentical Rössler oscillators. *Phys. Rev. E*, 55:2353–2361.

Pikovsky, A. S., Rosenblum, M. G., and Kurths, J. (2001). *Synchronization, a universal concept in nonlinear sciences.* Cambridge University Press, Cambridge.

Reddy, D. V. R., Sen, A., and Johnston, G. L. (1999). Time delay effects on coupled limit cycles at hopf bifurcation. *Physica D*, 129:15–34.

Richard, P., Bakker, B. M., Teusink, B., Van Dam, K., and Westerhoff, H. V. (1996). Acetaldehyde mediates the synchronization of sustained glycolytic oscillations in population of yeast cells. *Eur. J. Biochem.*, 235:238–241.

Rosenblum, M. G., Pikovsky, A. S., and Kurths, J. (1996). Phase synchronization of chaotic oscillators. *Phys. Rev. Lett.*, 76:1804.

Rössler, O. E. (1976). An equation for continous chaos. *Phys. Lett. A*, 57:397.

Sakaguchi, H. (1988). Cooperative phenomena in coupled oscillator systems under external fields. *Prog. Theor. Phys.*, 79:39–46.

Sakaguchi, H. and Kuramoto, Y. (1986). A soluble active rotator model showing phase transitions via mutual entertainment. *Prog. Theor. Phys.*, 76:576–581.

Schwartz, M. K., Mills, L. S., McKelvey, K. S., Ruggiero, L. F., and Allendorf, F. W. (2002). DNA reveals high dispersal synchronizing the population dynamics of Canada lynx. *Nature*, 415:520.

Shapiro, S. (1963). Josephson current in superconducting tunneling: The effect of microwaves and other observations. *Phys. Rev. Lett.*, 11:80–82.

Shapiro, S., Janus, A. R., and Holly, S. (1964). Effect of microwaves on Josephson currents in superconducting tunnelling. *Rev. Mod. Phys.*, 36:223–225.

Singer, W. (1999). Striving for coherence. *Nature*, 397:391–393.

Singer, W. and Gray, C. M. (1995). Visual feature integration and the temporal correlation hypothesis. *Annu. Rev. Neurosci.*, 18:555–586.

Steinmetz, P. N., Roy, A., Fitzgerald, P. J., Hsiao, S. S., Johnson, K. O., and Niebur, E. (2000). Attention modualtes synchronized neural firing in primate somatosensory cortex. *Nature.*, 404:187–190.

Stopfer, M., Bhagavan, S., Smith, B. H., and Laurent, G. (1997). Impaired odour discrimination on desynchronization of odour-encoding neural assemblies. *Nature.*, 390:70–74.

Strogatz, S. H. (1994). *Nonlinear dynamics and chaos.* Addison-Wesley, Reading.

Strogatz, S. H. (2000). From Kuramoto to Crawford: exploring the onset of synchronization in populations of coupled oscillators. *Physica D*, 143:1–20.

Strogatz, S. H. (2001). Exploring complex networks. *Nature*, 410:268–276.

Strogatz, S. H. and Mirollo, R. E. (1991). Stability of incoherence in a population of coupled oscillators. *J. Stat. Phys.*, 63:613–635.

Strogatz, S. H., Mirollo, R. E., and Matthews, P. C. (1992). Coupled nonlinear oscillators below the synchronization threshold: Relaxation by generalized Landau damping. *Phys. Rev. Lett.*, 68:2730–2733.

Stuart, J. T. (1960). On the nonlinear mechanics of wave disturbances in stable and unstable parallel flows. Part I: The basic behavior in plane Poseuille flow. *J. Fluid Mech.*, 9:353.

Taylor, G. I. (1951). Analysis of the swimming of microscopic organisms. *Proc. Roy. Soc. Lon. Ser. A*, 209:447–461.

Vandermeer, J., Stone, L., and Blasius, B. (2001). Categories of chaos and fractal basin boundaries in forced predator-prey models. *Chaos, Solitons and Fractals*, 12:265.

Varela, F., Lachaux, J. P., Rodriguez, E., and Martinerie, J. (2001). The brainweb: phase synchronization and large-scale integration. *Nature Rev. Neurosci.*, 2:229–239.

Walker, T. J. (1969). Two mechanisms in the snowy tree cricket. *Science*, 166:891–894.

Watanabe, S. and Strogatz, S. H. (1993). Integrability of a globally coupled oscillator array. *Phys. Rev. Lett.*, 70:2391–2394.

Wiener, N. (1958). *Nonlinear problems in random theory.* MIT press, Cambridge, MA.

Wiensenfeld, K. and Swift, J. W. (1995). Averaged equations for Josephson junction arrays. *Phys. Rev. E*, 51:1020–1025.

Wiesenfeld, K., Colet, P., and Strogatz, S. H. (1996). Synchronization transition in a disordered Josephson array. *Phys. Rev. Lett.*, 76:404–407.

Wiesenfeld, K., Colet, P., and Strogatz, S. H. (1998). Frequency locking in Josephson arrays: Connection with the Kuramoto model. *Phys. Rev. E*, 57:1563–1569.

Winfree, A. T. (1967). Biological rhythms and the behavior of populations of coupled oscillators. *J. Theor. Biol.*, 16:15–42.

Winfree, A. T. (1980). *The geometry of biological time.* Springer, New York.

Winfree, A. T. (2002). On emerging coherence. *Science*, 298:2336–2337.

Yamaguchi, Y. and Shimizu, H. (1984). Theory of self-synchronization in the presence of native frequency-distribution and external noise. *Science*, 11:212–226.